Ion Exchange in Natural Zeolite Packed Column

By

Özge CAN

A Dissertation Submitted to the
Graduate School in Partial Fulfillment of the
Requirements for the Degree of

MASTER OF SCIENCE

Department: Chemical Engineering
Major: Chemical Engineering

İzmir Institute of Technology
İzmir, Turkey

June, 2004

We approve the thesis of Özge CAN

Date of Signature

....2004

Prof. A. Semra ÜLKÜ

Supervisor

Department of Chemical Engineering

....2004

Prof. Devrim BALKÖSE

Co-Supervisor

Department of Chemical Engineering

....2004

Assoc. Prof. Ahmet Emin Eroğlu

Department of Chemistry

....2004

Assist. Prof. Fehime Özkan

Department of Chemical Engineering

....2004

Assist. Prof. Oğuz Bayraktar

Department of Chemical Engineering

....2004

Prof. Devrim BALKÖSE

Head of Department

ACKNOWLEDGEMENTS

I would like to express my intimate gratitude to my advisor, Prof. Semra Ülkü, for her guidance and support throughout this project. I am also grateful to my coadvisor Prof. Devrim Balköse for her precious suggestions. I would like to give my special thanks to Assoc. Prof. Dr. Mehmet Polat and Assist. Prof. Fehime Özkan for their valuable recommendations during the study.

I would like to thank all of the research scientists in the Chemical Engineering Department of İzmir Institute of Technology, especially Nesrin Gaffaroğulları and Handan Gaygısız for their contributions to the ICP-OES studies presented in this study.

Finally, my special thanks go to my fiancée Aslı Ertan for her encouragement, patience and understanding.

ABSTRACT

Turkish natural clinoptilolites were examined to evaluate their ion exchange performance for the removal of copper, nickel and cobalt ions by performing both batch and packed column experiments. Initial metal solutions were prepared using metal nitrate solutions at various concentrations. All of the experiments were carried out at 29^{o}C. Before performing the ion exchange experiments zeolites were characterized and their clinoptilolite contents were determined quantitatively as 80 and 64 % for zeolites named as CP1 and CP2, respectively. The copper exchange capacities of CP1 and CP2 were determined from equilibrium studies as 10.01 mg (0.32 meq) Cu^{2+} / g CP1 and 8.33 mg (0.262 meq) Cu^{2+} / g CP2. Ion exchange capacity of CP2 zeolite was determined as 6.64 mg (0.226 meq) Ni^{2+} / g and 4.55 mg (0.154 meq) Co^{2+} / g. The equilibrium behaviour of the system was best described by Langmuir model.

Experiments were designed to investigate the optimum parameters and significance of the interactions between these parameters. In column studies, the parameters such as packing height, inlet metal concentration and flow rate were investigated. The concentration of the metals in the sample solutions which were taken from the exit of the ion exchange column at specific time intervals were analyzed by using Optical Emission Spectrometry (ICP-OES). Afterwards, by making use of the data obtained from ICP-OES, breakthrough curves were constructed. By the help of these curves, breakthrough capacity and ion exchange capacity of natural zeolites were calculated. The ion exchange capacity of CP2 zeolite was calculated as 8.04 mg Cu^{2+}/g CP2, which was consistent with the capacity calculated from batch experiments, 8.33 mg Cu^{2+}/g CP2. Also, breakthrough points were determined. Furthermore, solid phase was also analysed for determining its crystal structure and chemical composition using Scanning Electron Microscopy (SEM) and Energy Dispersive X-Ray (EDX) devices (Philips XL 30S FEG).

In addition to these, natural zeolite particles which have been ion exchanged throughout this process were regenerated using 0.2M and 1.7M of NaCl solutions. According to regeneration studies, it was determined that 94 and 95% of copper were recovered within the first 100 minutes for both experiments.

After the experiments were performed, model equations were applied to the system in order to be able to investigate the dynamic behavior of the system. As a result of this simulation, breakthrough was well predicted.

ÖZ

Bu çalışmada, Türkiye'de bulunan yataklardan çıkan doğal zeolitlerin denge ve dolgulu kolonda dinamik çalışmaları ile bakır, nikel, kobalt gibi metalleri tutma performansları incelenmiştir. Bunun için kolon yüksekliği, giriş bakır konsantrasyonu ve debi gibi parametrelerin optimum değerleri saptanmıştır. Giriş metal çözeltileri farklı konsantrasyonlarda nitrat tuzları kullanılarak hazırlanmıştır. Bütün deneyler 29 ^{o}C'de gerçekleştirilmiştir. İyon değişimi deneylerinden önce, zeolitler kantitatif olarak karakterize edilip, klinoptilolit miktarları belirlenmiştir, CP1 ve CP2 zeolitlerinin klinoptilolit miktarları sırasıyla %80 ve %64 olarak bulunmuştur. CP1 ve CP2 zeolitlerinin bakır değiştirme kapasiteleri sırasıyla 10 mg Cu^{2+} / g CP1 ve 8.33 mg Cu^{2+} / g CP2 olarak hesaplanmıştır. Bunun yanısıra, CP2'nin farklı metaller için iyon değiştirme kapasiteleri 6.64 mg Ni^{2+} / g and 4.55 mg Co^{2+} / g olarak bulunmuştur.

Optimum parametrelerin ve bu parametrelerin birbirleri ile olan etkileşimlerinin öneminin incelenebilmesi için deneysel tasarım çalışmaları uygulanmıştır. Kolon çalışmalarında kolon boyu, giriş çözelti konsantrasyonu ve akış debisi gibi parametreler incelenmiştir. Öte yandan, iyon değişimi kolonundan çıkan çözeltiler belirli zaman aralıklarında toplanmış, içerdikleri metal konsantrasyonları ICP-OES cihazı kullanılarak belirlenmiştir. Daha sonra, ICP-OES'den alınan bilgiler kullanılarak eşzaman eğrileri oluşturulmuştur. Bu eğriler yardımıyla doğal zeolitlerin breakthrough ve iyon değişimi kapasiteleri hesaplanmıştır. CP2 zeolitinin iyon değiştirme kapasitesi 8.04 mg Cu^{2+}/g CP2 olarak hesaplanmış; denge çalışmalarından elde edilen sonuçla (8.33 mg Cu^{2+}/g CP2) karşılaştırıldığında iki sonucun birbiriyle uyumlu olduğu belirlenmiştir. Ayrıca breakthrough noktaları saptanmıştır. Bununla birlikte, SEM ve EDX cihazları (Philips XL 30S FEG) kullanılarak kristal yapısı ve kimyasal bileşiminin belirlenmesi amacıyla katı fazın analizi yapılmıştır.

İyon değişimi işlemi uygulanan zeolit partikülleri daha sonra 0.2M ve 1.7M NaCl çözeltileri kullanılarak rejenere edilmiş ve her iki deney için de ilk 100 dakikada bakırın yaklaşık %94'ünün geri kazanıldığı görülmüştür.

Sistemin dinamik davranışını inceleyebilmek için deneylerden elde edilen verilere daha sonra model denklemler uygulanmıştır. Bu çalışmanın sonucunda eşzaman eğrileri iyi bir şekilde temsil edilmiştir.

TABLE OF CONTENTS

LIST OF FIGURES

LIST OF TABLES

CHAPTER 1. INTRODUCTION

1.1. Importance of Heavy Metal Removal

Environmental conservation is of increasing social and economic importance. Particularly contamination of waters by heavy metals is an essential pollution problem. Industrial waste waters frequently contain high levels of heavy metals and treatment is needed in order to avoid water pollution. There are numerous sources for industrial effluents leading to heavy metal discharges apart from the mining and metal related industries. Heavy metal pollution frequently results from the industrial use of organic compounds containing metal additives in the petroleum and organic chemical industries such as textile mill products (Cr^{3+}), organic chemicals (Cr^{3+}, Pb^{2+}), petroleum refining, pulp industries and fertilizers (Cr^{3+}, Cu^{2+}, Pb^{2+}), iron and steel manufacturing plants (Inglezakis et al., 2001). Consequently, toxic metals which are produced and released by the stated industries seriously threat the environment. Because of the increased importance of related pollution aspects and the presence of water scarcity the separation and control of heavy metals during the treatment of most industrial waste waters has recently become an important issue.

Sources of copper and nickel pollutants include mining/smelting, agricultural materials, the electronics, chemical and metallurgical industries as well as waste disposal in the form of leachates from landfills. Metal ions in solution adsorbed by aquatic plants and animals are very toxic if the concentration is sufficiently high. Copper intake from drinking water can be around 1.4 mg per day from soft water and 0.05 mg per day from hard water, where the guideline for acceptable copper concentration in drinking water is less than 3 mg/L. Copper and nickel are among the most toxic metals for both plants and several microorganisms, whereas copper, along with arsenic and mercury, is recognised as exhibiting the highest relative mammalian toxicity (Keane, 1997).

1.2. The Methods Used in Removal of Heavy Metals

The removal of heavy metal cations from aqueous solutions can be achieved by several processes, such as chemical precipitation, adsorption, solvent extraction, reverse osmosis, ultrafiltration or ion exchange. Among these methods the currently used ones to eliminate metals are essentially precipitation followed by settling and/or filtration,

adsorption on activated carbon, extraction by solvent, and incineration. However, these processes have disadvantages such as low yield, high investment and running costs and high sludge production (Flores et al., 1999). Although there are many methods available for the removal of heavy metals, ion exchange is considered to be one of the most cost effective ones if low cost ion exchangers such as natural zeolites are used.

1.3. The scope of the Study

In this study, the performance of the natural zeolite as an ion exchanger taken from different deposits of Gördes/Manisa region for the removal of copper, nickel and cobalt ions were investigated. The effect of flow rate, initial metal concentration and packing height were the parameters investigated in packed bed column. Besides, batch and kinetic experiments were carried out to understand the equilibrium behavior of the system and to compare the results with those of column experiments.

As a result of column studies, breakthrough curves were constructed to calculate the breakthrough point, breakthrough capacity and ion exchange capacity of the natural zeolite by varying the parameters. Afterwards, regenaration experiments were carried out in order to be able to determine the reuseability of the natural zeolite.

Finally, model equations were applied to the system to describe its dynamic behaviour and to determine the most appropriate model representing system.

CHAPTER 2. MINERAL ION EXCHANGERS

Most natural ion-exchange minerals are crystalline aluminosilicates with cation-exchange properties. Characteristic representatives of this group of materials are the zeolites which include, among others, the minerals analcite, $Na[Si_2AlO_6]_2.H_2O$, chabazite, $(Ca,Na)[Si_2AlO_6]_2.6H_2O$, harmotome, $(K,Ba)[Si_5Al_2O_{14}].5H_2O$, heulandite, $Ca[Si_3AlO_8].5H_2O$, and natrolite, $Na_2[Si_3Al_2O_{10}].2H_2O$. All these materials have a relatively open three-dimensional framework structure with channels and interconnecting cavities in the aluminosilicate lattice (Helfferich, 1962).

2.1. Natural Zeolites

2.1.1. Definition

The term zeolite was originally coined in the 18th century by a Swedish mineralogist named Cronstedt who observed, upon rapidly heating a natural zeolite, that the stones began to dance about as the water evaporated. Using the Greek words which mean "stone that boils", he called this material zeolite. A commonly used description of a zeolite is a crystalline aluminosilicate with a cage structure.

The natural zeolites are a popular group of minerals for scientists and an important group of minerals for industrial and other purposes. They combine rarity, beauty, complexity and unique crystal habits. The unique physical and chemical properties of natural zeolites, combined with their abundance in nature have made them useful in many industrial and research applications. Recently, the zeolite group includes more than 40 naturally occuring species, and is the largest group of the minerals among the silicates (Tsitsishvili et al., 1992).

Natural zeolites are low cost aluminosilicates, with a cage-like structure suitable for ion exchange due to isomorphous replacement of Al^{3+} with Si^{4+} in the structure, giving rise to a deficiency of positive charge in the framework.

Typically forming in the cavities, or vesicles, of volcanic rocks, zeolites are the result of very low grade metamorphism. Some form from just subtle amounts of heat and pressure and can just barely be called metamorphic while others are found in obviously metamorphic regimes. Zeolite crystals have been grown on board the space shuttle and are undergoing extensive research into their formation and unique properties.

Clinoptilolite is probably the most abundant zeolite in nature because of its wide geographic distribution and large size of deposits. Characteristic clinoptilolite rocks consist of 60-90% clinoptilolite with the remaining being mainly feldspars, clays, glass, and quartz (Armbruster, 2001). Natural zeolites with ≈70–80% clinoptilolite content are often used in technological applications (Peric et al., 2003).

Clinoptilolite is very stable towards dehydration and its thermal stability, 700 °C in air, is considerably greater than the stability of other natural zeolites with a similar structure. The chemical composition of clinoptilolite is characterized by remarkable variations in the Si/Al ratio as well as in the composition of the exchangeable cations. The Si/Al ratio changes between 4 and 5.5 and low-silica members are enriched with calcium, whereas high-silica clinoptilolites are enriched with potassium, sodium, and magnesium (Çulfaz et al., 2003).

2.1.2. Structure

Clinoptilolite belongs to the heulandite group of minerals with the simplified formula $(Na,K)_6Si_{30}Al_6O_{72} \cdot nH_2O$ and found mainly in sedimentary rocks of volcanic origin. Because of its high content of silicon it is known as high-silica heulandite.

The primary building block of the zeolite framework is the tetrahedron, the center of which is occupied by a silicon or aluminum atom, with four atoms of oxygen at the vertices. Each oxygen atom is shared between two tetrahedra (Tsitsishvili et al., 1992).

The negative charge of the clinoptilolite framework, which comes from tetrahedrally coordinated aluminum, is counterbalanced mainly by monovalent cations (Na^+, K^+) and by divalent cations (Ca^{2+}, Mg^{2+}), which do not occupy fixed positions, but are free to move in the channels of the lattice framework. These ions act as counter ions and can be replaced by other cations (Doula et al., 2003).

The zeolite framework consists of an assemblage of SiO_4 and AlO_4 tetrahedra (Figure 2.1), joined together in various regular arrangements through shared oxygen atoms to form an open crystal lattice containing pores of molecular dimensions into which molecules can penetrate.

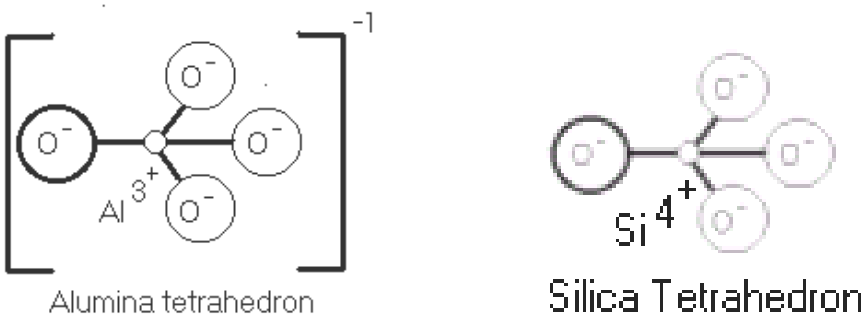

Figure 2.1. Primary Building Unit of Zeolites

The aluminosilicate framework is the most conserved and stable component and defines the structure type. The topology of the framework, the numbers and the distribution of the charges (aluminum sites) and stacking faults are basically formed at the crystal growth stage and define a series of technologically important properties of zeolites. Framework topology forms the basis of zeolite classification (Tsitsishvili et al., 1992). Clinoptilolite's framework consists of four channels. Three channels are formed of 8-membered rings of oxygen and one channel of 10-membered rings of oxygen. The 10-membered channel and one 8-membered channel are parallel with axis c, the second 8-membered channel is parallel with axis a, and the third channel lies at an angle of 50^{o} to axis a (Figure 2.2).

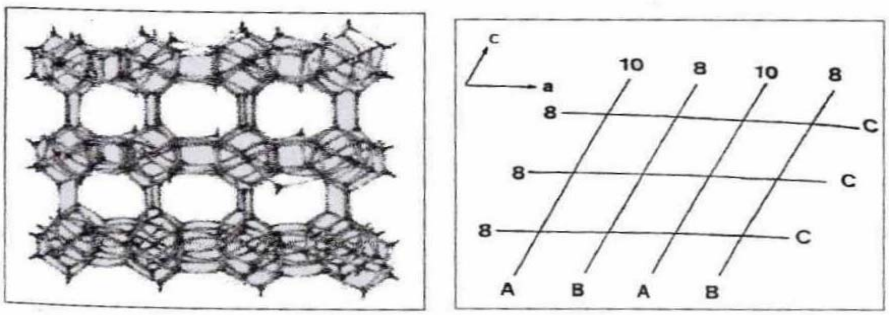

Figure 2.2. Schematic diagram of clinoptilolite structure

2.1.3. Uses and Applications

Zeolites have been recognized for more than 200 years, but only during the middle of the 20th century have attracted the attention of scientists and engineers who demonstrated their technological importance in several fields. Although most of the effort was devoted to synthetic zeolites, in recent years increasing attention has been

directed towards natural zeolites, whose status changed from that of museum curiosity to an important mineral commodity. Several hundred thousand tons of natural zeolite bearing materials are mined in the United States, Japan, Italy, Bulgaria, Cuba, Mexico, Korea and Germany but only those containing chabazite, clinoptilolite, erionite, ferrierite, phillipsite, mordenite and analcime are available in sufficient quantity and purity to be considered as exploitable natural resources (Cincotti et al., 2001).

The structure, the composition, the feasible phase transformations during hydrothermal, thermal, and tribochemical treatments, and the properties of adsorption, ionic exchange, catalysis, and cationic conduction are responsible for the large number of uses of natural zeolites. Natural zeolites can be used in wastewater cleaning, agriculture, fertilizers, aquaculture, animal health, animal nourishment, gas separation, solar refrigeration, gas cleaning, deodorization, solid electrolytes, construction materials, and cleanup of radioactive wastes.

Natural zeolites are also involved by mineral scientists for greater involvement in the surface, colloidal, and biochemical investigations that are needed in the future development of zeolite applications (Mumpton, 1999).

2.1.3.1. Zeolites as Ion Exchangers

Although the zeolite ion exchange has been well studied, often as an adjunct to their uses in catalysis and molecular sieving very few practical uses have emerged.

The economics of the use of natural zeolites in this way at present depends critically upon their availability and whereas quite extensive use of clinoptilolite columns is made worldwide, the source of mineral is usually geographically close to its end use.

The cation exchange property of zeolite minerals was first observed 100 years ago. The ease of cation exchange in zeolites and other minerals led to an early interest of ion exchange materials for use as water softening agents. Synthetic, noncrystalline aluminosilicate materials were primarily used; in more recent years, organic ion exchange resins are used. Crystalline zeolites have not been used commercially as water softeners. There are several applications of zeolites as ion exchangers (Table 2.1).

Table 2.1. Ion Exchange Applications of Zeolites

Applications	Advantage(s)
Removal of Cs^+ and Sr^+ radioisotopes - Linde AW-500, mordenite, clinoptilolite	Stable to ionization radiation Low solubility Dimensional stability High selectivity
Removal of NH_4^+ from wastewater-chabazite, clinoptilolite, mordenite	NH_4^+ - selective over competing cations
Detergent builder Linde A, Linde X (ZB-100, ZB-300)	Remove Ca^{2+} and Mg^{2+} by selective exchange No environmental problem
Radioactive waste water treatment	Same as Cs^+, Sr^{2+} removal
Aquaculture-AW-500, clinoptilolite	NH_4^+ - selective, direct addition of clinoptilolite to fish culture tanks
Regeneration of artificial kidney dialysate solution	NH_4^+ - selective
Animal Nourishment	Reduces NH_4^+ by selective exchange to non-toxic levels during digestion of food
Heavy Metals removal and recovery	High selectivities for various metals
Agricultural Applications (slow release fertilizers, soil conditioning and remediation)	Exchange with plant nutrients such as NH_4^+ and K^+ with slow release in soil

As mentioned above, ion exchange depends as much on the properties of the exchanger as on the properties of the ions undergoing exchange. The affinity of an ion towards a given ion exchanger, i.e. the ion exchangeability depends primarily on the charge of the ion, the ionic radius and the degree of hydration. The larger the charge on the ion the greater is the force with which it is attracted by the functional groups of opposite charge on the ion exchanger and hence the larger is its exchange capacity, i.e. the more difficult it's to remove during the exchanger - regeneration process.

In the case of equivalent ions the magnitude of their radii is decisive for their ion exchange capacity. The greater the volume of the ion, the weaker is its electric field in the solution and thus the smaller is its degree of hydration. The so-called hydrodynamic radii of ions decrease with increasing atomic weight and hence their exchange energy (energy with which the ion is transported from the solution to the ion exchanger).

CHAPTER 3. ION EXCHANGE THEORY

3.1. Definition of the Process

Ion exchange is often used for removing a certain ion from a solution or for replacing it by another ion. Ion exchange reactions are important in chemical processes, food and pharmaceutical industries. Application areas of ion-exchange also includes removal of heavy metals from waste water and major cationic constituents from ground water due to cation exchange.

Ion exchange in zeolites is a complicated process involving two particles which are the extraframework charge balance cation present in the zeolite, and the ion dissolved in the solution (Malherbe, 2001).

The ion exchange process may be presented by the following equation:

$$z_B A^{ZA} + z_A \overline{B}^{ZB} \rightleftharpoons z_B \overline{A}^{ZA} + z_A B^{ZB} \quad (3.1)$$

where,

z_A & z_B are the valances of the ions

A^{ZA}, initially in the solution

B^{ZB}, initially in the zeolite

- Characters with a bar related to a cation inside the zeolite crystal.

***Simple examples are*:**

$$Na^+ + \overline{K}^+ \rightleftharpoons \overline{Na}^+ + K^+ \quad (3.2)$$

$$2\,Na^+ + \overline{Ca}^{+2} \rightleftharpoons 2\,\overline{Na}^+ + Ca^{+2} \quad \text{for uni-divalent exchange} \quad (3.3)$$

These stoichiometric reactions can be conveniently characterized by the construction of an ion exchange isotherm. This is a pictorial presentation of the equilibrium of the representative ions in both solution and zeolite phase.

Clearly, before making up such an isotherm it's necessary to ensure that ion exchange equilibrium has been reached, so same simple kinetic exchange measurements must be performed.

3.2. Ion Exchange Equilibrium

Cation exchange in zeolites leads to alteration of stability, adsorption behavior, and selectivity, catalytic activity and other important physical properties so ion exchange should also be considered as a modification process as well as a direct application. Since many of these properties depend on controlled cation exchange with particular cation species, detailed information on the cation exchange equilibria is important (Breck, 1974).

Equilibrium behavior is usually described in terms of equilibrium isotherms which depend on the system temperature, the total initial concentration of the solution in contact with the exchanger and on characteristics of the ion exchange system, such as solution composition, mineral type and pH. One of the models which describe the equilibrium behavior of the system is the Langmuir model.

$$\frac{q}{q_{\max}} = \frac{bC}{1+bC} \tag{3.4}$$

Where, q is the amount of solute passing through the solid phase, q_{max} is the maximum amount of solute which can be passed through the solid phase, C is concenration and b is the Langmuir constant.

Another equilibrium parameter is the ion exchange capacity, or the total exchange capacity, which, in common usage, is defined as the number of ionogenic groups, in equivalents, present in a specified amount of the material, and is a constant used for characterizing ion exchangers.

However, not all of these ionogenic groups are always available for ion exchange. Zeolites for example, exclude some of the incoming ions, which are too large to fit into the channels of the aluminosilicate framework. Furthermore, some of the present ionogenic groups (cations for cation exchange process) are components of impurities such as feldspar, quartz and salts, especially in the case of natural zeolites, or they are located at inaccessible sites of the material structure. From a practical point of view, the number of ions, which can be sorbed or exchanged, is more important than the number of ionogenic groups. The maximum exchange level, measured by ion exchange methods is expressed in terms of exchangeable ions and depends on the experimental conditions and on the specific nature of the ions involved (Inglezakis et al., 2001). Maximum exchange level of clinoptilolite samples determined by many scientists were given in Table 3.1.

The ion exchange capacity of zeolite ion exchangers is a function of their silicon oxide/aluminum oxide mole ratio, since each AlO_4 tetrahedra in the zeolite framework provides a single cation exchange site. On a weight basis, the exchange capacity also depends on the cation form (Sherman et al., 1978).

Table 3.1. Maximum Exchange Level Data Available for Cu^{2+} Exchange on Clinoptilolite

METAL	Method	Sample	MEL (meq/g)	References
Cu^{2+}	Column exhaustion	Na-clinoptilolite	1.10-1.25	Nikashina et al., 1984
	Column exhaustion	Na-clinoptilolite	0.68-0.84	Mondale et al., 1995
	Column exhaustion	Natural clinoptilolite	0.16-0.55	Mondale et al., 1995
	Column exhaustion	Natural clinoptilolite	0.08-0.55	Mondale et al., 1995
	Equilibrium isotherms	Natural clinoptilolite	1	Assenov et al., 1988
	Column exhaustion	Na-clinoptilolite	1.39	Guangsheng et al., 1988
	Repeated batch eqls.	Na-clinoptilolite	1.76	Langella et al., 2000
	Equilibrium isotherms	Natural clinoptilolite	0.7	Kurama et al., 1995
	Equilibrium isotherms	Natural clinoptilolite	0.88-1.42	Semmens et al., 1988
	Repeated batch eqls.	Natural clinoptilolite	0.093	Cincotti et al., 2001
	Repeated batch eqls.	Na-clinoptilolite	0.38	Cincotti et al., 2001
	Equilibrium isotherms	Natural clinoptilolite	0.539	Top A., 2001
	Kinetic measurements	Natural clinoptilolite	0.057	Türkmen M., 2001

At equilibrium solution and solid phases should be analyzed to determine the distributions of A^{ZA} & B^{ZB} between the phases. An isotherm can now be plotted which records the equivalent fraction of the entering ion in the solution (A_S) against that in the zeolite (A_Z) at constant temperature. Equilibrium data available for clinoptilolite samples with different forms were presented in Table 3.2 for copper exchange.

The equivalent fractions of the exchanging cation in the solution and zeolite are defined by:

$$A_S \equiv \frac{z_A m_S^A}{z_A m_S^A + z_B m_S^B} \tag{3.5}$$

m_S^A *and* m_S^B are the molalities of the ions A and B, respectively.

$$A_Z \equiv \frac{no.\ equivalents\ of\ exchanging\ cation\ A}{total\ equivalents\ of\ cations\ in\ the\ zeolite} \tag{3.6}$$

$$\bar{A}_Z + \bar{B}_Z = 1 \tag{3.7}$$

$$A_S + B_S = 1 \quad \text{in the equilibrium.} \tag{3.8}$$

Table 3.2. Equilibrium Data Available for Clinoptilolite/Cu^{2+}

Metal	Initial Conc.(meq/dm^3)	Sample	Isotherm Type	Literature
Cu^{2+}	15	NH_4-Clino.	Unfavorable	Blanchard G. et al., 1984
	10	Na-Clino.	Favorable	Nikashina V.A. et al., 1984
	100	Ca-Clino.	Favorable	Nikashina V.A. et al., 1984
	2	NH_4-Clino.	Favorable	Assenov A. et al., 1988
	14	Pretreated Clinos.	Sigmoid	Semmens M.J. et al., 1988
	100	Na-Clino.	Unfavorable	Langella A. et al., 2000

3.2.1. Equilibrium Isotherms

The ion exchange isotherm is a plot of A_Z (mole fraction of component A in zeolite phase) as a function of A_S (mole fraction of component B in solution phase) at a given total concentration in the equilibrium solution and at a constant temperature.

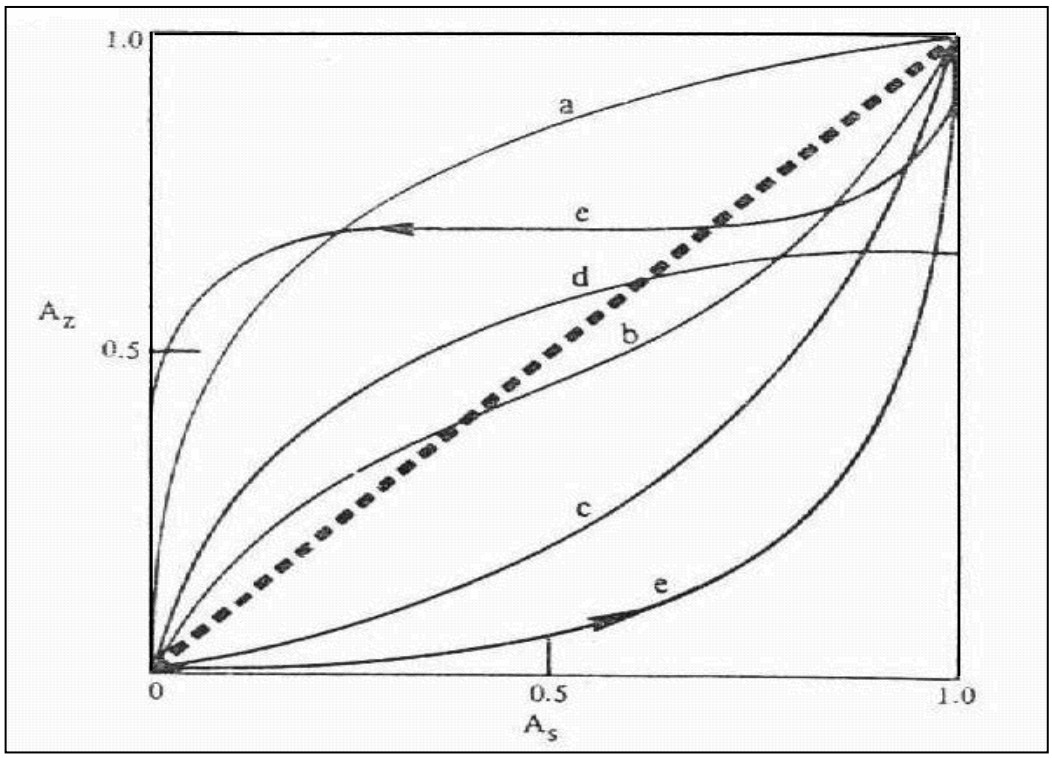

Figure 3.1. Types of ion exchange isotherms for the reaction

The exchange isotherms for exchange of cations in zeolites may be classified into five types;

In curve a: The zeolite exhibits a preference for the entering ion A ($\alpha_B^A > 1$) and isotherm lies above the diagonal.

In curve b: In many cases, the selectivity varies with the degree of exchange and sigmoidal isotherm illustrated.

In curve c: $\alpha_B^A < 1$ the isotherm lies below the diagonal.

In curve d: Complete exchange is not attained, by the entering ion, $x_{max} < 1$, due to an ion sieve effect.

In curve e: It represents an unusual case where exchange results in two zeolite phases and produces a hysteresis loop.

3.2.2. Selectivity and Ion Sieving

The preference of zeolite for one of two ions is expressed by the separation factor,

$$\alpha_{B}^{A} = \frac{A_z B_s}{B_z A_s} = \frac{areaI}{areaII} \tag{3.9}$$

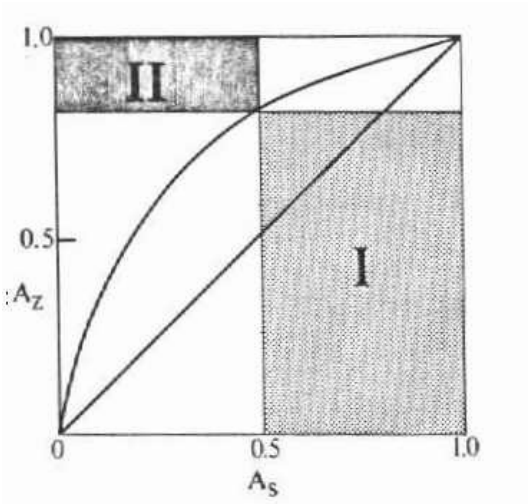

Figure 3.2. Derivation of the Separation Factor from the Isotherm

If ion A is preferred, α_B^A is greater than unity. The separation factor depends on the total concentration of the solution, the temperature, and A_S. Selectivity series of zeolites determined by the indicated scientists for many different cations were listed in Table 3.3.

If α_B^A=1, the exchange is ideal and obeys the law of mass action. Normally, however, the isotherm deviates from the diagonal line, represented as α_B^A=1, and thus shows a selectivity for one of the two ions. In most crystalline exchangers, the isotherms terminate at the lower left and upper right corners of the diagrams. In zeolites, however, there are many exceptions due to exclusion of the entering ions or trapped cations in the zeolite structure. This is referred to as the ion-sieve effect, that is, the entering ions cannot reach all of the sites occupied by the ions initially in the zeolite. The isotherm then terminates at a point where the degree of exchange, x, is less than 1.

General statements on the parameters controlling zeolite cation exchange properties;

- The nature of both the competing ions with respect to their relative sizes and to their states of solvation inside & outside the zeolite
- The charge on the zeolite framework coupled with framework geometry
- The heteroenergetic nature of the cation sites available for occupation inside the framework
- The temperature at which exchange is carried out, this can influence the removal of water of hydration and the accessibility of sites and improve exchange kinetics
- The concentration of the external solution coupled with the presence of (or absence) of ligands other than water molecules.

The sieving & partial sieving effect of zeolites toward various cations have been attributed to one or more three possible mechanisms;

1. The cation may be too large to enter the small channels and cavities within the zeolite structure, or in some zeolites exchangeable cation is locked in during synthesis
2. The distribution of charge on the zeolite structure may be unfavorable for the cation
3. The size of the hydrated cation in aqueous solution or solvation in non- aqueous solution, may influence and retard exchange of cation since an exchange of solvent molecules must occur for the cation to diffuse through zeolite structure.

Table 3.3. Molecular Sieve Zeolite Ion Exchange Selectivity Patterns [Sherman, John D., 1978]

Selectivity Series	**Reference**
$NC_4H_9NH_3^+$<$nC_3H_7NH_3^+$<NH_4^+<$C_2H_5NH_3^+$	Barrer, Papadopoulos, and Rees
Li<Na<Rb<K<Cs	Sherry
Li<Ca<Sr<Ba<Na<K<Rb	Filizova
Na<K<Cs	Ames
Na<NH_4^+<Cs	Howery and Thomas
Cu<Zn<Cd<Pb<Ba	Semmens and Seyforth
Zn<Cu<Cd<Pb	Fujimori and Moriya
Mg<Ca<Na<NH_4^+<K	Sherman and Ross
Li<Na<NH_4^+<K<Rb<Cs Mg<Ca<Sr<Ba	Ames
Na<Ag<Pb At low loadings: Na<Cu<Zn<Cd<Ag<Pb	Chelishchev et al.

CHAPTER 4. ION EXCHANGE IN PACKED COLUMN

Most ion exchange operations, whether in the laboratory or in plant-scale processes, are carried out in columns. A solution is passed through a bed of ion-exchanger beads where its composition is changed by ion exchange or sorption. The composition of the effluent and its change with time depend on the properties of the ion exchanger (ionic form, capacity, degree of crosslinking, etc.), the composition of the feed, and the operating conditions (Helfferich, 1962). The principle operating conditions influencing the ion exchange processes are the flow rate and the quality of flow. Furthermore, flow rate controls the contact time between any part of the solution which is in contact with a given layer of the bed.

Generally, ion exchange in fixed beds is favored by strong preference and high capacity of the ion exchange for the cation from the feed, high solid diffusion coefficients of the exchanging cations and low flow rate (Inglezakis et al., 2001).

4.1. Breakthrough Curve

Breakthrough curve is the effluent concentration history. The time when the cations of the feed first appear in the effluent is termed as breakthrough point. In practice, breakthrough point is defined as the time when the effluent concentration is reaching a percentage of the influent concentration which is considered unacceptable, e.g. 10%. Then the operation is stopped and the exchanger can be regenerated or replaced by a fresh one. The entire breakthrough curve and the breakthrough point depend on the properties of the ion exchanger, the composition of the feed solution and the operating conditions. The main relevant properties of the ion exchanger are considered to be the equilibrium behaviour and the diffusion rate through the material, expressed by solid diffusion coefficients.

4.2. Performance of an Ion Exchange Column

When the solution containing heavy metal ions is first fed to the column, it will exchange all its ions for ions that are initially present in the zeolite phase in a comparatively narrow zone at the top of the bed. The solution, now containing electrolyte in the form of ions which are initially present in the zeolite phase, passes through the upper part of the column, in the upflow mode, without further change in composition. As the feed is continued, the bottom layers of the bed are constantly exposed to fresh heavy metal solution. Eventually, they completely converted to metal form and lose their efficiency and they become exhausted. Thus, the time when the heavy metal ions are first appear in the effluent is the breakthrough point. Afterwards, continuation beyond breakthrough results in complete displacement of ions initially present in zeolite phase by heavy metal ions in the column. After that, the whole bed is in equilibrium with the feed which then passes through without change in composition.

At breakthrough, the top layers of the bed are not yet completely converted to metal form. Thus, breakthrough capacity is less than the overall ion exchange capacity of the column. The breakthrough capacity can be defined as the amount of ions initially present in the metal solution taken up prior to the breakthrough. The breakthrough and overall capacities of a column are readily determined by the effluent concentration history. The breakthrough capacity depends on the nature of the process and the operating conditions and is a meaningless figure unless these are specified (Helfferich, 1962).

CHAPTER 5. MODELING

Mathematical models are developed to describe the dynamic behaviour of the system. The differential mass balance equations for an element of the ion exchange column and for an ion exchanger particle within such an element provide the starting point for the development of models.

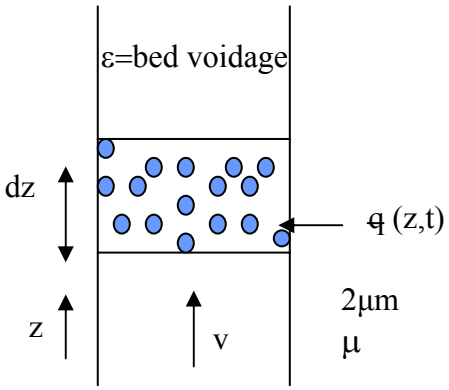

Figure 5.1. Element of Packed Bed

Fluid stream containing concentration c(z, t) of an exchangeable species is flowing through an element of packed bed sketched in Figure 5.1. If the flow pattern can be represented as axially dispersed plug flow the differential fluid phase mass balance is (Ruthven, 1984)

$$-D_L \frac{\partial^2 c}{\partial z^2} + \frac{\partial}{\partial z}(\upsilon c) + \frac{\partial c}{\partial t} + \left(\frac{1-\varepsilon}{\varepsilon}\right)\frac{\partial \bar{q}}{\partial t} = 0 \qquad (5.1)$$

where, D_L is the axial dispersion coefficient, c is the fluid phase concentration, z is the distance measured from the column inlet, υ is the interstitial velocity, ε is the bed voidage and $\bar{q}$ is the volume average concentration of the pollutant in the solid phase.

When the equilibrium isotherm yields favorable isotherm, concentration front approaches constant pattern form. Analytical solutions for the asymptotic constant pattern profile are easily obtained, but a general analytic solution for the breakthrough curve or pulse response is only possible in a few special cases (Ruthven, 1984). Heat

transfer resistance can be neglected in isothermal systems. Also, when plug flow is considered axial dispersion is neglected so that the term $-D_L \frac{\partial^2 c}{\partial z^2}$ can be dropped.

Thus the general mass balance equation reduces to a first order hyperbolic equation. Although, such a system is not common in practice, its analysis can provide useful insight into the behaviour of more complex systems.

For such a system the differential fluid phase mass balance for the exchangeable species reduces to

$$\upsilon \frac{\partial c}{\partial z} + \frac{\partial c}{\partial t} + \left(\frac{1-\varepsilon}{\varepsilon}\right)\frac{\partial \bar{q}}{\partial t} = 0 \tag{5.2}$$

Representing the equilibrium isotherm in general form by

$$q^* = f(c) \tag{5.3}$$

and assuming mass transfer equilibrium:

$$\left(\frac{\partial \bar{q}}{\partial t}\right)_z = \left(\frac{\partial q^*}{\partial t}\right)_z = \frac{dq^*}{dc}\left(\frac{\partial c}{\partial t}\right)_z \tag{5.4}$$

$$\left(\frac{\partial c}{\partial t}\right)_z + \frac{\upsilon}{\left[1+\left(\frac{1-\varepsilon}{\varepsilon}\right)\left(\frac{dq^*}{dc}\right)\right]}\left(\frac{\partial c}{\partial z}\right)_t = 0 \tag{5.5}$$

This equation has the form of kinematic wave equation. After determining the isotherm type that the system obeys, above equation can be integrated analytically or numerically and thus it yields the exit concentration profile of the pollutant.

5.1. Frequently Used Models for the Prediction of Breakthrough Curves

In a study of Cincotti et al. in 2000, they have performed breakthrough experiments of lead solutions and they have simulated fixed bed runs using a mathematical model which includes axial dispersion as well as a new approximate rate

law for non-linear adsorption and diffusion in spherical adsorbent particle based on a equivalent film resistance model. Breakthrough experiments were conducted at 25 °C using 65 ppm lead solutions at an inlet flow rate of 1.2 L h^{-1}, 50 g of Sardinian natural zeolite and a column with 1.6 cm diameter and 23 cm depth). Samples of the column effluent were collected at selected time intervals, and the composition was measured using an atomic absorption spectrophotometer.

They have used heterogeneous axial-dispersion model to simulate the transient behavior of the fixed-bed column. The column was assumed isothermal and monodimensional flux was considered. Parallel pore and surface diffusion was considered to take place in spherical and uniformly sized adsorbent particles. Local equilibrium between pore fluid and adsorbent surface was assumed.

They used several mass balance equations which were written for the pollutant in aqueous phase and solid phase. The corresponding boundary conditions were also used.

Mass balance equation in the aqueous phase,

$$\varepsilon \frac{\partial C}{\partial t} = -\varepsilon \upsilon_{\text{int}} \frac{\partial C}{\partial z} + \varepsilon E_D \frac{\partial^2 C}{\partial z^2} - \frac{3(1-\varepsilon)}{R_p} k_f (C - C_p^*) \tag{5.6}$$

Initial and boundary conditions were,

$$\text{t} = 0, \qquad \text{C} = C_p^* = 0 \tag{5.7}$$

$$\text{z} = 0, \qquad \upsilon_{\text{int}} C^f = \upsilon_{\text{int}} C - E_D \frac{\partial C}{\partial z} \tag{5.8}$$

$$\text{z} = \text{L}, \qquad \frac{\partial C}{\partial z} = 0 \tag{5.9}$$

Where C represents the aqueous phase concentration of the pollutant, ε is bed void fraction, υ_{int} interstitial fluid velocity, E_D is dispersion coefficient, z is the distance through the bed and k_f is the intraparticle diffusivity.

They have represented the intraparticle diffusional resistance by pseudo-steady state diffusion through a hypothetical flat film thickness $\delta = R_p/5$, where R_p represents the particle radius.

$$\frac{\partial \bar{q}}{\partial t} = \frac{3/R_p}{\rho_p + \varepsilon_p (d(f_{eq}^{-1}(\bar{q})))/d\bar{q}} k_f (C - C_p^*) \tag{5.10}$$

where due to the local equilibrium assumption,

$$q^* = f_{eq}(C_p^*) \qquad \bar{q} = f_{eq}(\bar{C}_p) \tag{5.11}$$

They have used f_{eq} as Langmuir equilibrium isotherm, and they have calculated average solid phase and pore fluid concentration of the pollutant as,

$$\bar{q} = \frac{\int_0^{R_p} q 4\pi r^2 dr}{(4/3)\pi R_p^3} \qquad \bar{C}_p = \frac{\int_0^{R_p} C_p 4\pi r^2 dr}{(4/3)\pi R_p^3} \tag{5.12}$$

They have solved those systems of non-linear partial differential equations by the method of lines, which was consisted in adopting a central finite difference scheme for the spatial derivatives in order to convert the equations above into a set of ordinary differential equations at the internal node points. Afterwards, they have integrated the resulting system of ordinary differential equations numerically as an initial value problem with Gear's method (subroutine DIVPAG of the IMSL libraries).

Finally, the corresponding fitting results were satisfactory and it was found that the model was to be able to predict fairly well the corresponding breakthrough curve. Also, bed volumes of different natural zeolite-lead systems were found as 250 and 700 and those values were of same magnitude of typical bed volume values reported in the literature for the removal of various pollutants using natural zeolite-bearing materials.

In a study of Inglezakis et al. in 2003, they have performed modeling of ion exchange of Pb^{2+} in fixed beds of clinoptilolite. They have conducted fixed bed experiments by natural clinoptilolite in 0.7 m long plexiglass column of 2.1 cm internal diameter, using three different volumetric flow rates 5-15 BV/h, under total normality of 0.01 N and ambient temperature (25°C).

They have considered the rate of diffusion into a uniformly porous spherical particle for solid diffusion controlled process. After solving a partial differential mass balance equation by using Crank- Nicholson method, they have found average fluid phase and solid phase concentrations of pollutant using numerical integration.

Finally they have found that the deviation between experimental and the model (C/C_0) values for the same time (t) was within the limits of ±22%, for (C/C_0)>0.06. For (C/C_0)<0.06 the model was totally failed to fit the experimental data. Also, they have

found the increase of contact time was leading to higher operating exchange capacity and lower solid diffusion coefficient, both approaching those calculated in batch-type reactors.

In another study performed by Lin and his coworkers in 2003, they have adopted theoretical column model and this model was found to describe well the ion exchange breakthrough characteristics. In the column ion exchange test runs, they have used a pyrex tube of 2 cm i.d. and 30 height containing 10 g of OH-type strong acid anionic resin in which the chromic acid solution with a Cr^{6+} concentration between250 and 750 ppm passed through at a desired rate between 10 and 30 ml/min. In this study, they have used an alternative model which was developed from the original microscopic model by Bohart and Adams and Thomas for describing the solute breakthrough behavior of a column adsorber.

The macroscopic model was represented by

$$\ln\left(\frac{C_0 - C}{C}\right) = \ln\left[\exp\left(\frac{k_1 Q_e M}{F}\right) - 1\right] - k_1 C_0 t \tag{5.13}$$

where C is the solute concentration in the aqueous stream at time t, k_1 the rate constant of adsorption, Q_e the equilibrium solid phase concentration of sorbed solute, M the mass of adsorbent, F the flow rate and t the time.

After making some assumptions, they have used the simplified logistic function:

$$\ln\left(\frac{C}{C_0 - C}\right) = k(t - \tau) \tag{5.14}$$

Using simple linearization techniques they have easily calculated k and τ values from the equation above and using the estimated parameters, they have reconstructed the breakthrough curves for different inlet concentration and flow rate conditions. As a result, they have found reasonably well predictions with observed data.

In a study of Lehmann and his friends in 2000, they have column tests consisted of a peristaltic pump and a vertical plastic column having inner diameter 1.5 cm and height 10 cm. Goethite was used as an adsorbent and chromate and zinc solutions at a volumetric flow rate of 100 ml/h were used as feed solutions. The only parameter investigated in this study was packing height which was between 1.98 and 7.92 cm.

In the modeling part they have used BDST model which relates the service time of a fixed bed with the height of adsorbent material in the bed. They have found the following equation to describe the BDST model (Chung et al., 1998):

$$t = \frac{q_0}{C_0 V} M - \frac{1}{kC_0} \ln\left(\frac{C_0}{C_t} - 1\right) = aM + b \tag{5.15}$$

where t is the service time, q_0 the adsorption capacity, C_0 the initial concentration of adsorbate, V the applied flow rate, M the quantity of sorbent inside the column, k is the rate constant of adsorption, and C_t the respective effluent concentration of adsorbate at time t.

Afterwards, they have performed scaled-up of column system using obtained parameters of the BDST model. Besides, they have found good prediction for the case of changing flow rates during tests of a number of complex mixtures. For this, they have used following correcting calculations:

$a_{new} = a_{old} (C_0/C_n)$ (5.16)

and

$b_{new} = b_{old} (C_0/C_n)[\ln(C_n-1)/\ln(C_0-1)]$. (5.17)

Finally, they have found that this method for estimating the effect of changing feed concentrations appeared to work well when removing one-component impurities from water.

In another work performed by Sağ et al. in 2001, mass transfer models to dynamic removal of Cr(VI) ions by chitin in packed column reactor were studied. In this study two identical packed columns, 2.5 cm in diameter and 3.25 and 6.0 cm in height, were used and experiments were carried out at 25°C. The masses of sorbent were set at 1.5 and 2.75 g for depths of 3.25 and 6 cm, respectively. The influent was introduced by an upflow of varying volumetric flow rate from 2.5 to 10 ml min^{-1}.

In that study, the breakthrough curves for the sorption of Cr(VI) ions onto chitin were measured as a function of flow rate, bed depth, amount of chitin in the column and inlet metal ion concentration.

One of the models used in this study was the Adams-Bohart model which was used for the description of the initial part of the breakthrough curve. According to this model, the mass transfer rates obey the following equations:

$$\frac{\partial q}{\partial t} = -kqC \tag{5.18}$$

$$\frac{\partial C}{\partial Z} = -\frac{k}{U_0} qC \tag{5.19}$$

where q is the metal ion content in the sorbent at t, C the solute concentration in solution, Z the column depth, k the kinetic constant and U_0 the linear flow rate. In this model the concentration field was considered to be low. The following equation was obtained:

$$\ln \frac{C_s}{C_0} = kC_0 t - kN_0 \frac{Z}{U_0} \tag{5.20}$$

where N_0 is the saturation concentration.

According to this study, Wolborska model was also used for the description of adsorption dynamics in the range of the low-concentration breakthrough curve. The following equations represent the approximated solution:

$$\ln \frac{C_s}{C_0} = \frac{\beta_a C_0}{N_0} t - \frac{\beta_a Z}{U_0} \tag{5.21}$$

with

$$\beta_a = \frac{U_0^2}{2D}\left(\sqrt{1 + \frac{4\beta_0 D}{U_0^2}} - 1\right) \tag{5.22}$$

where β_a is the external mass transfer coefficient with a negligible axial dispersion coefficient D.

The third model used in this study was Clark model which associates the Freundlich equation and the mass transfer concept according to following equations:

$$q_{eq} = K_F C_{eq}^{1/n} \tag{5.23}$$

$$U_0 \frac{dC}{dZ} = k_T (C - C_{eq}) \tag{5.24}$$

where k_T is the mass transfer rate coefficient.

The solution of the system was given by

$$\left(\frac{C_0^{n-1}}{1 + Ae^{-rt}}\right)^{1/n-1} = C_s \quad \text{, generalized logistic function} \tag{5.25}$$

where

$$A = \left(\frac{C_0^{n-1}}{C_b^{n-1}} - 1 \right) e^{rt_b} \tag{5.26}$$

and

$$R(n-1) = r \qquad R = \frac{k_T}{U_0} \upsilon \tag{5.27}$$

υ, n, C_b and t_b are the migration velocity, the Freundlich constant, the concentration at breakthrough, and the time at beakthrough, respectively.

Finally, they have found that breakthrough was well predicted by Adams-Bohart, whereas they could not defined the whole breakthrough curve. However, they have found that simulation of the whole breakthrough curve was effective with the Clark model.

Analytical solution of breakthrough curves for the limiting cases of solid diffusion control was solved by Cooper (Rutven, 1984).

In this model, linear rate solid film equation is represented as

$$\frac{\partial \bar{q}}{\partial t} = k(q_s - \bar{q}) \tag{7.9}$$

where q_s and $\bar{q}$ are the sorbate concentration at saturation limit and the value of sorbate concentration averaged over crystal.

According to Cooper model, solution for breakthrough curve given by,

$$\frac{C}{C_0} = 1 - \xi e^{-\tau} \ , \qquad \xi \le 1.0 \tag{7.10}$$

$$\frac{C}{C_0} = 1 - e^{\xi - \tau - 1} \ , \qquad 1 \le \xi \le 1 + \tau \tag{7.11}$$

$$\frac{C}{C_0} = 0 \ , \qquad \xi \ge 1 + \tau \tag{7.12}$$

$$\tau = k(t - \frac{z}{v}) \quad \text{and} \quad \xi = \frac{kKz}{v}(\frac{1-\varepsilon}{\varepsilon}) \tag{7.13}$$

Where, τ is the dimensionless time, ξ is the dimensionless column length, k is the overall effective mass transfer coefficient (s^{-1}), t is the time and z is the column length.

CHAPTER 6. EXPERIMENTAL

6.1. Materials

In this study, clinoptilolite rich natural zeolite taken from different deposites of Gördes/Manisa region was used. The zeolites used were defined as CP1 or CP2 depending on the clinoptilolite content equal to 80 % or 64 ± 5 %, respectively. The zeolitic content of CP1 was determined in the study of Top et al., 2004 and CP2 was characterized in this study. The initial moisture of the samples were determined by moisture analyzer (Sartorius, MA 100).

6.2. Methods

Before performing the experiments natural zeolites used in this study were characterized by using several methods. For this, natural clinoptilolite samples were taken representatively from Gördes/Manisa region, Enli Madencilik A.Ş. In order to be able to prevent contamination excavator was not used during the sample collection operation. Approximately 500 kg samples were collected and then simultaneously divided into four groups until the desired amount of samples were obtained. These samples were firstly crushed into 1-2 cm range of particle size and then into < 2 mm size range with a jaw crusher (Fritsch, Pulverisette 1). Particles smaller than 2 mm size were then wet sieved into five groups namely; > 1.7 mm, 425 μm – 1.7 mm, 106 – 425 μm, 25 – 106 μm and finally smaller than 25 μm. The reason for applying wet sieving was to prevent the smaller particles to stick on the larger ones and hence change the ion exchange capacity of these particles. It was observed that during wet sieving some of the particles were precipitated while the others were dispersed within the deionized water for 25 μm fraction. The ones precipitated within three days are called “very fine” and the ones dispersed in water are called “ultrafine” particles in this study. Later on, the water containing ultrafine particles were first separated from the precipitate by overflowing and then centrifuged (Sigma Laboratory Centrifuges, 6K15). After the wet sieving process all zeolite fractions were dried at 105 ^{o}C overnight. In further characterization studies to eliminate the effect of particle size all fractions were ground under 25 μm (Fritsch, Pulverisette 9). In order to determine the optimum grinding time to reduce the particles under 25 μm, the same amount of samples (30 g) were ground with different time intervals such as 1, 2 and 4 minutes and then the samples were analysed using Sedigraph (Micromeritics, Sedigraph 5100). From each time interval one

gram of sample was taken representatively, it was replaced in 50 ml of calgon (Sodiummetaphosphate 50w%) solution and was stirred in an ultrasonic bath (Ultrasonic LC30). Afterwards, to determine if the particles were dispersed within the solution properly or not, a drop of the solution was analysed under optic microscope (Olympus CH40) and scanning electron microscopy (SEM, Philips XL 30S FEG).

Standard materials used for quantitative analyses were obtained from Mineral Research, Clarkson, New York with +90 % pure, clinoptilolite, IDA, (# 27031, Castle Creek, Idaho) and CAL, (# 27023, Hector, California) supplied kindly by F. Mumpton. RIR standard mixtures were prepared by mixing 1.0 μm α-alumina powder (corundum) to each mineral standard in a 50:50 ratio by weight. XRD data were collected on a X-ray diffractometer, Philips X'pert Pro employing the Cu Kα radiation of power settings of 30 kV and 30 mA. Data were collected using a step size of 0.02^o 2θ and a count time of 2 s/step. Several discrete 2θ ranges between 5 and 40^o 2θ were used to measure only the reflections of interest.

Natural zeolites were prepared and ground in order to reduce it to the appropriate size for ion exchange experiments. Afterwards, solutions with varying concentrations (100 to 200 ppm) were prepared to investigate the effects of the initial concentration of the feed metal solutions to ion exchange behaviour of the system. In the experiments two different natural zeolites were taken from different deposits of Gördes/Manisa region and three metals namely, Cu^{2+}, Ni^{2+} and Co^{2+} were used to be investigated in the studies. Furthermore, to determine the effect of the solution flow rate, three different flow rates (2.86, 3.6, 4.75 ml/min) were selected. Besides, the experiments were conducted by using different packing heights ranging between 12 and 25 cm. Later on, EDX analyses of the ion-exchanged clinoptilolite samples were performed.

Throughout the studies, deionized water used in the preparation of solutions was produced by using Dowex cation exchange resin (HCR S/S) and Labconco instrument. Besides, pH values were measured with a pH-meter (Metrohm 744).

In the ion exchange experiments, both batch and packed column studies, Copper(II)nitrate hemipentahydrate ($Cu(NO_3)_2.2.5H_2O$) (Aldrich, ACS Reagent, 98% pure), Nickel(II)nitrate hexahydrate ($Ni(NO_3)_2.6H_2O$) (Aldrich, ACS Reagent, 98% pure) and Cobalt(II)nitrate hexahydrate ($Co(NO_3)_2.6H_2O$) (Sigma, ACS Reagent, 98.3% pure) solutions were used as the feed solution. Small amount of nitric acid was added to the solutions to avoid metal precipitation. In order to do this, the solutions were titrated

until the final pH reaches 4. Beyond fixed bed runs, clinoptilolite samples were analysed by EDX (Philips XL 30S FEG).

6.2.1. Ion Exchange Experiments

6.2.1.1. Material Preparation for Ion Exchange Experiments

Clinoptilolite samples taken from two different deposits of Manisa/Gördes region were first crushed and reduced to particle size range of 2-0.85 mm. Then, in order to determine the dry weight of clinoptilolite samples, the moisture of the samples was determined by using moisture analyzer (Sartorius, MA 100). For this, the samples were kept in the device for 2 hours at 105 °C. Consequently, the moisture content of the clinoptilolite samples were determined. Afterwards, the crushed samples were placed in the plexi-glass column without any further pretreatment.

6.2.1.2. Batch Kinetic and Equilibrium Experiments

Equilibrium behaviour of the system and the effect of initial concentration were investigated by performing twenty experiments for both zeolites (CP1, CP2) given in Table 6.1. As can be seen from Table 6.1, 100 ml of $Cu(NO_3)_2$, $Ni(NO_3)_2$, $Co(NO_3)_2$ solutions with different concentrations were prepared. Then 1 g of each zeolite sample was placed in the volumetric flasks and mixed at 130 rpm, 29 ^oC in the water bath. For five days long, samples were taken at specific time intervals until no further metal uptake from zeolite was observed. However, for each set of experiment the number of solutions prepared for the sampling stage was equal to the number of samples taken to maintain the solid to solution ratio constant. In addition, pH of the solutions were measured. Finally, solutions were analysed using ICP-OES.

Table 6.1. Process Parameters in Batch Studies for two Different Clinoptilolite Deposits

Ion Exchanger		**CP1**	**CP2**
Metal	**Cu^{2+}**	+	+
	Ni^{2+}	-	+
	Co^{2+}	-	+
Initial Conc. [mg/L]		50, 75, 100, 150, 200	
Zeolite mass [g]		1	
SolutionVolume [ml]		100	
Shaking Rate [rpm]		130	

6.2.1.3. Packed Column Studies

In the fixed bed studies ion exchange experiments were carried out in plexiglass ion exchange column of 30 cm height and 1.5 cm inner diameter. The feed was introduced to the system using a diaphram pump (Cole- Parmer) in upflow mode with adjustible flow rate between 1 and 50 ml/min. The adjusted flow rate was controlled by a flow meter (Gilmont Instruments). The fluid is transferred within the system with the aid of the Cole Parmer tygon tubing. In these experiments, samples were collected at specific time intervals by using automatic fraction collector namely, Atto Biocollector, AC-5750. Drainage solutions were kept in 4L volumetric flasks (Ilmabor TGI). In order to be able to determine the effluent concentration of samples Inductively Coupled Plasma- Atomic Emission Spectrometry (Axial ICP-OES 96, Varian Liberty Series) was used.

As a result of these studies the effects of two ion exchangers (CP1 and CP2), different heavy metal ions (Cu^{2+},Ni^{2+}, Co^{2+}) as well as packing height, flow rate, initial metal concentration were determined. During the studies, the exchange temperature was kept constant in water bath at 29 ± 1 ^{o}C. The corresponding parameters are given in Tables 6.2, 6.3, 6.4 and 6.5.

Table 6.2. Process Parameters to Investigate the Effect of Packing Height for CP1 Zeolite Using Cu^{2+}

C_o [mg/L]	200	200	200
Flow rate [ml/min]	4.75	4.75	4.75
Bed height [cm]	12.5	18.75	25
Amount of Ixer [g]	14.06	19.95	26.75
Initial pH	4.82	4.64	4.72
Final pH	5.33	5.86	5.93

Table 6.3. Process Parameters to Investigate the Effect of Packing Height for CP2 Zeolite Using Cu^{2+}

C_o [mg/L]	200	200	200
Flow rate [ml/min]	1.87	1.87	1.87
Bed height [cm]	12.5	18.75	25
Amount of Ixer [g]	14.06	19.95	26.75
Initial pH	4.46	4.48	4.54
Final pH	5.38	5.42	5.61

Table 6.4. Process Parameters to Investigate the Effect of Flow Rate for CP1 Zeolite Using Cu^{2+}

C_o [mg/L]	200	200	200	200
Flow rate [ml/min]	1.87	2.86	3.6	4.75
Bed height [cm]	25	25	25	25
Amount of Ixer [g]	26.75	26.75	26.75	26.75
Initial pH	4.53	4.6	4.84	4.72
Final pH	5.86	5.84	5.96	5.93

Table 6.5. Process Parameters to Investigate the Effect of Initial Copper Concentration for CP1 Zeolite Using Cu^{2+}

C_o [mg/L]	100	158.5	200
Flow rate [ml/min]	4.75	4.75	4.75
Bed height [cm]	18.75	18.75	18.75
Amount of Ixer [g]	19.95	19.95	19.95
Initial pH	4.4	4.5	4.6
Final pH	5.83	5.96	5.86

Table 6.6. Process Parameters to Investigate the Column Performance of CP2 Zeolite for Different Metals

Metal	Initial Conc. [mg/L]	Flow Rate [ml/min]	Packing Height [cm]
Cu^{2+}, Ni^{2+}, Co^{2+}	150	3.8	21.88

6.2.1.4. Regeneration Studies

In order to check the reusability of the natural zeolite, regenaration experiments were performed after ion exchange process. For this, 0.2 M and 1.7 M of NaCl solutions were prepared and were passed through the column. Samples taken from the exit solutions were collected within specific time intervals. Afterwards, the solutions were get prepared for the ICP-OES analysis.

Table 6.7. Process Parameters in Regeneration Experiments

Ion Exchanger	CP1 from Table 6.4- set 2	CP1 from Table 6.2- set 1
Flow rate [ml/min]	2.86	4.75
Bed height [cm]	25	12.5
Regenerant	1.7 M NaCl	0.2 M NaCl
Amount of Ixer [g]	26.75	14.06
Initial pH	6.74	6.32
Final pH	5.16	5.36

6.3. Analyses of the Solutions

In the preparation of the solutions of copper, nickel and cobalt, metal nitrate solutions and deionized water were used. After ion exchange experiments, stock solutions of 10 % (w/w) of nitric acid together with the sample solutions taken from the fixed bed experiments were prepared to be analyzed by using ICP-OES. The nitric acid stock solution was prepared by mixing 110 ml of 65 % (w/w) of HNO_3 with deionized water which adds up to 1 liter of solution. Therefore, the final solution produced is 10 % (w/w) of HNO_3. The sample solutions can be diluted by adding deionized water to the mixture of 10 ml of sample solution and 10 ml of 10 % (w/w) of HNO_3 which adds up to 100 ml. The final solution contains 1 % (w/v) of HNO_3 and hence the solution was diluted by ten fold.

Other than nitric acid stock solution, standard copper solution was also prepared by using 100 ml of 1000 mg/L copper standard solution for ICP. Then this copper standard was diluted to 100 mg/L by taking 10 ml of this solution, 10 ml of 10 % (w/w) of HNO_3 and 80 ml of deionized water. Finally, 100 ml of 100 mg/L copper standard solution was obtained to be used in further dilutions. Also, 100 ml blank solution including was prepared by adding 90 ml of deionized water to 10 ml of 10 wt% of HNO_3.

In this study, all solutions prepared contains 1 % (w/v) of HNO_3 in order to prevent precipitation of metal hydroxides and also the matrix effect during ICP analyses.

6.4. Analyses of the Solid Phase

After the ion exchange experiments, clinoptilolite samples taken from the column exit and from the batch experiments were kept in the oven overnight at 105 °C to prepare them for EDX analyses. During EDX analyses data taken from 10 different parts of the samples were evaluated using SPSS computer program in order to determine the standard deviation.

CHAPTER 7. RESULTS AND DISCUSSION

7.1. Batch Kinetic and Equilibrium Studies

In order to evaluate the ion exchange capacity of the natural zeolites namely, CP1 and CP2, the experiments were carried out by performing both batch and fixed bed modes by using Cu^{2+}, Ni^{2+} and Co^{2+} ions. In this part of the study, the kinetic runs were conducted in batch mode on the clinoptilolite samples until equilibrium was reached. In performing the batch experiments, 1 g of each zeolite sample was placed in different concentrations of metal nitrate solution of 100 ml at 29 °C. The reason for working with different concentrations of metal nitrate solution was to construct equilibrium isotherm for the determination of the equilibrium behavior of the system.

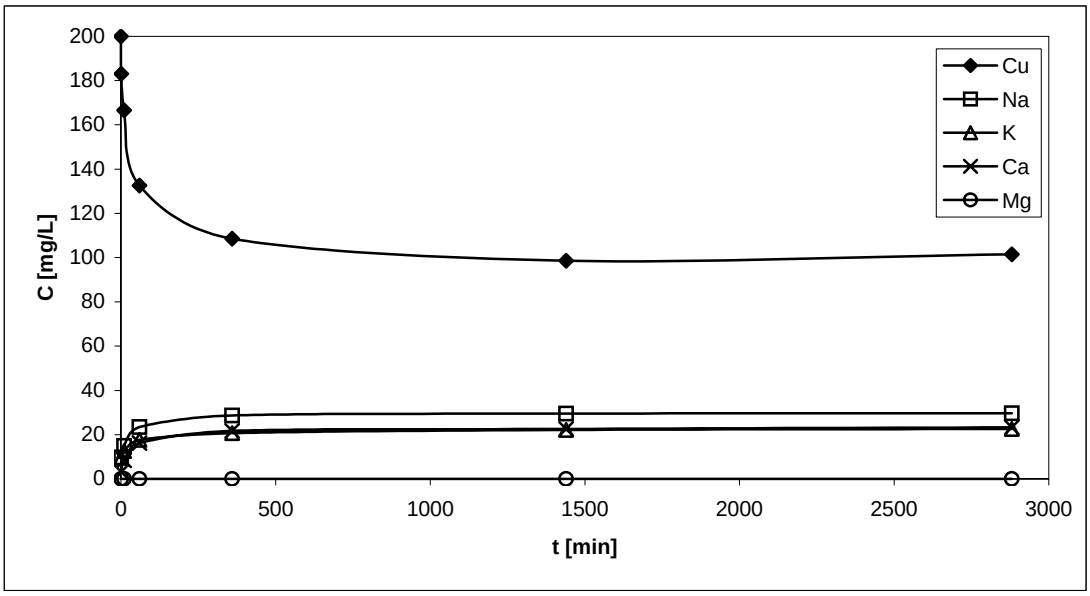

Figure 7.1. The Kinetic Curves for Ion Exchange Between Cu^{2+} and Na^{+}, K^{+}, Ca^{2+}, Mg^{2+} ions with 1 g of CP1 in 100 ml, 200 mg/L Copper Nitrate Solution at 130 rpm.

Table 7.1. Variation of the Ion Concentrations with Respect to Time at 29°C, 130 rpm, 1 g of CP1 in 100 ml of 200 mg/L Copper Nitrate Solution.

t [min]	Cu^{2+} [mg/L]	Na^{+} [mg/L]	K^{+} [mg/L]	Ca^{2+} [mg/L]
0	200	0	0	0
1	183	10	10	3
10	166	14	12	8
60	132	23	17	16
360	108	28	20	21
1440	98	29	22	22
2880	101	29	22	23

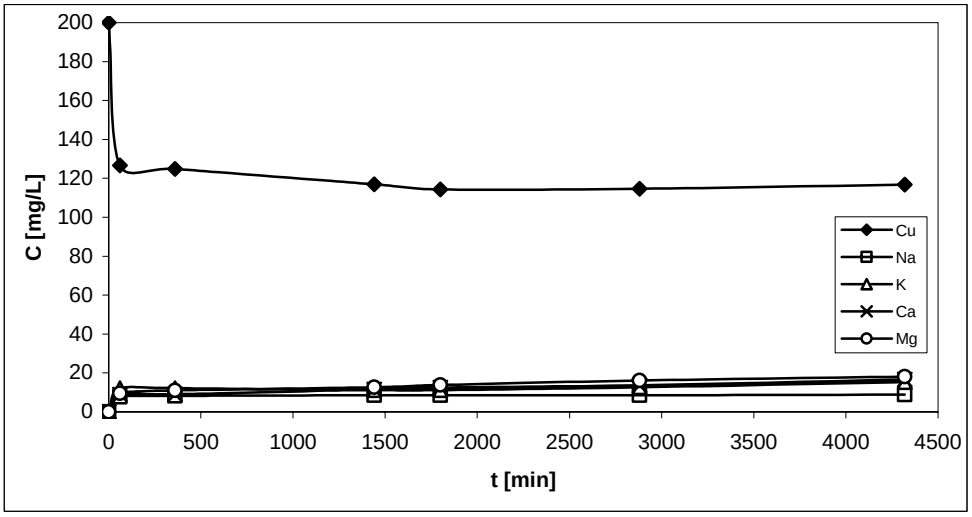

Figure 7.2. The Kinetic Curves for Ion Exchange Between Cu^{2+} and Na^{+}, K^{+}, Ca^{2+}, Mg^{2+} ions with 1 g of CP2 in 100 ml, 200 mg/L Copper Nitrate Solution at 130 rpm.

Table 7.2. Variation of the Ion Concentrations with Respect to Time at 29°C, 130 rpm, 1 g of CP2 in 100 ml of 200 mg/L Copper Nitrate Solution.

t [min]	Cu^{2+} [mg/L]	Na^{+} [mg/L]	K^{+} [mg/L]	Ca^{2+} [mg/L]	Mg^{2+} [mg/L]
0	200	0	0	0	0
60	126	7	12	9	9
360	124	8	12	9	11
1440	116	8	11	11	12
1800	114	8	11	12	13
2880	114	8	12	13	16
4320	116	9	15	16	18

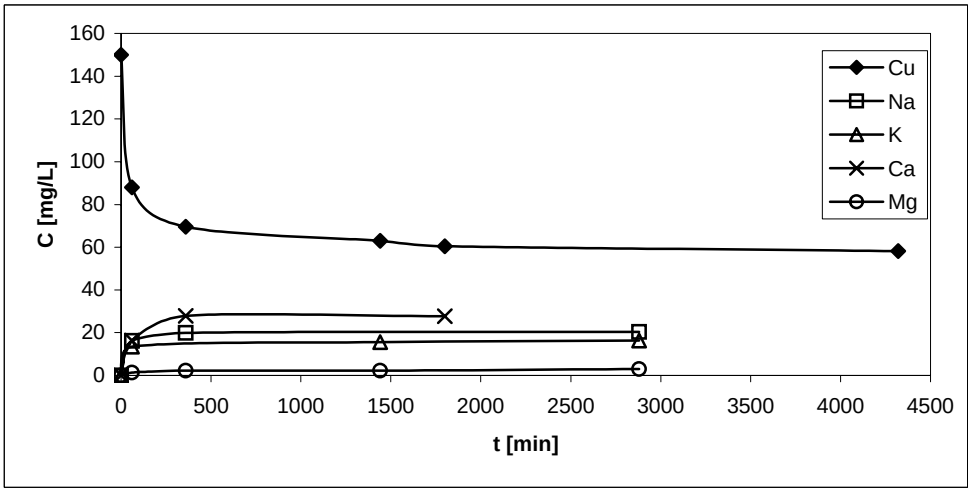

Figure 7.3. The Kinetic Curves for Ion Exchange Between Cu^{2+} and Na^{+}, K^{+}, Ca^{2+}, Mg^{2+} ions with 1 g of CP1 in 100 ml, 150 mg/L Copper Nitrate Solution at 130 rpm.

Table 7.3. Variation of the Ion Concentrations with Respect to Time at 29°C, 130 rpm, 1 g of CP1 in 100 ml of 150 mg/L Copper Nitrate Solution.

t [min]	Cu^{2+} [mg/L]	Na^{+} [mg/L]	K^{+} [mg/L]	Ca^{2+} [mg/L]	Mg^{2+} [mg/L]
0	150	0	0	0	0
60	87.95	16.13	13.44	16.33	1.42
360	69.64	19.95	17.39	27.89	2.18
1440	63.01	19.55	15.49	17.79	2.28
1800	60.43	19.12	12.88	27.64	2.12
2880	61.39	20.32	16.31	26.79	2.98

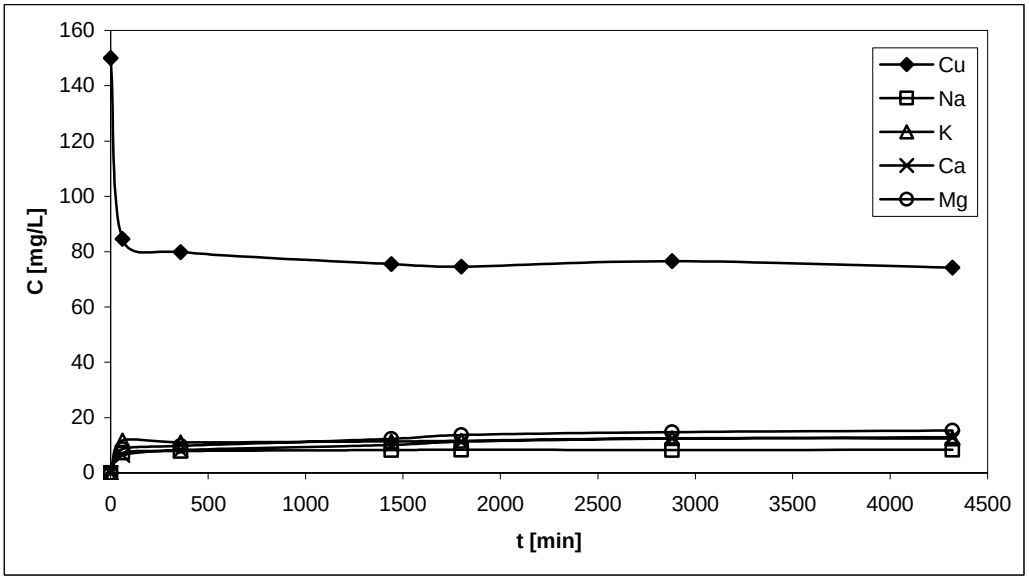

Figure 7.4. The Kinetic Curves for Ion Exchange Between Cu^{2+} and Na^{+}, K^{+}, Ca^{2+}, Mg^{2+} ions with 1 g of CP2 in 100 ml, 150 mg/L Copper Nitrate Solution at 130 rpm.

Table 7.4. Variation of the Ion Concentrations with Respect to Time at 29°C, 130 rpm, 1 g of CP2 in 100 ml of 150 mg/L Copper Nitrate Solution.

t [min]	Cu^{2+} [mg/L]	Na^{+} [mg/L]	K^{+} [mg/L]	Ca^{2+} [mg/L]	Mg^{2+} [mg/L]
0	150	0	0	0	0
60	84.61	7.34	11.72	6.45	8.59
360	79.87	7.85	11.05	8.23	9.71
1440	75.49	8.26	11.33	10.14	12.31
1800	74.59	8.36	11.59	11.29	13.69
2880	76.57	8.25	12.55	12.36	14.74
4320	74.30	8.37	12.44	12.85	15.36

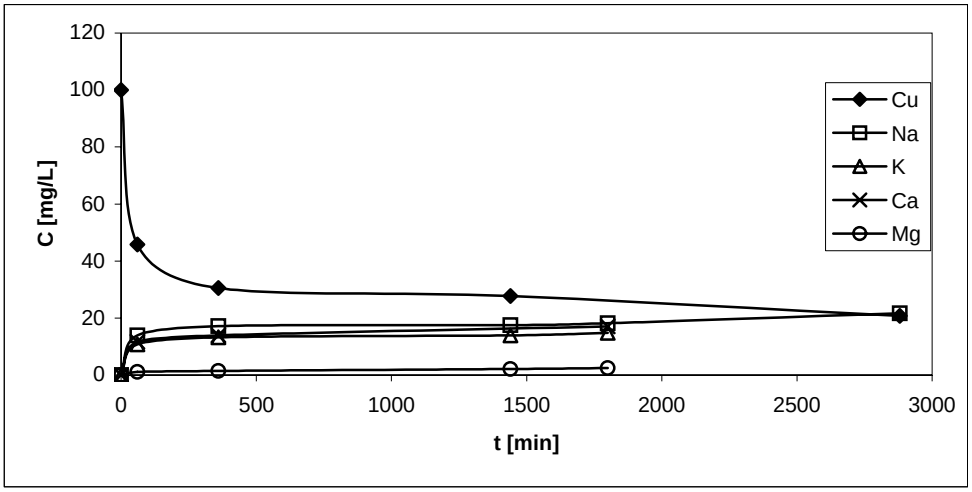

Figure 7.5. The Kinetic Curves for Ion Exchange Between Cu^{2+} and Na^{+}, K^{+}, Ca^{2+}, Mg^{2+} ions with 1 g of CP1 in 100 ml, 100 mg/L Copper Nitrate Solution at 130 rpm.

Table 7.5. Variation of the Ion Concentrations with Respect to Time at 29°C, 130 rpm, 1 g of CP1 in 100 ml of 100 mg/L Copper Nitrate Solution.

t [min]	Cu^{2+} [mg/L]	Na^{+} [mg/L]	K^{+} [mg/L]	Ca^{2+} [mg/L]	Mg^{2+} [mg/L]
0	100	0	0	0	0
60	45.77	13.93	10.81	11.65	1.11
360	30.58	17.22	13.23	13.92	1.48
1440	27.74	17.55	13.87	20.22	2.16
1800	28.68	18.24	14.84	17.09	2.45
2880	20.73	21.62	11.22	12.17	1.53

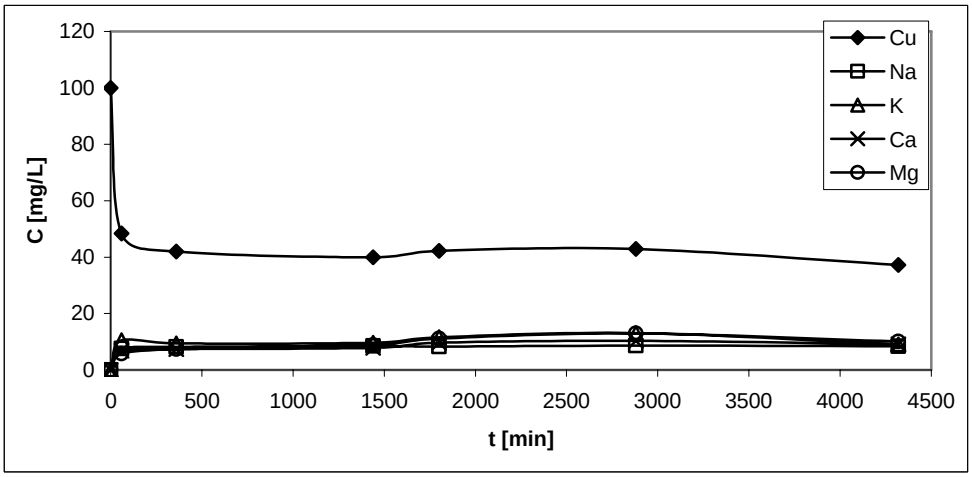

Figure 7.6. The Kinetic Curves for Ion Exchange Between Cu^{2+} and Na^{+}, K^{+}, Ca^{2+}, Mg^{2+} ions with 1 g of CP2 in 100 ml, 100 mg/L Copper Nitrate Solution at 130 rpm.

Table 7.6. Variation of the Ion Concentrations with Respect to Time at 29°C, 130 rpm, 1 g of CP2 in 100 ml of 100 mg/L Copper Nitrate Solution.

t [min]	Cu^{2+} [mg/L]	Na^{+} [mg/L]	K^{+} [mg/L]	Ca^{2+} [mg/L]	Mg^{2+} [mg/L]
0	100	0	0	0	0
60	48.39	7.66	10.58	6.79	5.85
360	42.03	8.19	9.49	7.35	7.39
1440	40.01	8.50	9.73	7.83	8.85
1800	42.29	8.30	11.57	9.65	11.21
2880	42.94	8.70	13.05	10.38	12.99
4320	37.24	8.38	9.16	9.06	10.08
7200	38.26	8.16	10.35	9.10	11.25

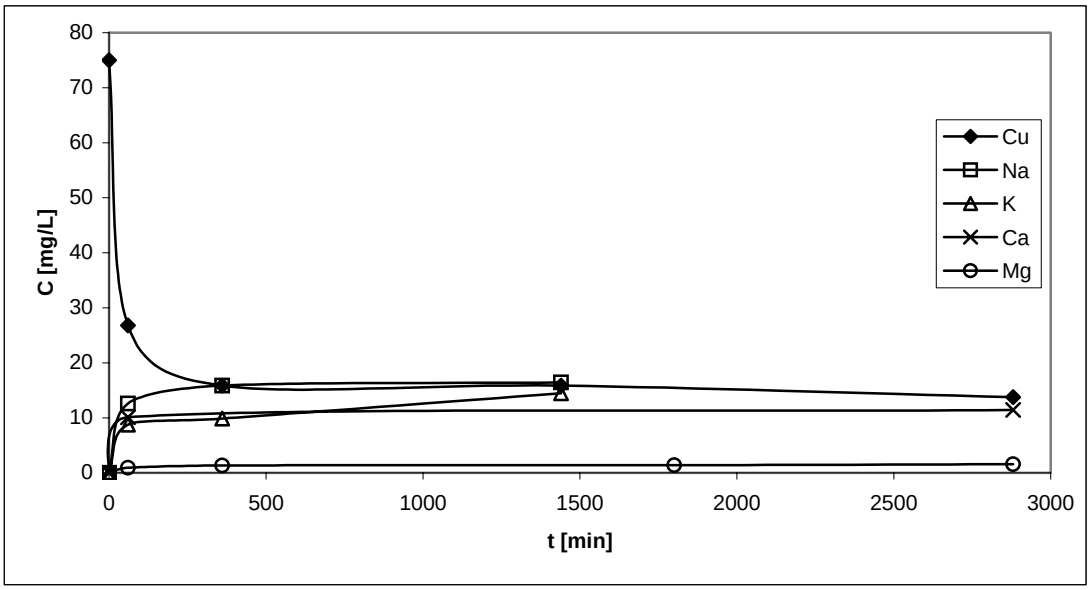

Figure 7.7. The Kinetic Curves for Ion Exchange Between Cu^{2+} and Na^{+}, K^{+}, Ca^{2+}, Mg^{2+} ions with 1 g of CP1 in 100 ml, 75 mg/L Copper Nitrate Solution at 130 rpm.

Table 7.7. Variation of the Ion Concentrations with Respect to Time at 29°C, 130 rpm, 1 g of CP1 in 100 ml of 75 mg/L Copper Nitrate Solution.

t [min]	Cu^{2+} [mg/L]	Na^{+} [mg/L]	K^{+} [mg/L]	Ca^{2+} [mg/L]	Mg^{2+} [mg/L]
0	75	0	0	0	0
60	26.80	12.59	8.79	10.12	0.94
360	15.88	15.86	9.86	26.85	1.33
1440	15.86	16.43	14.49	13.72	2.49
1800	13.18	15.24	9.00	9.25	1.40
2880	13.78	15.27	10.92	11.44	1.58

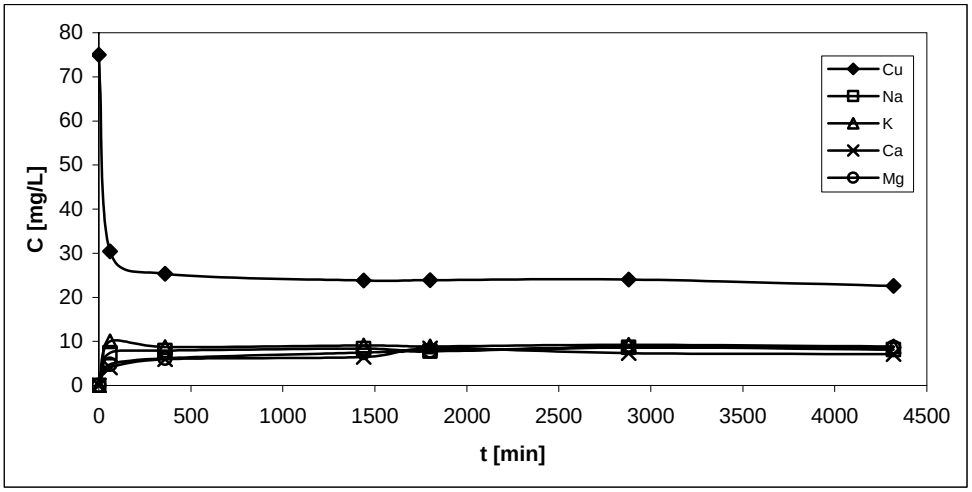

Figure 7.8. The Kinetic Curves for Ion Exchange Between Cu^{2+} and Na^{+}, K^{+}, Ca^{2+}, Mg^{2+} ions with 1 g of CP2 in 100 ml, 75 mg/L Copper Nitrate Solution at 130 rpm.

Table 7.8. Variation of the Ion Concentrations with Respect to Time at 29°C, 130 rpm, 1 g of CP2 in 100 ml of 75 mg/L Copper Nitrate Solution.

t [min]	Cu^{2+} [mg/L]	Na^{+} [mg/L]	K^{+} [mg/L]	Ca^{2+} [mg/L]	Mg^{2+} [mg/L]
0	75	0	0	0	0
60	30.44	7.43	10.03	4.09	4.76
360	25.37	7.89	8.73	5.93	6.14
1440	23.80	8.34	9.05	6.49	7.51
1800	23.89	7.79	8.83	8.45	7.84
2880	24.05	8.62	9.24	7.35	8.62
4320	22.57	8.10	8.88	7.12	8.63
7200	25.79	8.38	13.19	9.56	12.78

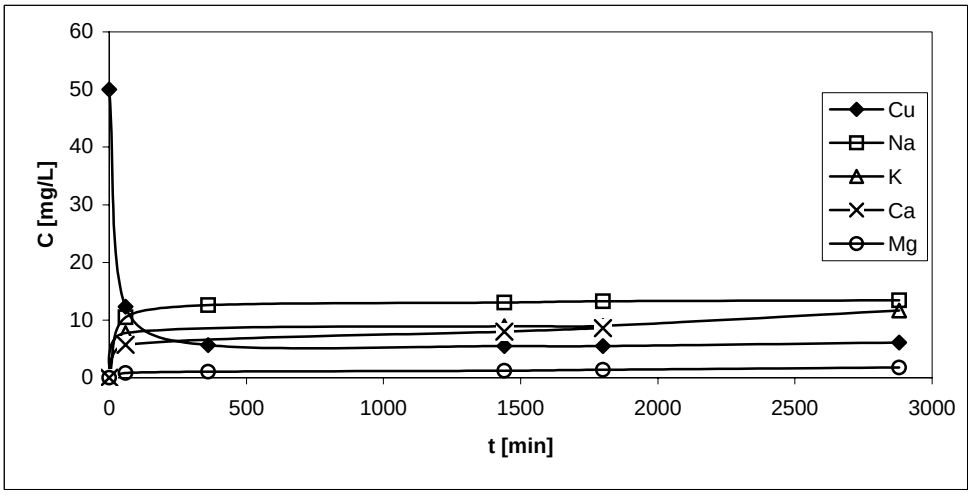

Figure 7.9. The Kinetic Curves for Ion Exchange Between Cu^{2+} and Na^{+}, K^{+}, Ca^{2+}, Mg^{2+} ions with 1 g of CP1 in 100 ml, 50 mg/L Copper Nitrate Solution at 130 rpm.

Table 7.9. Variation of the Ion Concentrations with Respect to Time at 29°C, 130 rpm, 1 g of CP1 in 100 ml of 50 mg/L Copper Nitrate Solution.

t [min]	Cu^{2+} [mg/L]	Na^{+} [mg/L]	K^{+} [mg/L]	Ca^{2+} [mg/L]	Mg^{2+} [mg/L]
0	50	0	0	0	0
60	12.33	10.49	7.78	5.72	0.82
360	5.68	12.59	7.66	12.92	1.08
1440	5.48	13.05	8.93	8.01	1.24
1800	5.48	13.25	9.01	8.61	1.36
2880	6.10	13.42	11.65	7.82	1.76

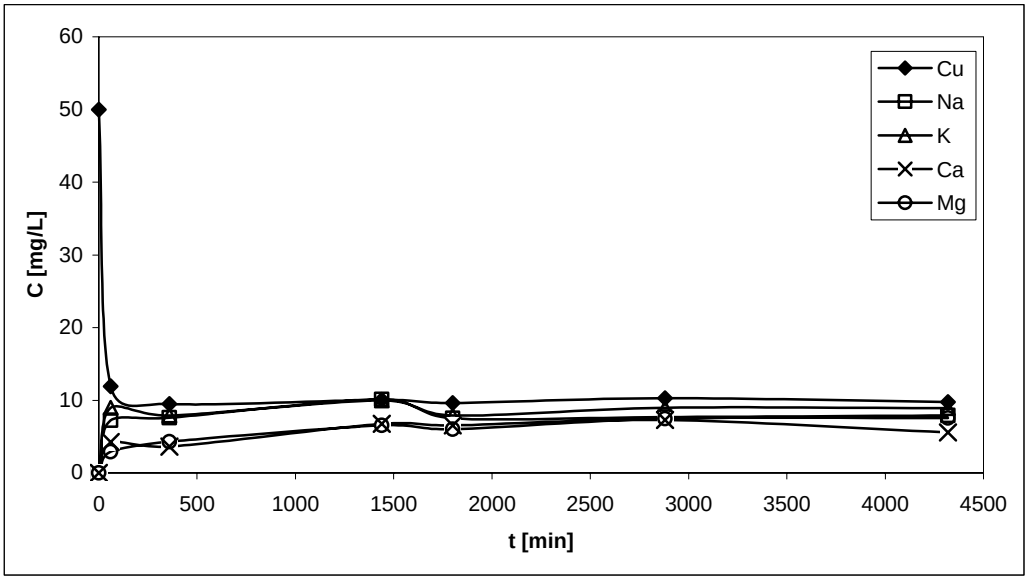

Figure 7.10. The Kinetic Curves for Ion Exchange Between Cu^{2+} and Na^{+}, K^{+}, Ca^{2+}, Mg^{2+} ions with 1 g of CP2 in 100 ml, 50 mg/L Copper Nitrate Solution at 130 rpm.

Table 7.10. Variation of the Ion Concentrations with Respect to Time at 29°C, 130 rpm, 1 g of CP2 in 100 ml of 50 mg/L Copper Nitrate Solution.

t [min]	Cu^{2+} [mg/L]	Na^{+} [mg/L]	K^{+} [mg/L]	Ca^{2+} [mg/L]	Mg^{2+} [mg/L]
0	50	0	0	0	0
60	11.90	7.26	8.96	4.25	2.89
360	9.50	7.59	7.91	3.61	4.29
1440	10.05	10.09	9.99	6.77	6.52
1800	9.63	7.52	7.89	6.55	6.03
2880	10.29	7.69	8.97	7.29	7.46
4320	9.75	7.89	8.91	5.54	7.55

In Figure 7.1, copper concentration decreased from 200 mg/L to about 100 mg/L while the major exchangeable cations in CP1 zeolite such as sodium, potassium and calcium concentrations increased to 29, 22 and 23 mg/L, respectively. Of all the ions, the maximum exchange was observed between Cu^{2+} and Na^{+} ions. Figure 7.1 clearly indicates that an ion exchange mechanism exists between the copper ions and the exchangeable cations of the CP1 zeolite. Furthermore, for CP1 zeolite, it seems that the amount of Mg^{2+} ions passed through the solution were determined to be lower than the others. Besides, cations interact with water molecules to form clusters and the characteristics of these clusters depend on the size and charge of the cation. In general, hydrated radius is inversely proportional to cation radius, and divalent cations usually have a higher hydrated radius than monovalent cations. Thus, small alkaline earth cations such as Mg^{2+}, cannot move easily out of the channels due to their considerably higher hydrated radii. This fact explains why it is more difficult to remove the smaller Mg^{2+} ions.

According to Figure 7.2, copper concentration decreased from 200 mg/L to about 116 mg/L while the major exchangeable cations in CP2 zeolite such as sodium, potassium, calcium and magnesium concentrations increased to 9, 15, 16 and 18 mg/L, respectively. In CP2 zeolite, the maximum exchange was observed between Cu^{2+} and Mg^{2+} ions. Therefore, Figure 7.2 similarly indicates that an ion exchange mechanism exists between the copper ions and the exchangeable cations of the zeolite. In CP2 zeolite, the amount of Mg^{2+} ions present in the zeolite structure were not as low as in CP1 zeolite.

When the initial copper concentration is 150 mg/L for CP1 zeolite, Ca^{2+}, Na^{+}, K^{+} and Mg^{2+} ion concentrations have increased to 46, 20, 16 and 3 mg/L, respectively (Table 7.3). Besides, the copper concentration has decreased to 61 mg/L while for CP2 zeolite it has decreased to 74 mg/L after six hours, which was the time required to reach equilibrium. The maximum ion exchange has occurred between Ca^{2+} and Cu^{2+} ions for CP1 zeolite while it's between Mg^{2+} and Cu^{2+} for CP2 zeolite (Figures 7.3-7.4).

In Figure 7.5, the initial copper concentration of 100 mg/L has decreased to 20.73 while Ca^{2+}, Na^{+}, K^{+} and Mg^{2+} ion concentrations have increased to 12, 21, 11 and 2 mg/L, respectively for CP1 zeolite (Table 7.5). Consequently, the highest ion exchange was determined to be between Na^{+} and Cu^{2+} ions. As in general the lowest increase was observed for Mg^{2+} ions for CP1 zeolite. In contrast to this, the highest increase belongs to Mg^{2+} ions for CP2 zeolite (Figure 7.6). Besides, Ca^{2+}, Na^{+}, K^{+} and

Mg^{2+} ion concentrations have increased to 9, 8, 10 and 11 mg/L, respectively for CP2 zeolite (Table 7.6). Similarly, the amount of Cu^{2+} removed from the solution is greater in CP1 than in CP2 zeolite.

When the initial copper concentration is 75 mg/L, a similar observation was obtained such that the amount of Cu^{2+} removal for CP1 zeolite is greater than that of CP2 zeolite. Furthermore, Ca^{2+}, Na^{+}, K^{+} and Mg^{2+} ion concentrations have increased to 11, 15, 10 and 1 mg/L for CP1 zeolite (Table 7.7) while for CP2 zeolite they are 9, 8, 13 and 12, respectively (Table 7.8).

Finally, when the initial copper is 50 mg/L, similarly, the performance of CP1 zeolite was better for removing Cu^{2+} ions from the solution than CP2 zeolite because the initial Cu^{2+} concentration has decreased to 6.10 for CP1 while to 10.29 mg/L for CP2 zeolite (Figures 7.9-7.10). The maximum ion exchange occurred between Cu^{2+} and Na^{+} ions for CP1 while it was occurred between Cu^{2+} and K^{+} ions for CP2 zeolite. The lowest ion exchange was observed between Cu^{2+} and Mg^{2+} ions for CP1 zeolite (Table 7.9) and it was between Cu^{2+} and Ca^{2+} ions for CP2 zeolite (Table 7.10).

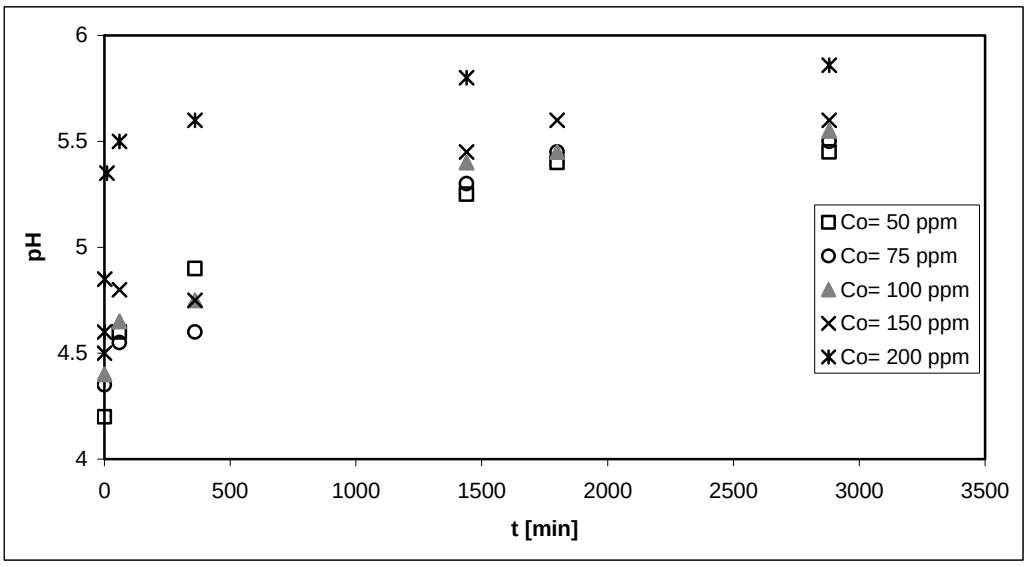

Figure 7.11. Investigation of pH of the Solutions at Varying Initial Metal Concentrations for CP1 Zeolite.

The pH profiles of CP1 zeolite in varying concentrations of copper nitrate solutions, 50 to 200 mg/L, as a function of time are presented in Figure 7.11. The initial pH of all solutions were about 4.2-4.6. After CP1 zeolite addition, the solution pH rised to 4.60, 4.55, 4.65, 4.80 and 4.85 in 1 hour and then increased until they reached equilibrium around 5.45, 5.50, 5.55, 5.60 and 5.86 after 30 hours, for initial Cu^{2+} concentrations of 50, 75, 100, 150 and 200 mg/L, respectively. The reason for the rise in

the solutions pH was due to the exchange of H^+ ions from water onto the negatively charged clinoptilolite surface and as a potential determining ion (pdi), ions that establish or change the surface charge of a solid since they control the surface reactions, in the electrical double layer (EDL) in order to provide electroneutrality (Ersoy et al., 2002). In a study performed by Rivera et al., 2000, pH experiments were carried out for purified natural clinoptilolite in aqueous medium and they collected a lot of data up to 1500 minutes. According to their results, pH of the solution was increased quickly after zeolite was added. After that, a decrease of the pH values towards the neutral pH area was observed, followed by its stabilization at around 6000 min. These results clearly indicate that clinoptilolite tends to neutralize the aqueous medium acting either as proton acceptor or as a proton donor, which makes evident its amphoteric character. This phenomena has been reported by other authors for the case of zeolites with lower Si/Al ratio (Filippidis et al., 1996). In addition, the H^+ ions in solution undergo exchange with some of the cations of clinoptilolite lattice leading to the consumption of H^+ ions in solution. It has been reported that natural clinoptilolite exhibits pH values in the range of pH 7-9 (Breck, 1974).

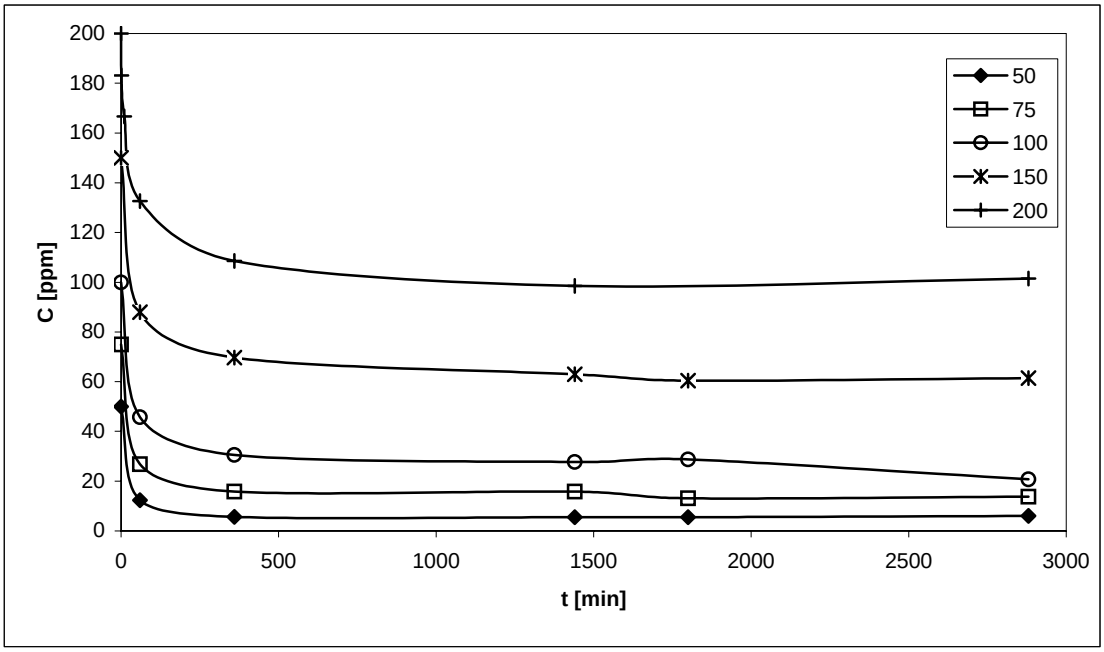

Figure 7.12. The Kinetic Curve for Ion Exchange Between Cu^{2+} ions with 1 g of CP1 in 100 ml at Varying Initial Concentrations of Copper Nitrate Solution at 130 rpm.

When Figures 7.12 and 7.13 are investigated, for the same initial zeolite amounts, as the initial copper ion concentration was increased the amount of copper removed from the solution increased, which were determined as 4.4, 6.2, 8.0, 9.0 and

10.0 mg for CP1 zeolite and 4.03, 5.24, 6.28, 7.57 and 8.33 mg for CP2 zeolite at initial concentrations of 50, 75, 100, 150 and 200 mg/L, respectively. For both zeolites, the time required to reach equilibrium was determined as approximately six hours for all initial copper concentrations. After 30 hours no further exchange was observed, which indicated that the system has reached equilibrium.

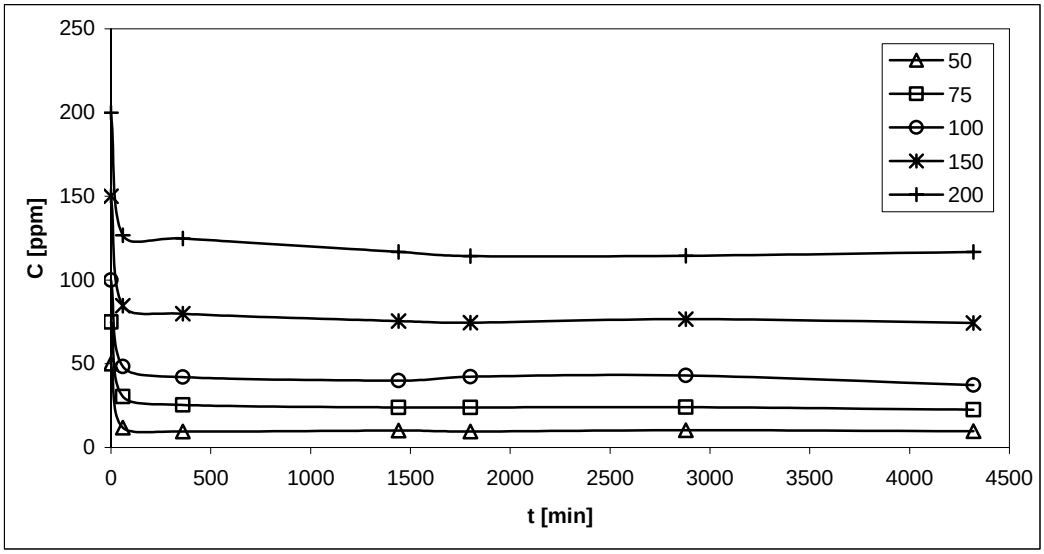

Figure 7.13. The Kinetic Curve for Ion Exchange Between Cu^{2+} ions with 1 g of CP2 in 100 ml at Varying Concentrations of Copper Nitrate Solution at 130 rpm.

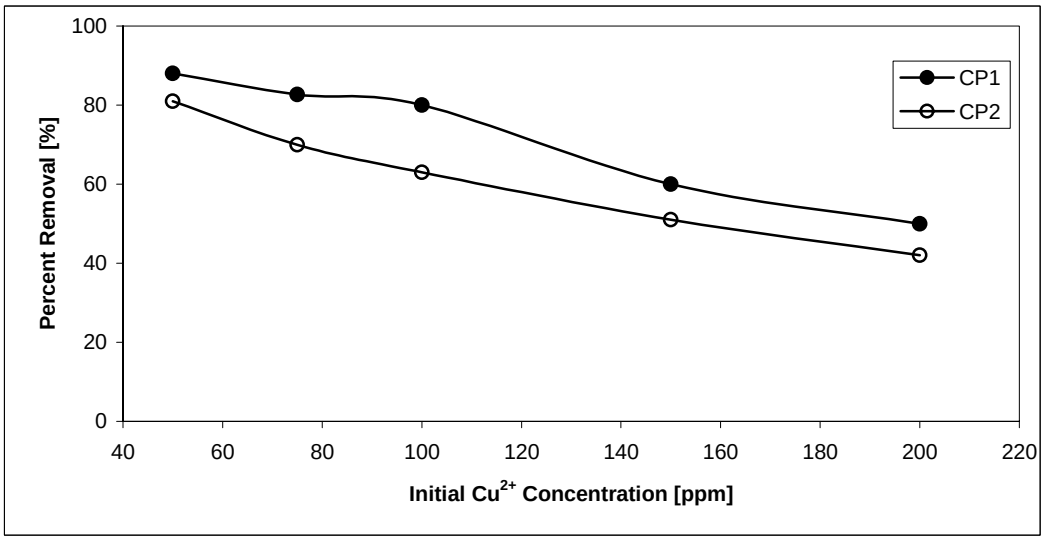

Figure 7.14. Percent Removal with Respect to Initial Cu^{2+} Concentration at 130 rpm, 29°C Using 1 g of Each Zeolite Sample.

Although the amount of copper removed from the solution increased with increasing initial copper ion concentration, the percent removal of the copper ions decreased with increasing initial copper ion concentration as can be seen from Figure

7.14, for both zeolites. It's clearly seen in Figure 7.14 that, the percent removal of Cu^{2+} ions from the solution was greater for CP1 zeolite for all initial ion concentrations. At copper concentration of 50 mg/L, removal efficiencies of CP1 and CP2 zeolites were achieved as 88, 81 %, respectively. At higher copper concentrations, the removal efficiency decreased to a value of 50, 42 % for CP1 and CP2 zeolites, respectively, at 200 mg/L of Cu^{2+}. Same observations were found in literature, ammonia treatment of Porsuk River was studied by using Balıkesir natural zeolite and almost 91% of ammonia was removed from the river (Kaban et al., 1980). Also, in a study performed by Ülkü, S. in 1984, ammonia removal from waste water of the Nitrogen Fertilizer plant by using Bigadiç-Balıkesir natural zeolite has been investigated and it was found that ammonia removal efficiency has been reached to a value around 98%.

Table 7.11. Equilibrium Uptake Data for Copper Exchange of the Clinoptilolite Samples at 29°C

	CP1			**CP2**		
C_o (Cu^{2+}) [mg/L]	**q_{eq}^{a} [meq/g]**	**q_{eq}^{b} [meq/g]**	**% difference**	**q_{eq}^{a} [meq/g]**	**q_{eq}^{b} [meq/g]**	**% difference**
50	0.140	0.146	4.07	0.127	0.147	-15.75
75	0.193	0.179	7.21	0.165	0.166	-0.61
100	0.249	0.238	4.73	0.197	0.189	4.06
150	0.289	0.293	1.42	0.238	0.261	-9.66
200	0.319	0.303	5.26	0.262	0.312	-19.08

a= from Cu^{2+} measurements directly
b= from K^{+}+Na^{+}+Ca^{2+}+Mg^{2+} measurements

Since ion exchange is a stoichiometric reaction, total equivalents of exchanging cations between the solution and the ion exchanger should be equal to each other. Therefore, a mole balance was constructed between the major exchangeable cations initially present in the zeolite structure and the copper ions in the solution. In Table 7.11, amount of Cu^{2+} ion sorbed by the solid phase was determined by the difference in the concentration of Cu^{2+} ion in equivalents and also it was calculated by summing up the concentrations of Na^{+}, K^{+}, Mg^{2+} and Ca^{2+} ions similarly, in equivalents. The percent differences of the Cu^{2+} ion sorbed by the solid phase between both methods were generally within tolerable limits for both zeolites.

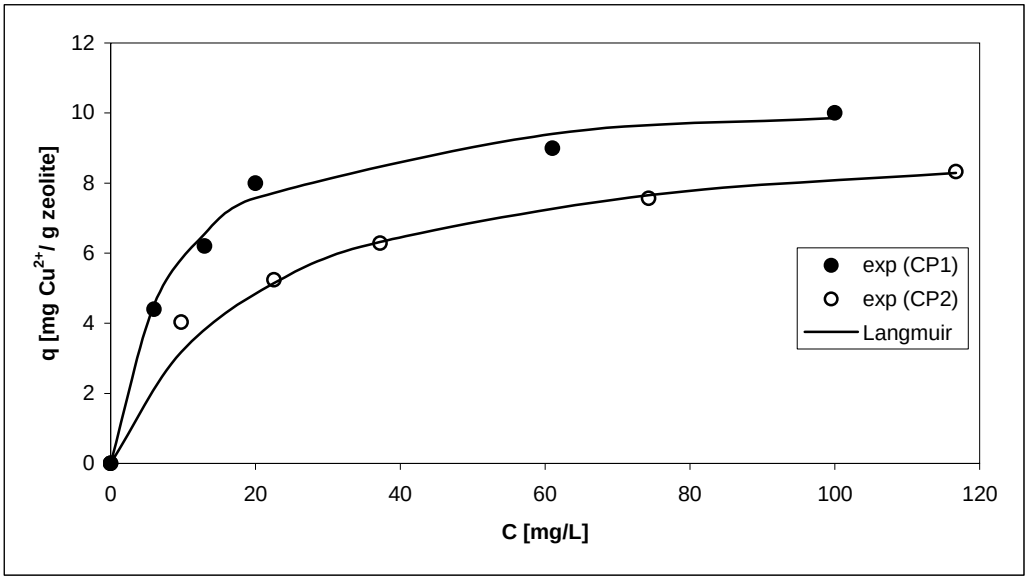

Figure 7.15. Equilibrium Uptake Isotherms of Copper with Clinoptilolite Samples and Langmuir Model at 29°C.

Ion exchange isotherms of copper were constructed on the same graph for CP1 and CP2 zeolites with corresponding Langmuir Model in terms of species concentration in the solid phase as a function of its value in solution (Figure 7.15). Langmuir model described the equilibrium behavior of both systems quite well. It can be seen from Figure 7.15 that natural zeolite containing 80% clinoptilolite, CP1, gave rise to better ion exchange capacity for copper than CP2 zeolite containing 64% clinoptilolite. Ion exchange capacities were determined as 10 mg (0.32 meq) Cu^{2+} / g CP1 zeolite and 8.33 mg (0.26 meq) Cu^{2+} / g CP2 zeolite. These values determined from the zeolites in this work can be compared in Table 3.1 for Cu^{2+} ion investigated with the corresponding values reported in the literature for other natural clinoptilolite based ion exchangers. The ion exchange capacities for Cu^{2+} determined in this work fall within the corresponding range reported in the literature, e.g. Mondela et al., 1995. On the contrary, in the studies performed by Cincotti et al., 2001 and Türkmen, 2001 the ion exchange capacities determined by using natural clinoptilolite were much lower than the values indicated in this study. On the other hand, in the studies performed by Nikashina at al., 1984, Guangsheng et al., 1988, Langella et al., 2000, ion exchange capacities determined by using sodium form of clinoptilolite were higher. The reason for obtaining such results are due to the usage of different forms of natural material (Table 3.1).

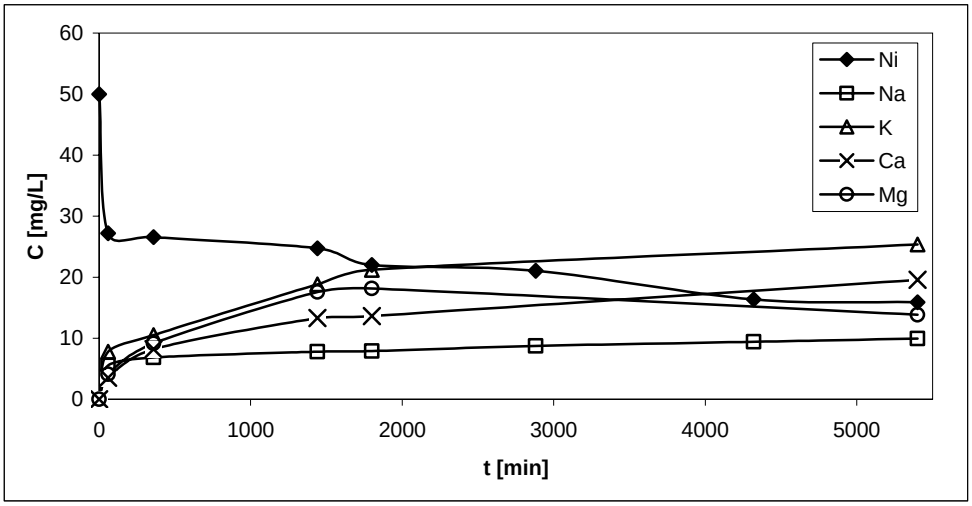

Figure 7.16. The Kinetic Curves for Ion Exchange Between Ni^{2+} and Na^{+}, K^{+}, Ca^{2+}, Mg^{2+} ions with 1 g of CP2 in 100 ml, 50 mg/L Nickel Nitrate Solution at 130 rpm.

Table 7.12. Variation of the Ion Concentrations with Respect to Time at 29°C, 130 rpm, 1 g of CP2 in 100 ml of 50 mg/L Nickel Nitrate Solution.

t [min]	Ni^{2+} [mg/L]	Na^{+} [mg/L]	K^{+} [mg/L]	Ca^{2+} [mg/L]	Mg^{2+} [mg/L]
0	50	0	0	0	0
60	27	5	8	3	4
360	26	6	10	8	9
1440	24	7	19	13	17
1800	22	8	21	13	18
2880	21	8	29	19	25
4320	16	9	35	22	28
5400	15	9	25	19	13

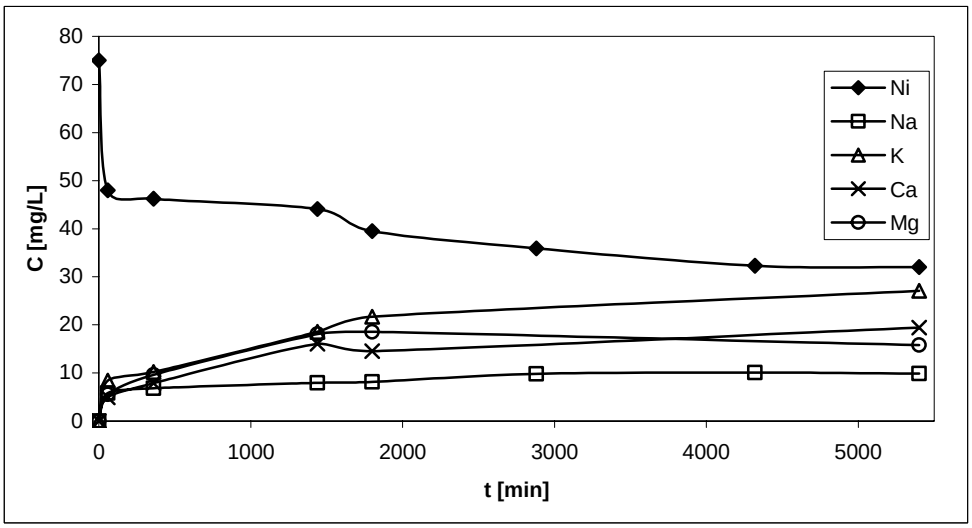

Figure 7.17. The Kinetic Curves for Ion Exchange Between Ni^{2+} and Na^{+}, K^{+}, Ca^{2+}, Mg^{2+} ions with 1 g of CP2 in 100 ml, 75 mg/L Nickel Nitrate Solution at 130 rpm.

Table 7.13. Variation of the Ion Concentrations with Respect to Time at 29°C, 130 rpm, 1 g of CP2 in 100 ml of 75 mg/L Nickel Nitrate Solution.

t [min]	Ni^{2+} [mg/L]	Na^{+} [mg/L]	K^{+} [mg/L]	Ca^{2+} [mg/L]	Mg^{2+} [mg/L]
0	75	0	0	0	0
60	47	5	8	5	5
360	46	6	10	8	9
1440	44	8	18	16	18
1800	39	8	21	14	18
2880	35	10	30	26	28
4320	32	10	40	25	31
5400	32	10	27	19	15

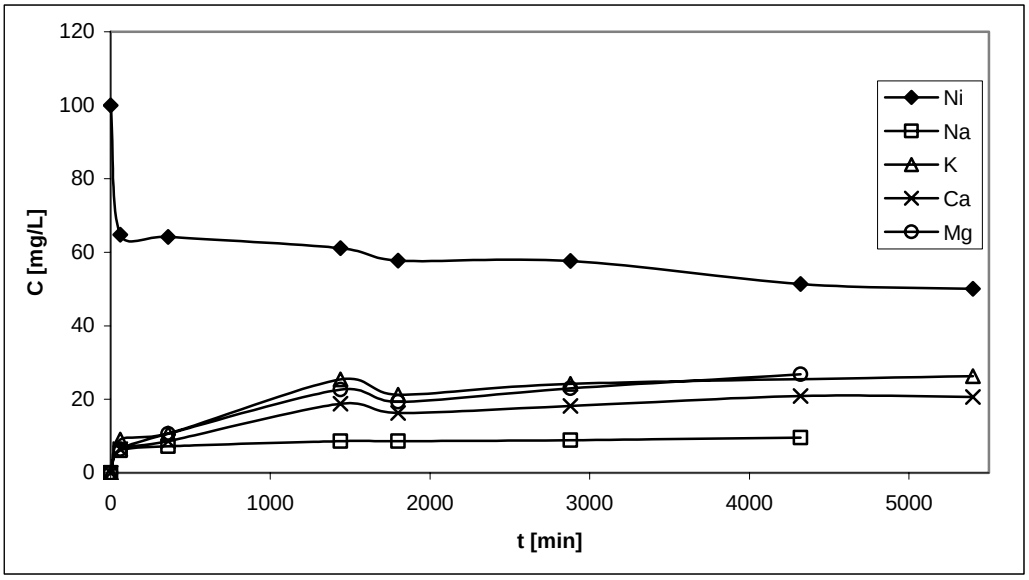

Figure 7.18. The Kinetic Curves for Ion Exchange Between Ni^{2+} and Na^{+}, K^{+}, Ca^{2+}, Mg^{2+} ions with 1 g of CP2 in 100 ml, 100 mg/L Nickel Nitrate Solution at 130 rpm.

Table 7.14. Variation of the Ion Concentrations with Respect to Time at 29°C, 130 rpm, 1 g of CP2 in 100 ml of 100 mg/L Nickel Nitrate Solution.

t [min]	Ni^{2+} [mg/L]	Na^{+} [mg/L]	K^{+} [mg/L]	Ca^{2+} [mg/L]	Mg^{2+} [mg/L]
0	100	0	0	0	0
60	64	6	9	6	6
360	64	7	10	8	10
1440	61	8	25	18	22
1800	57	8	21	16	19
2880	57	8	24	18	22

4320	51	9	33	20	26
5400	50	17	26	20	15

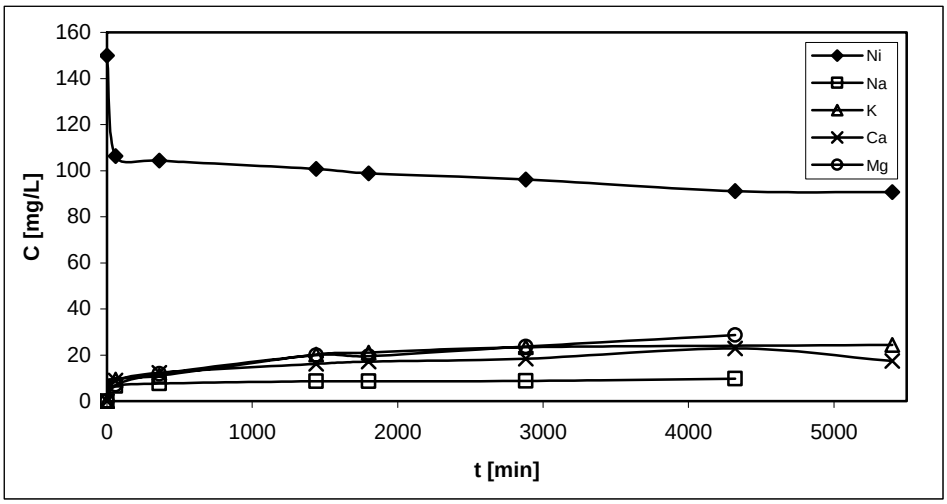

Figure 7.19. The Kinetic Curves for Ion Exchange Between Ni^{2+} and Na^{+}, K^{+}, Ca^{2+}, Mg^{2+} ions with 1 g of CP2 in 100 ml, 150 mg/L Nickel Nitrate Solution at 130 rpm.

Table 7.15. Variation of the Ion Concentrations with Respect to Time at 29°C, 130 rpm, 1 g of CP2 in 100 ml of 150 mg/L Nickel Nitrate Solution.

t [min]	Ni^{2+} [mg/L]	Na^{+} [mg/L]	K^{+} [mg/L]	Ca^{2+} [mg/L]	Mg^{2+} [mg/L]
0	150	0	0	0	0
60	106	6	9	9	7
360	104	7	10	12	11
1440	100	8	20	16	20
1800	98	8	20	17	19
2880	96	8	23	18	23
4320	91	9	35	23	28
5400	91	15	24	17	15

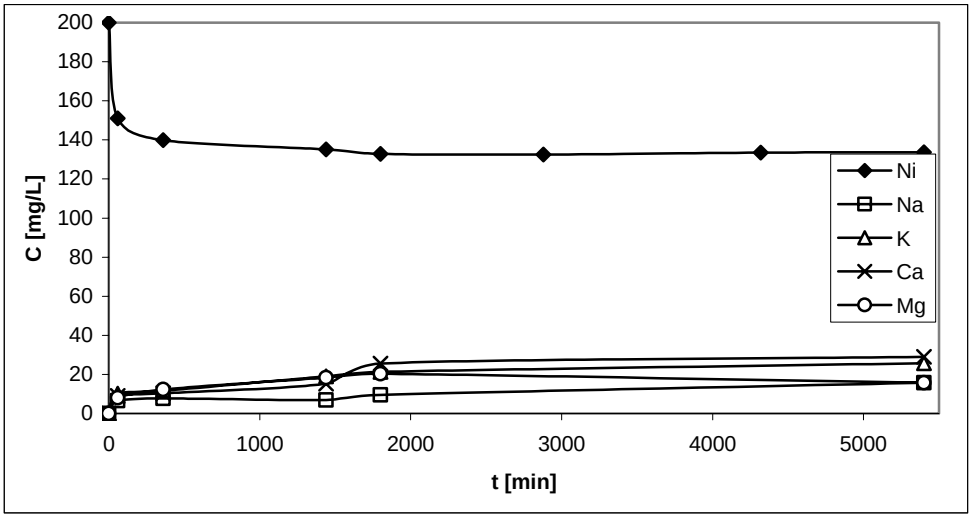

Figure 7.20. The Kinetic Curves for Ion Exchange Between Ni^{2+} and Na^{+}, K^{+}, Ca^{2+}, Mg^{2+} ions with 1 g of CP2 in 100 ml, 200 mg/L Nickel Nitrate Solution at 130 rpm.

Table 7.16. Variation of the Ion Concentrations with Respect to Time at 29°C, 130 rpm, 1 g of CP2 in 100 ml of 200 mg/L Nickel Nitrate Solution.

t [min]	Ni^{2+} [mg/L]	Na^{+} [mg/L]	K^{+} [mg/L]	Ca^{2+} [mg/L]	Mg^{2+} [mg/L]
0	200	0	0	0	0
60	151	6.5	10	9	8
360	140	7.7	11.6	10	12
1440	135	7	19	15	18
1800	132	9.5	21	25	20
2880	132	17.5	40	33	39
4320	133	21.6	79	49	57
5400	133	16	26	29	15

Besides Cu^{2+}, batch experiments were also performed for Ni^{2+} and Co^{2+} ions with CP2 zeolite. In experiments with Ni^{2+}, the maximum ion exchange generally took place with Ni^{2+} and K^{+} ions in which the K^{+} ion concentrations were 25, 27, 26, 24 and 26 mg/L for initial Ni^{2+} concentrations of 50, 75, 100, 150 and 200 mg/L, respectively. In general the lowest ion exchange has occured between Ni^{2+} and Na^{+} ions. In batch experiments with Cu^{2+} also the lowest ion exchange has taken place with Na^{+}. Unlike experiments with Cu^{2+}, the time required to reach near equilibrium was higher than the experiments performed with Ni^{2+} at different concentrations. With the experiments conducted with nickel, as concentration increased from 50 to 200 mg/L, the time to reach near equilibrium became lower which were 72 hours for 50 and 75 mg/L, 30 hours for 100 mg/L, 6 hours for 150 and 200 mg/L.

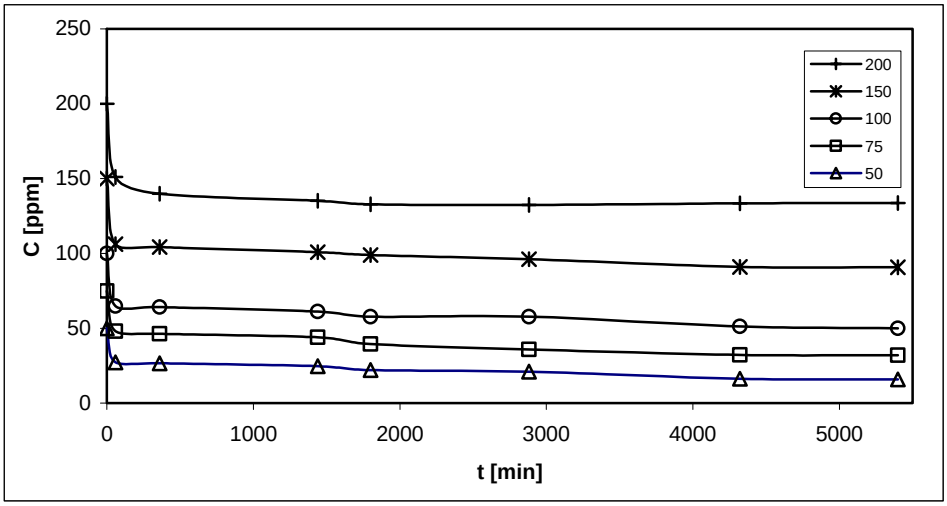

Figure 7.21. The Kinetic Curve for Ion Exchange Between Ni^{2+} ions with 1 g of CP2 in 100 ml at Varying Concentrations of Nickel Nitrate Solution at 130 rpm.

When Figure 7.21 is investigated, for the same initial zeolite amounts, as the initial nickel ion concentration was increased the amount of nickel removed from the solution increased, which were determined as 3.41, 4.30, 4.99, 5.93 and 6.64 mg for CP2 zeolite at initial concentrations of 50, 75, 100, 150 and 200 mg/L, respectively. These values were much lower than the values obtained from the batch studies performed with copper.

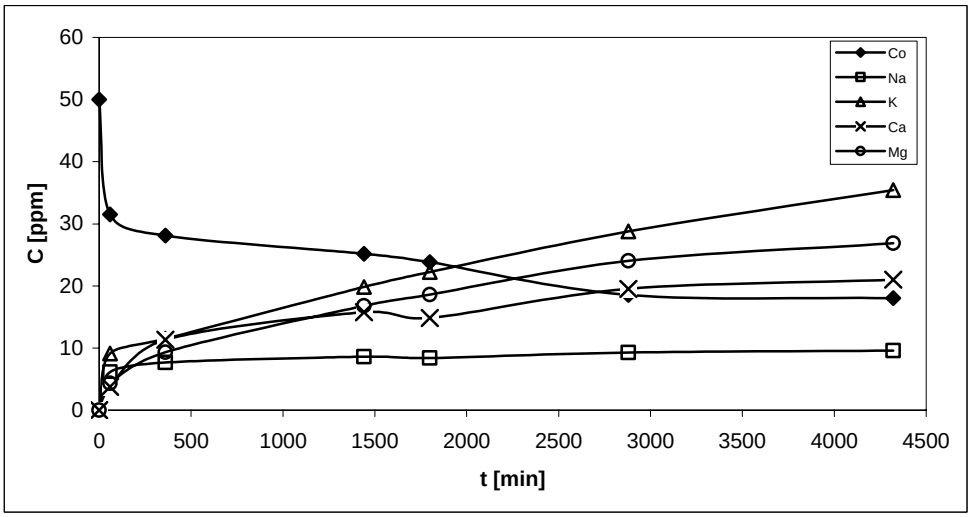

Figure 7.22. The Kinetic Curves for Ion Exchange Between Co^{2+} and Na^{+}, K^{+}, Ca^{2+}, Mg^{2+} ions with 1 g of CP2 in 100 ml, 50 mg/L Cobalt Nitrate Solution at 130 rpm.

Table 7.17. Variation of the Ion Concentrations with Respect to Time at 29°C, 130 rpm, 1 g of CP2 in 100 ml of 50 mg/L Cobalt Nitrate Solution.

t [min]	Co^{2+} [mg/L]	Na^{+} [mg/L]	K^{+} [mg/L]	Ca^{2+} [mg/L]	Mg^{2+} [mg/L]
0	50	0	0	0	0
60	31.5	6	9	4	4
360	28	7.6	11.5	11	9
1440	25	8.5	20	15	16
1800	24	8	22	15	18
2880	18	9	29	20	24
4320	18	9	35	21	26

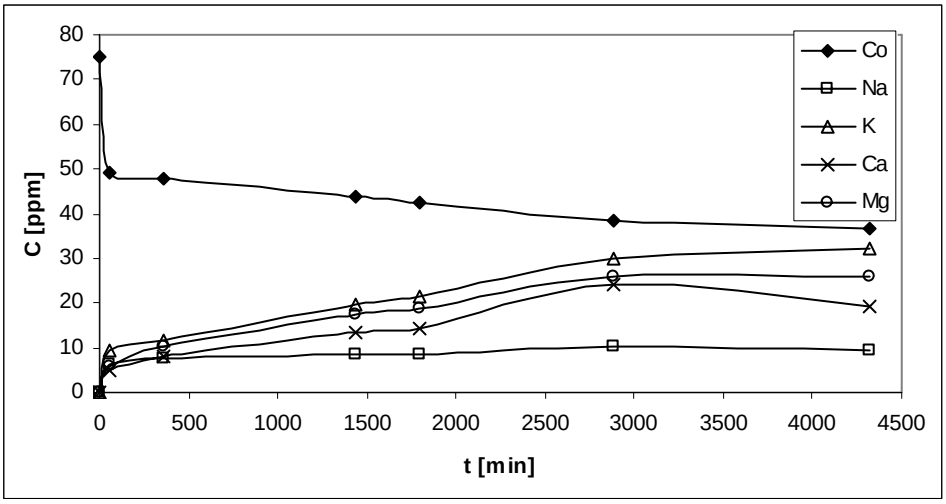

Figure 7.23. The Kinetic Curves for Ion Exchange Between Co^{2+} and Na^{+}, K^{+}, Ca^{2+}, Mg^{2+} ions with 1 g of CP2 in 100 ml, 75 mg/L Cobalt Nitrate Solution at 130 rpm.

Table 7.18. Variation of the Ion Concentrations with Respect to Time at 29°C, 130 rpm, 1 g of CP2 in 100 ml of 75 mg/L Cobalt Nitrate Solution.

t [min]	Co^{2+} [mg/L]	Na^{+} [mg/L]	K^{+} [mg/L]	Ca^{2+} [mg/L]	Mg^{2+} [mg/L]
0	75	0	0	0	0
60	49	6	9	5	6
360	47	7	12	8	10
1440	44	8.5	20	13	17
1800	42.5	8.5	21	14.5	19
2880	38	10	30	24	26
4320	37	10	32	19	26

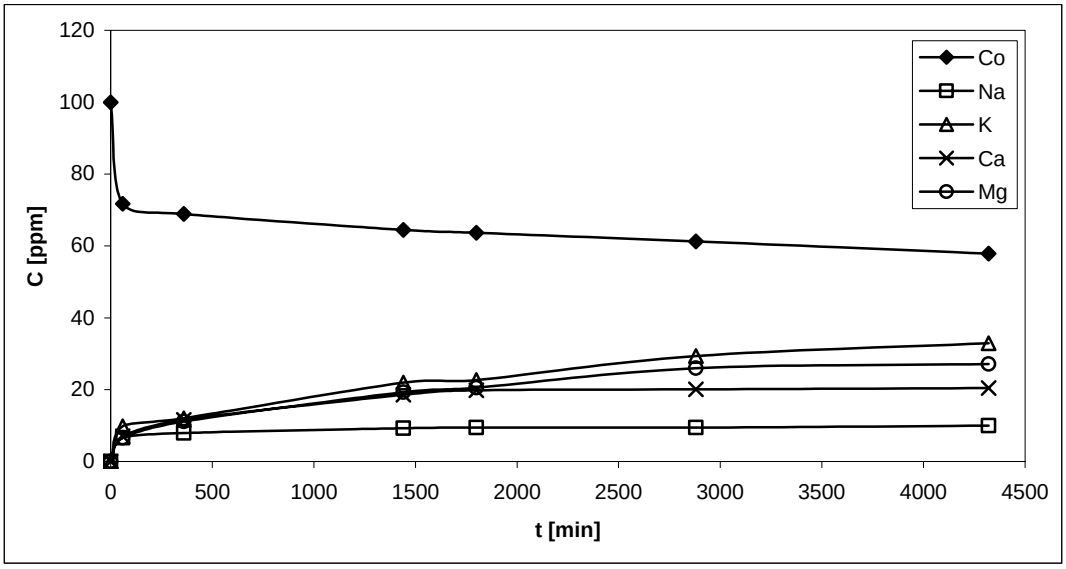

Figure 7.24. The Kinetic Curves for Ion Exchange Between Co^{2+} and Na^{+}, K^{+}, Ca^{2+}, Mg^{2+} ions with 1 g of CP2 in 100 ml, 100 mg/L Cobalt Nitrate Solution at 130 rpm.

Table 7.19. Variation of the Ion Concentrations with Respect to Time at 29°C, 130 rpm, 1 g of CP2 in 100 ml of 100 mg/L Cobalt Nitrate Solution.

t [min]	Co^{2+} [mg/L]	Na^{+} [mg/L]	K^{+} [mg/L]	Ca^{2+} [mg/L]	Mg^{2+} [mg/L]
0	100	0	0	0	0
60	72	7	10	7	6.5
360	69	8	12	11	11
1440	64	9	22	18	19
1800	63	9	23	20	21
2880	61	9	29	20	26
4320	58	10	33	20	27

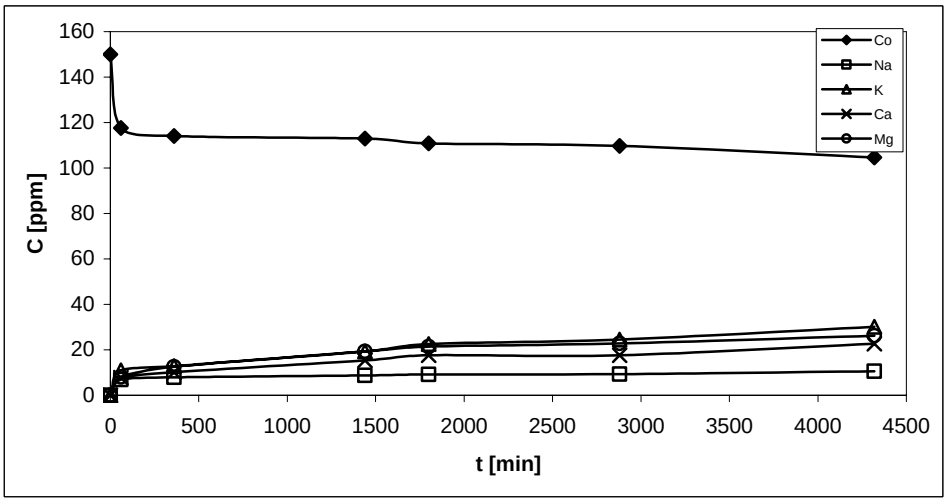

Figure 7.25. The Kinetic Curves for Ion Exchange Between Co^{2+} and Na^{+}, K^{+}, Ca^{2+}, Mg^{2+} ions with 1 g of CP2 in 100 ml, 150 mg/L Cobalt Nitrate Solution at 130 rpm.

Table 7.20. Variation of the Ion Concentrations with Respect to Time at 29°C, 130 rpm, 1 g of CP2 in 100 ml of 150 mg/L Cobalt Nitrate Solution.

t [min]	Co^{2+} [mg/L]	Na^{+} [mg/L]	K^{+} [mg/L]	Ca^{2+} [mg/L]	Mg^{2+} [mg/L]
0	150	0	0	0	0
60	117	7	11	8	8
360	114	8	13	10	12
1440	113	9	19	15	19
1800	111	9	22.5	17	21
2880	109	9	24.5	17	23
4320	104	10	30	22	26

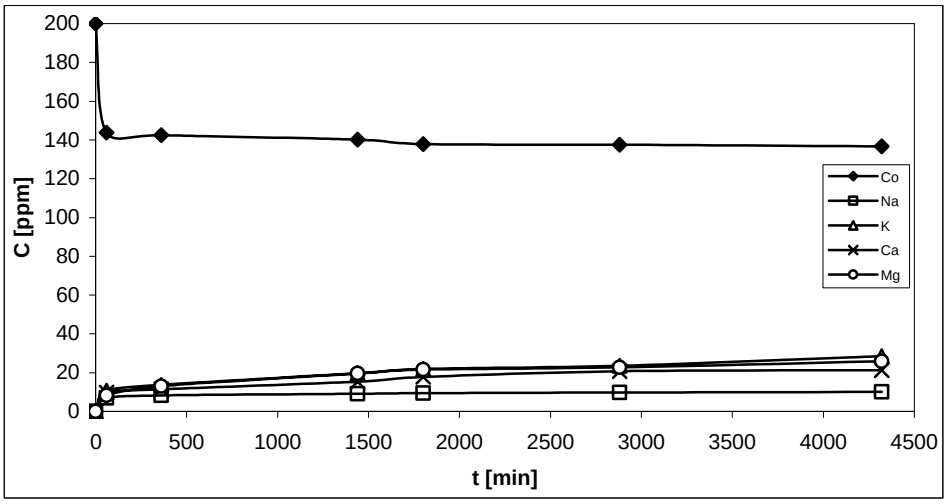

Figure 7.26. The Kinetic Curves for Ion Exchange Between Co^{2+} and Na^{+}, K^{+}, Ca^{2+}, Mg^{2+} ions with 1 g of CP2 in 100 ml, 200 mg/L Cobalt Nitrate Solution at 130 rpm.

Table 7.21. Variation of the Ion Concentrations with Respect to Time at 29°C, 130 rpm, 1 g of CP2 in 100 ml of 200 mg/L Cobalt Nitrate Solution.

t [min]	Co^{2+} [mg/L]	Na^{+} [mg/L]	K^{+} [mg/L]	Ca^{2+} [mg/L]	Mg^{2+} [mg/L]
0	200	0	0	0	0
60	143	7	11	10	8
360	142	8	13	11	13
1440	140	9	19	15	19
1800	138	9	22	17	21
2880	137	10	23	20	23
4320	136	10	28.5	21	26

In experiments with Co^{2+}, the maximum ion exchange took place with Co^{2+} and K^{+} ions in which the K^{+} ion concentrations were 35, 32, 33, 30 and 28.5 mg/L for initial Co^{2+} concentrations of 50, 75, 100, 150 and 200 mg/L, respectively. The lowest ion exchange has occured between Co^{2+} and Na^{+} ions, as well as batch experiments carried

out with copper and nickel. Unlike experiments with nickel, the highest exchange was observed with K^+ ions. In experiments with Co^{2+} and Ni^{2+}, the time required to reach equilibrium was higher than the experiments performed with Cu^{2+} at different concentrations. With the experiments conducted with cobalt, as concentration increased from 50 to 200 mg/L, the time to reach near equilibrium became lower which were 72 hours for 50 and 75 mg/L, 30 hours for 100 mg/L, 6 hours for 150 and 200 mg/L as in the case of experiments with Ni^{2+}.

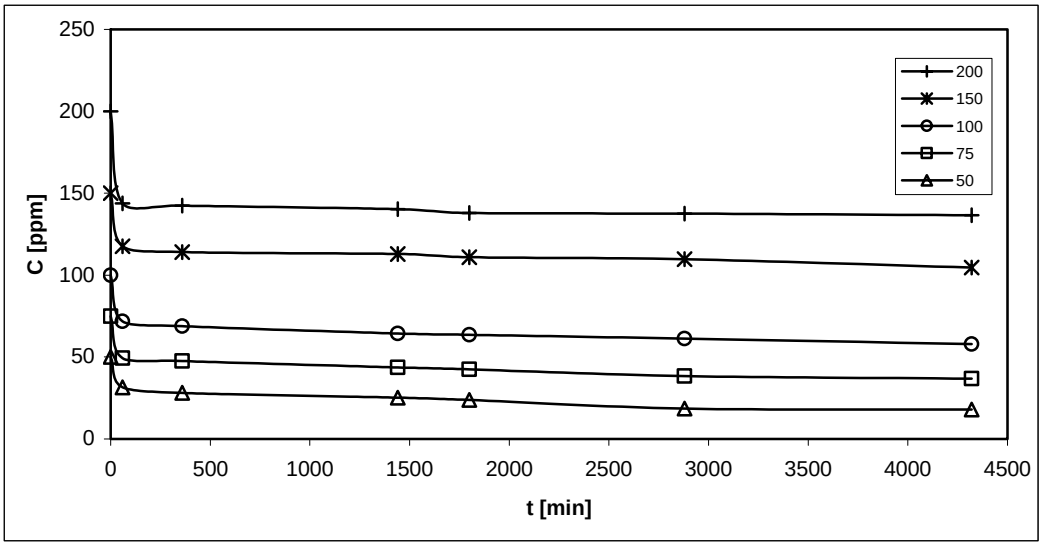

Figure 7.27. The Kinetic Curve for Ion Exchange Between Co^{2+} ions with 1 g of CP2 in 100 ml at Varying Concentrations of Cobalt Nitrate Solution at 130 rpm.

In Figure 7.27, as the initial cobalt concentration was increased the amount of cobalt removed from the solution increased, which were determined as 3.2, 3.82, 4.21, 4.54 and 6.34 mg for the same initial CP2 zeolite amount at initial concentrations of 50, 75, 100, 150 and 200 mg/L, respectively. These values were lower than the values obtained from the batch studies performed with copper and nickel.

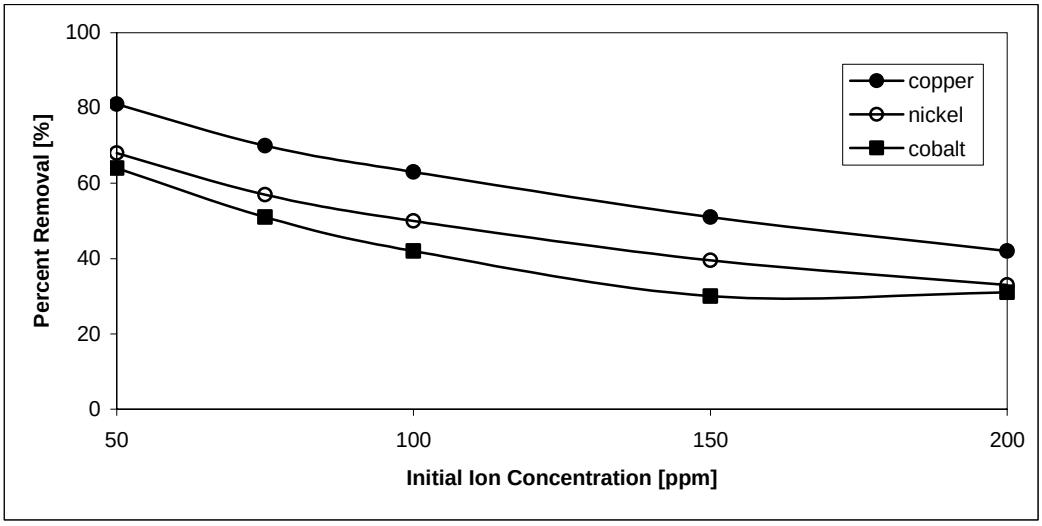

Figure 7.28. Percent Removal with Respect to Initial Ion Concentration at 130 rpm, 29°C Using 1 g of CP2 Zeolite.

Although the amount of cations removed from the solution increased with increasing initial cation concentration, the percent removal of the cations decreased with increasing initial cation concentration as can be seen from Figure 7.28, for both cations. For CP2 zeolite, it's clearly seen in Figure 7.28 that, the percent removal of the cations from the solution in decreasing order were; $Cu^{2+} > Ni^{2+} > Co^{2+}$ for all initial ion concentrations. At initial cation concentration of 50 mg/L, removal efficiencies of CP2 zeolites were achieved as 81, 68 and 64% for Cu^{2+}, Ni^{2+} and Co^{2+} ions respectively. In the study of Ajmal et al., 1995, Ni^{2+} removed from the solution, with the sawdust to solution ratio being 1:50 at 30 ^{o}C was reported as 50% for initial concentration of 14 mg/L. At higher ion concentrations, at 200 mg/L, the percent removal decreased to a value of 42, 33 and 31%, of Cu^{2+}, Ni^{2+} and Co^{2+}, respectively. Hence, CP2 zeolite has higher removal efficiency towards copper.

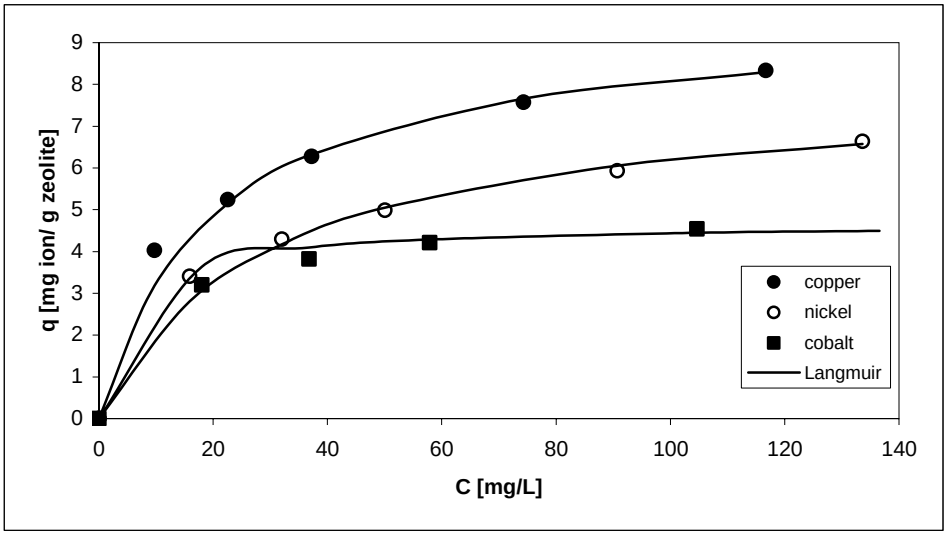

Figure 7.29. Equilibrium Uptake Isotherm of Different Metals with CP2 Zeolite and Langmuir Model at 29°C.

Table 7.22. Langmuir Model Parameters.

	Copper	**Nickel**	**Cobalt**
Slope	0.10	0.12	0.21
Intercept	2.06	3.69	1.09
R	0.9996	0.9979	0.9922
q_{max} (mg/g zeolite)	9.72	8.03	4.66
b	0.05	0.30	0.19

Ion exchange capacity of CP2 towards the ions studied was determined to be the greatest for Cu^{2+} and smallest for the Co^{2+} ions. In Figure 7.29, ion exchange isotherms of these cations were constructed for CP2 zeolite with the corresponding Langmuir Model in terms of species concentration in the solid phase as a function of its value in solution. Langmuir model represented the systems of Ni^{2+} and Cu^{2+} by far better than Co^{2+} ion as can be seen from Table 7.22. Ion exchange capacity of CP2 zeolite was determined as 8.33 mg (0.26 meq) Cu^{2+} / g, 6.64 mg (0.23 meq) Ni^{2+} / g and 4.55 mg (0.15 meq) Co^{2+} / g. Based on these results, the following general trend for ion exchange capacity series was obtained as; $Cu^{2+} > Ni^{2+} > Co^{2+}$. In the study of Wang et al., 2003, it's reported that the percent removal of Co^{2+} using coal with the initial concentration of 6.7 mg/L was achieved as 38%. On the other hand, Ming et al., 1993 reported that, with the initial Ni^{2+} concentration of 350 mg/L, the effective ion exchange capacities of the five zeolites at 48 hr for Ni^{2+} was determined as 0.24, 0.20, 0.31, 0.14

and 0.14 meq/g for the zeolites from Barstow, Buckhorn, Hector, Death Valley Junction and Pine Valley, respectively. The ion exchange capacity reported in this study was determined as 0.23 meq/g, which is in very good agreement with the literature data.

7.2. Packed Bed Studies

In this part of the study, packed bed runs were carried out in upflow mode to investigate the column efficiency of Turkish clinoptilolites (CP1, CP2). The reason for operating the system in upflow mode was to make sure the perfect wetting of the particles. Different parameters such as initial metal concentration, packing height and flow rate were investigated throughout the study. Furthermore, in order to investigate the column performance of the zeolites towards copper, nickel and cobalt ions.

7.2.1. Interpretation of the Breakthrough Curves

Breakthrough curves were constructed and ion exchange capacities were calculated for each run. The effect of several parameters on breakthrough curves was discussed for understanding ion exchange behavior of clinoptilolite rich natural zeolite in packed bed column. Breakthrough curves were presented for copper, nickel and cobalt, where C represents the time-dependent outlet metal concentration of the bed, C_o the inlet concentration and BV is the bed volume. In the interpretation of the breakthrough curves, the breakthrough point was set at C/C_o=5%.

7.2.1.1. Effect of Initial Copper Concentration

Three experiments were conducted with the initial copper concentrations of 100, 158 and 200 mg/L to investigate the effect of initial copper concentration on the ion exchange behavior of CP1 at a flow rate of 4.75 ml/min in 18.75 cm packed bed column.

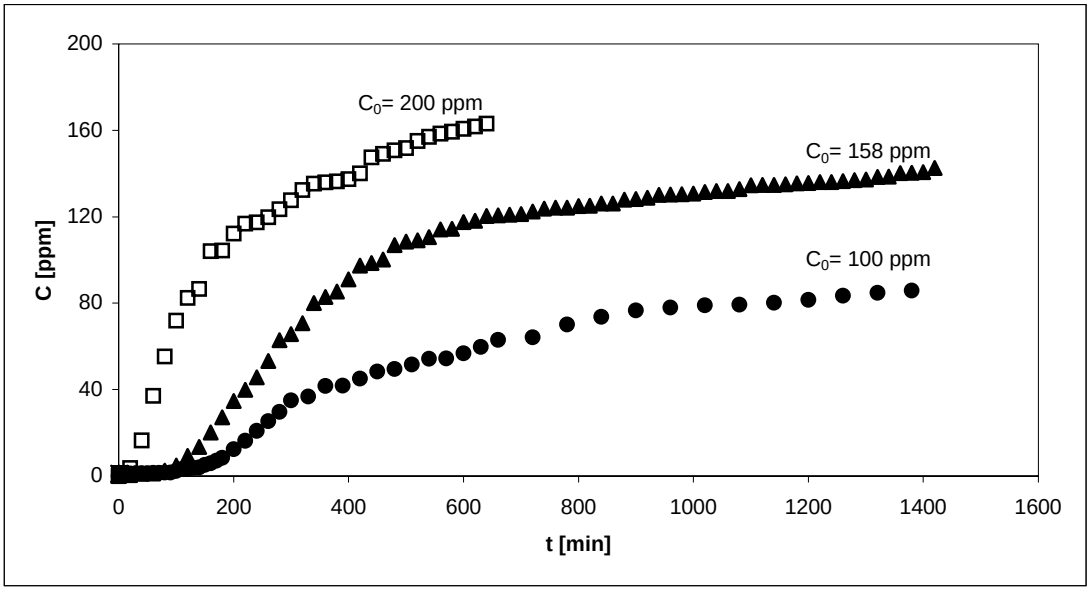

Figure 7.30. Breakthrough Curves for Cu^{2+} Exchange on CP1 with Respect to Concentration and Time at 29°C with varying Cu^{2+} Concentrations (Flow Rate= 4.75 ml/min, Packing Height= 18.75 cm).

In Figure 7.30, it is seen that decreasing the feed concentration increased the breakthrough time, which were 150, 120 and 30 min for initial copper concentrations of 100, 158 and 200 mg/L, respectively and thus shifted the breakthrough curve to the right. As the concentration of Cu^{2+} ions increased in the feed, the breakthrough curves became steeper. The reason for having sharp increases at higher concentrations is due to the fact that as the concentration gradient increases which is the driving force for mass transfer, the system reaches equilibrium faster. Similar findings are available in the literature. For example, in a study performed by Sag et al., 2001, the breakthrough curves of Cr(VI) obtained at increasing ion concentrations in the 0.920-5.055 mmol/liter range, as the ion concentration decreases breakthrough curves shifted to the right. In the study of Lin and his coworkers, 2003, similarly as the chromate ion concentration increased from 200 to 750 mg/L, breakthrough time decreases accordingly, thus, breakthrough curves shift to the left.

Ion exchange capacities were calculated by taking the integration using "Trapezoidal Rule" from the experimental breakthrough curves obtained in the column studies. The results of integration yielded the area above the breakthrough curves indicating that metal retained in the column. Therefore, the capacities calculated from column studies and batch equilibrium studies can be compared.

7.2.1.2. Effect of Flow Rate

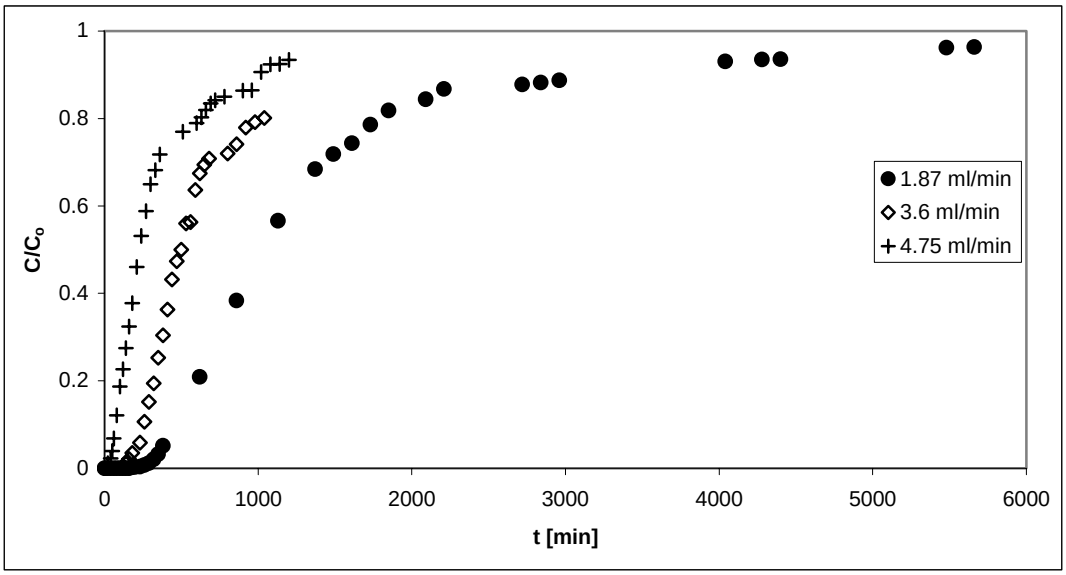

Figure 7.31. Breakthrough Curves for Cu^{2+} Exchange on CP1 with Respect to Concentration Ratio and Time at 29°C with Varying Flow Rates (Packing Height= 25 cm, Initial Cu^{2+} Concentration= 200 mg/L).

The principal operating conditions influencing the ion exchange process are the flow rate and the quality of the flow. Any volume element of the solution is in contact with a given layer of the bed for only a limited time, and flow rate is controlling this contact time.

It can be seen that at higher flow rate, a steeper breakthrough curve was obtained and the breakthrough point, set at C/C_o = 5%, was moved towards left on the C/C_o vs. time diagram (Figure 7.31) as expected from the literature (Inglezakis et al., 2001). Maximum column capacity is generally expected to increase with increasing flow rates because of high metal loading. However, the longer the contact time between metal solution and ion exchanger in packed column the greater the amount of metal exchanged (Sag et al., 2001).

In this study, the used volumetric flow rates were 1.87, 3.6 and 4.75 ml/min These rates were corresponding to relative flow rates of 2.54, 4.89 and 6.45 BV/h respectively. A wide range of flow rates for the treatment of heavy metal solutions using zeolites is presented in the literature. For example, flow rates between 0.75 and 25 BV/h are used for the treatment of the solutions containing Pb^{2+}, Cu^{2+} and Fe^{2+} with natural clinoptilolite (Zamzow et al., 1995). In the study of Guangsheng et al., 1988, for Cu^{2+}

exchange on Na-clinoptilolite, at concentrations between 25 and 320 mg/L and flow rates between 7.5 and 22.5 BV/h, breakthrough point was strongly influenced by the flow rate and increased by 24%, lowering the flow capacity from 22.5 to 7.5 BV/h. In a similar manner, in this study, as the flow rate increased from 2.54 to 6.45 BV/h, breakthrough time decreased from 380 to 58 min (85%). In the study of Hlavay et al., 1982, flow rates between 5 and 15 BV/h were used for ammonia removal using natural and modified clinoptilolite at 25 mg/L. They have determined that by changing the flow rate from 10 to 5 BV/h the ammonia breakthrough point was increased as much as 34%. Lower flow rates ranging from 2.4 to 13.4 BV/h were used for ammonia removal at 600 mg/L, using modified clinoptilolites. Breakthrough point was as much as 17 times higher for 2.4 BV/h, compared to 13.4 BV/h (Milan et al., 1997).

7.2.1.3. Effect of Packing Height

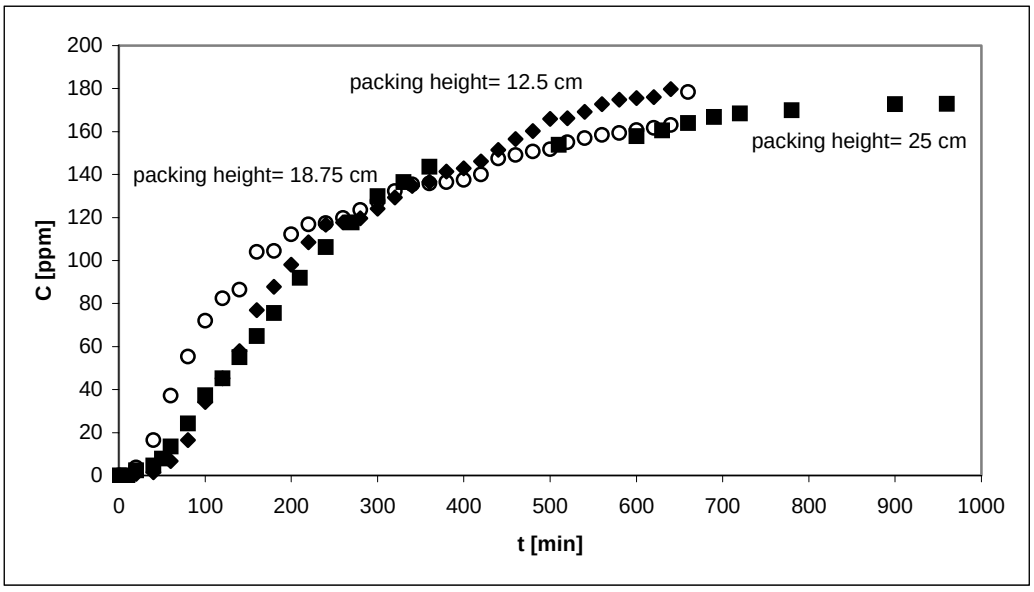

Figure 7.32. Breakthrough Curves for Cu^{2+} Exchange on CP1 with Respect to Concentration and Time at 29°C with Varying Packing Heights (Flow Rate= 4.75 ml/min, Initial Cu^{2+} Concentration= 200 mg/L).

Six experiments were carried out to investigate the effect of packing height on the ion exchange behavior of CP1 and CP2 in packed bed column.

To assess the influence of packing height on column performance of CP1, an influent containing 200 mg/L Cu^{2+} was passed through columns with various packing heights, 12.5, 18.75 and 25 cm, at a flow velocity of 4.75 ml/min. Although slight differences were observed between the breakthrough curves, breakthrough point was

shifted to the right 20% when packing height increased from 18.75 to 25 cm (Figure 7.32).

To see the effect of packing height on column performance of CP2 zeolite, lower flow rate was chosen which was 1.87 ml/min. Since decreasing flow rate inceases the liquid hold up and contact time between the metal solution and CP2 particles, more clear results were expected. For this, three experiments were conducted by using the copper nitrate solutions having same concentrations, 200 mg/L, which were passed through the column with 12.5, 18.75 and 25 cm packing heights. As can be seen from Figures 7.31 and 7.32, breakthrough curves shifted to the right with increasing packing height.

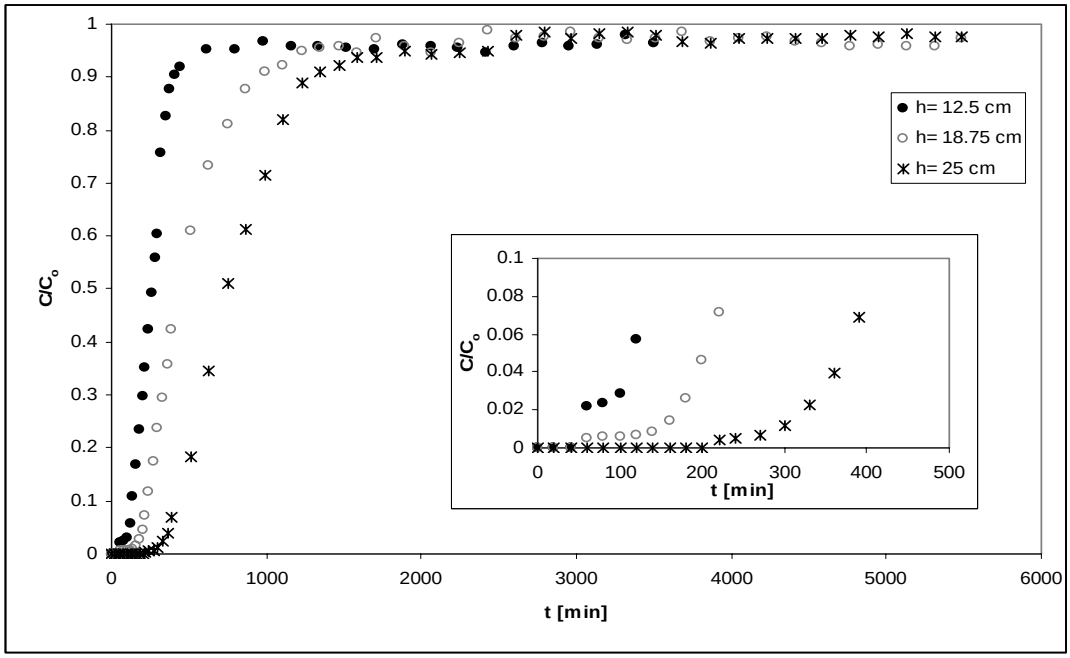

Figure 7.33. Breakthrough Curves for Cu^{2+} Exchange on CP2 with Respect to Concentration Ratio and Time at 29°C with Varying Packing Heights (Flow Rate= 1.87 ml/min, Initial Cu^{2+} Concentration= 200 mg/L).

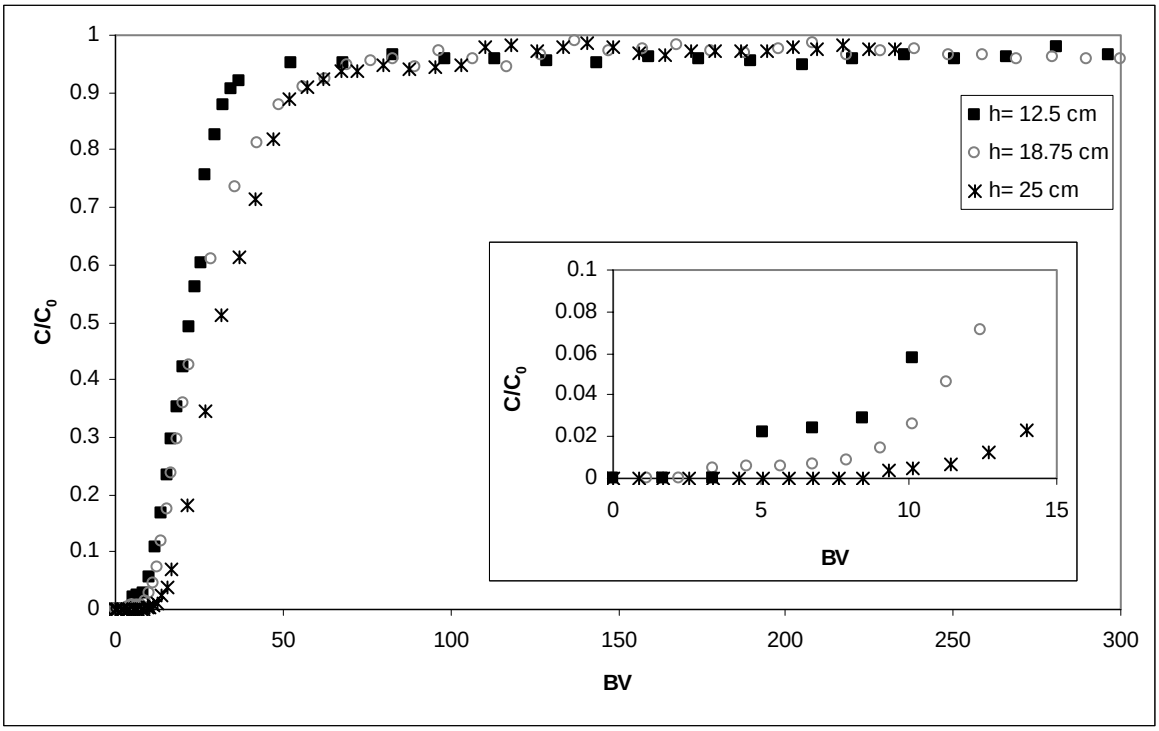

Figure 7.34. Breakthrough Curves for Cu^{2+} Exchange on CP2 with Respect to Concentration Ratio and Bed Volume at 29°C with Varying Packing Heights (Flow Rate= 1.87 ml/min, Initial Cu^{2+} Concentration= 200 mg/L).

Obviously, it is seen from the Figure 7.33 that, increasing packing height increases the time for the system to reach eqilibrium, $C/C_o=1$. After 600 minutes, the column with 12.5 cm of packing height reached the saturation point, while 1200 and 1700 minutes were required to reach to this point for the columns having 18.75 and 25 cm packing heights, respectively. Also it is seen that increasing packing height from 12.5 cm to 18.75 cm increased the breakthrough time by 66% and operating capacity 5 %, while increasing packing height from 18.75 cm to 25 cm was increased the breakthrough time by 80% and operating capacity 20 %. The ion exchange capacity was calculated as 8.04 mg Cu^{2+}/g CP2, which was consistent with the capacity calculated from batch experiments, 8.33 mg Cu^{2+}/g CP2.

7.2.1.4 Comparison of the Column Performance of Zeolites, CP1 and CP2

Figure 7.35 was constructed to compare the ion exchange capacities of the zeolites used in this work with the packing height, flow rate and the initial copper concentration of 25 cm, 1.87 ml/min and 200 mg/L, respectively. According to the figure, it was determined that the breakthrough time for both zeolites were 380 min. Besides, the system has reached equilibrium at around 2500 and 4000 min for CP2 and CP1 at which the saturation point, C/C_o, for these zeolites were approximately 1. Although the breakthrough curves were generally close to each other, there was a slight difference between the time interval of 1000-4000 min, CP2 was on the right hand side of CP1 zeolite.

When the batch studies were compared with the column studies, in batch experiments, copper removed from the solution was determined as 10 mg and 8.33 mg for 1 g of CP1 and CP2 zeolites, respectively. In column studies, at the same initial Cu^{2+} concentrations of 200 mg/L, copper exchange capacities were calculated as 9.46 mg Cu^{2+}/ g CP1 and 8.04 mg Cu^{2+}/ g CP2.

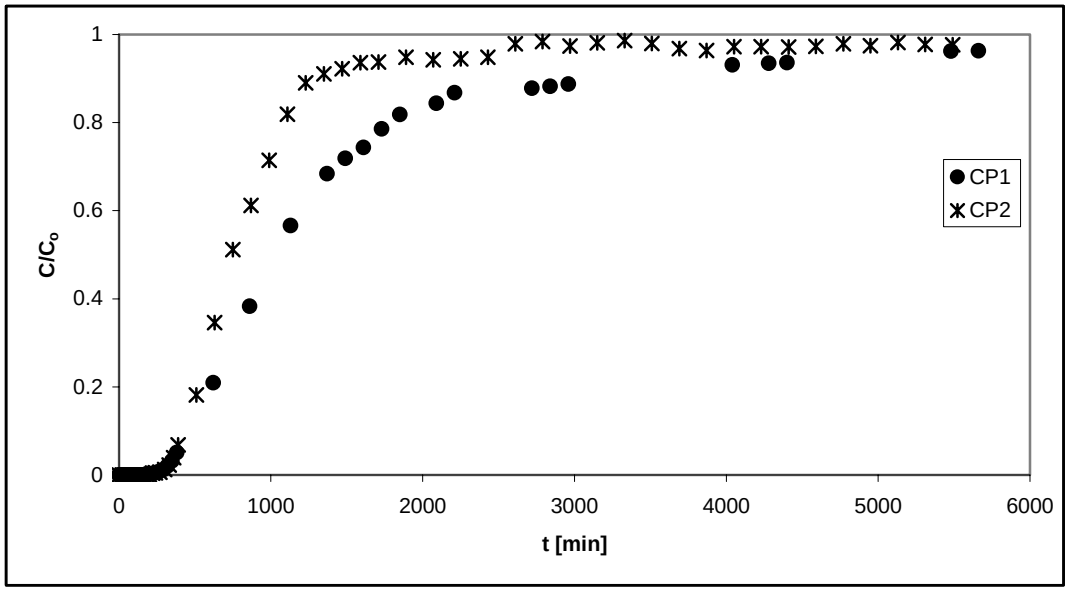

Figure 7.35. Comparison of the Breakthrough Curves for Cu^{2+} Exchange on CP1 and CP2 with Respect to Concentration Ratio and Time at 29°C (Packing Height= 25 cm, Flow Rate= 1.87 ml/min, Initial Cu^{2+} Concentration= 200 mg/L).

7.2.1.5 Comparison of the Column Performance of CP2 for Cu^{2+}, Ni^{2+} and Co^{2+}

Figure 7.36 represents the breakthrough curves of CP2 zeolite for Cu^{2+}, Ni^{2+} and Co^{2+} ions with the packing height, flow rate and initial ion concentration of 21.88 cm, 3.8 ml/min and 150 mg/L, respectively. The breakthrough times obtained for Cu^{2+}, Ni^{2+} and Co^{2+} ions were 250, 119 and 118 min, respectively which were consistent with the results obtained from batch studies. As was also understood from the batch studies, the ion exchange capacity of CP2 zeolite towards Cu^{2+} was much higher than Ni^{2+} and Co^{2+} ions. When Figure 7.36 is investigated, it can be seen that, the breakthrough times for Co^{2+} and Ni^{2+} are nearly the same and the system has reached the saturation point ($C/C_o \approx 1$) at about 500 min for these ions. However, it took much greater time for the system to reach equilibrium for Cu^{2+} ion which was around 2000 min.

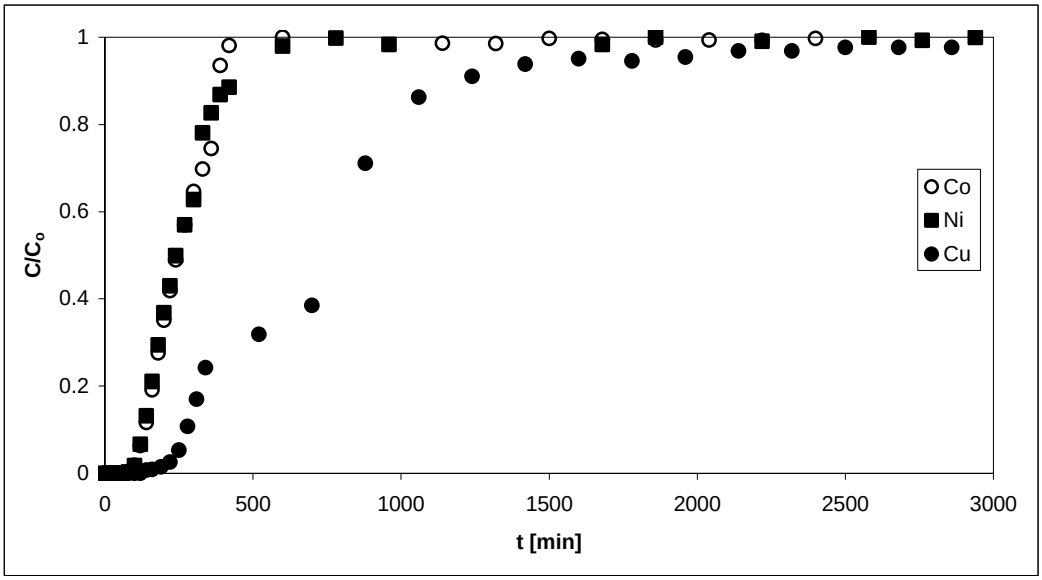

Figure 7.36. Comparison of the Breakthrough Curves for Cu^{2+}, Ni^{2+} and Co^{2+} Exchange on CP2 with Respect to Concentration Ratio and Time at 29°C (Packing Height= 21.88 cm, Flow Rate= 3.8 ml/min, Initial Ion Concentration= 150 mg/L).

Three factorial design model which was previously applied to copper-CP1 zeolite system by using "Design of Expert" program predicted the breakthrough time of Cu^{2+} with CP1 zeolite. The breakthrough time for Cu^{2+} was predicted as 294.12 min which afterwards was determined as 250 min for CP2 zeolite as a result of the experiments being performed at the same conditions.

7.2.1.6. Regeneration Results

Regeneration of natural zeolites after ion exchange operation plays a crucial role due to the need of repeated use of the ion exchangers for cost effectiveness. Therefore, regenerability of CP1 zeolite was investigated after having passed 200 mg/L copper solution through the column having packing heights of 12.5 and 25 cm at 29 ^{o}C.

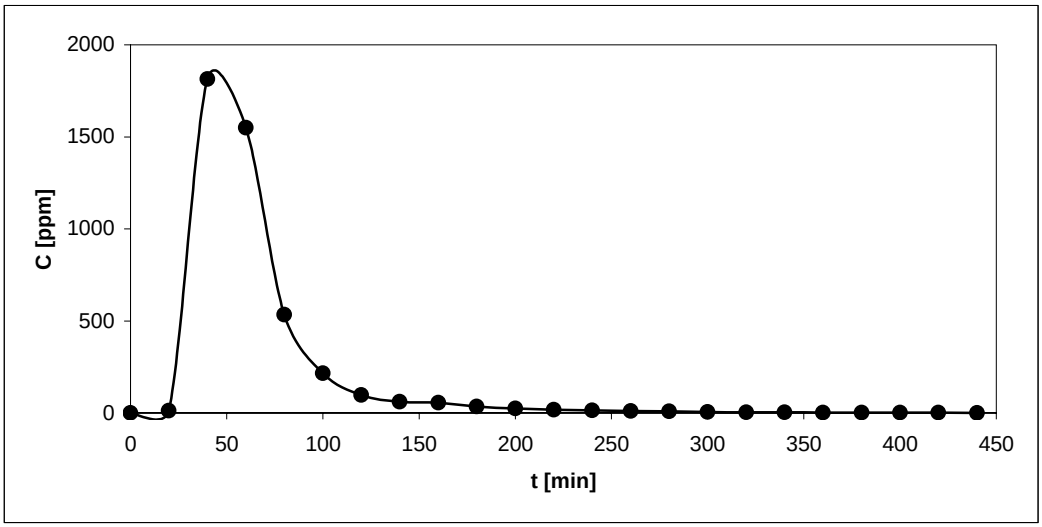

Figure 7.37. Regeneration of CP1 with 0.2 M NaCl after 200mg/L solution passed through the column having packing height of 12.5 cm at 29 ^{o}C.

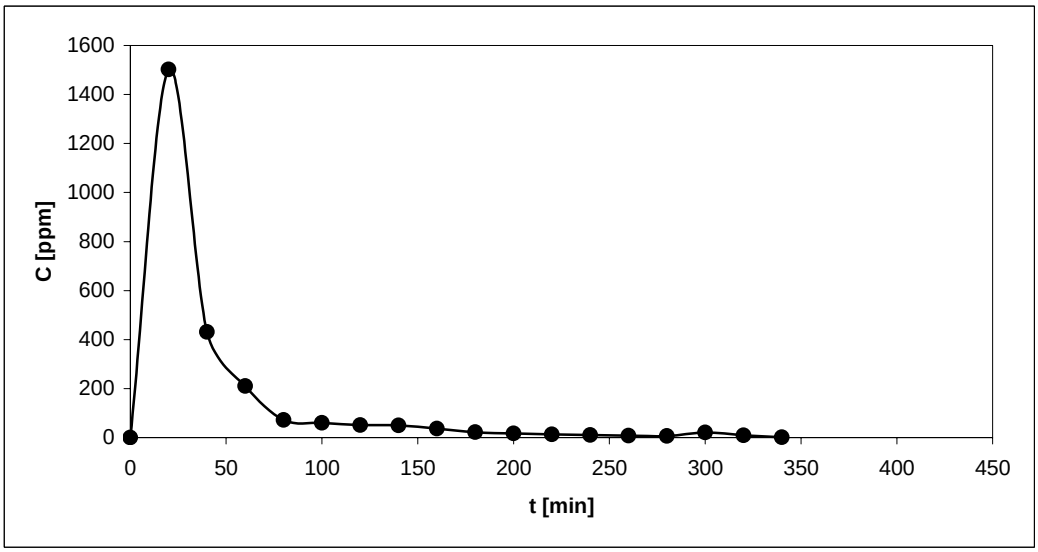

Figure 7.38. Regeneration of CP1 with 1.7 M NaCl after 200mg/L solution passed through the column having packing height of 25 cm at 29 ^{o}C.

Regeneration of exhausted CP1 zeolite was achieved by using 0.2 and 1.7 M of NaCl solutions passed through the columns having packing heights of 12.5 and 25 cm.

In the regeneration of CP1 zeolite using NaCl solution, the copper on the solid phase was replaced by exchange with sodium. Figure 7.37 and 7.38 demonstrate the copper concentration change in the exit solution as a function of time after ion exchange using 0.2 and 1.7 M of NaCl solutions. The time to reach zero Cu^{2+} concentration (complete desorption of Cu^{2+}) was 440 min when using 0.2 M NaCl solution, while it required 340 min to reach zero Cu^{2+} concentration when 1.7 M NaCl solution was used. The time required to regenerate the zeolite when the NaCl solution concentration is low however, 94 and 95% of copper were recovered within the first 100 minutes for both experiments. Therefore, it is unnecessary to use approximately 8 fold greater amount of NaCl, 1.7 M, to regenerate CP1 zeolite effectively.

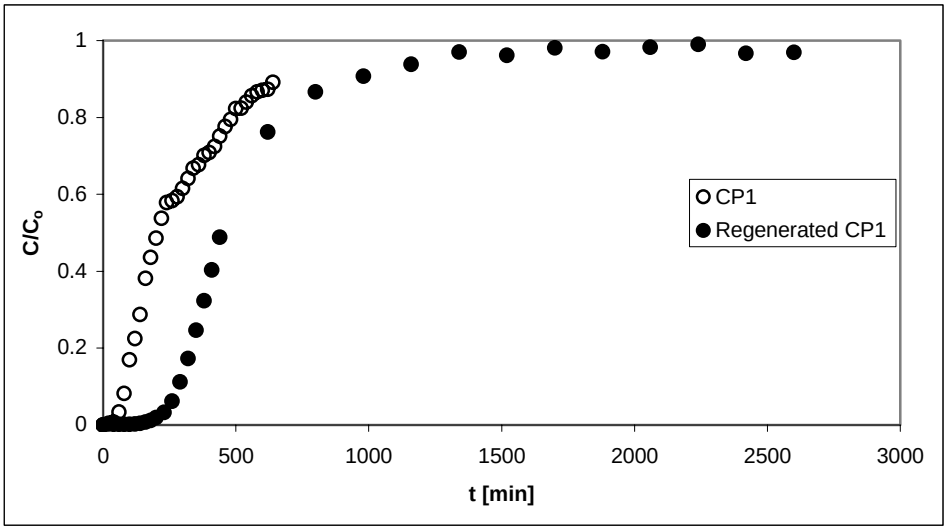

Figure 7.39. Comparison of Breakthrough Curves for Cu^{2+} Exchange on CP1 and Regenerated CP1 with Respect to Concentration Ratio and Time at 29°C (Flow Rate= 4.75 ml/min, Initial Cu^{2+} Concentration= 200 mg/L).

Regenerated CP1 sample given in Figure 7.37 by using 0.2M NaCl solution was then reused for the removal efficiency of copper ions at the same conditions, which were 12.5 cm packing height, 200 mg/L $Cu(NO_3)_2$ solution and flow rate of 4.75 ml/min at 29 ^oC. As can be seen from Figure 7.39, regenerated sample has the highest capacity to remove copper ions from the solution which were 7.41 mg Cu^{2+}/g CP1 and 9.7 mg Cu^{2+}/g regenerated CP1. This situation may be explained as washed particles with NaCl solution during regeneration process was resulted in the cleaning of blocked pores within the CP1 structure and thus improved the copper exchange capacity. Also, clinoptilolite particles in sodium form could readily exchange its ions for copper. Similar observations were found in a previous study performed by Top, A. in 2001.

7.3. Evaluation of the SEM & EDX Results

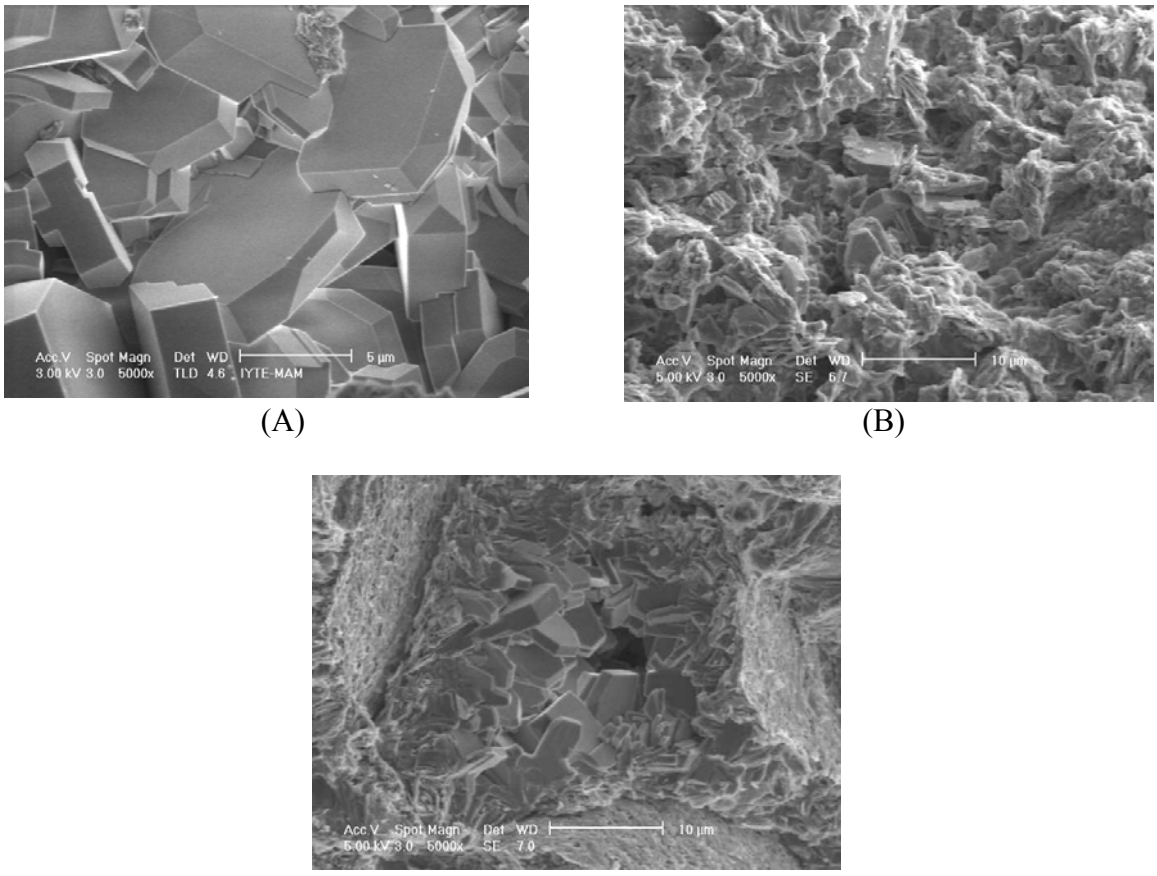

(A) (B)

(C)

Figure 7.40. SEM Micrographs of (A) Natural Zeolite (CP1), (B) Outer Surface of CP1 after Ion Exchange, (C) Inner Surface of CP1 After Ion Exchange

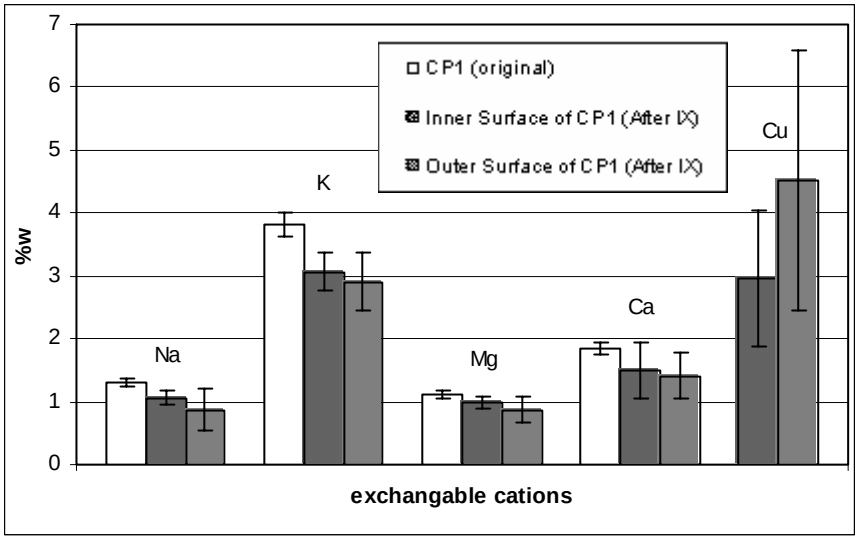

Figure 7.41. EDX Results of CP1 Zeolite, Before and After Ion Exchange Process

Analyses of solid phase was carried out using scanning electron microscopy and energy dispersive x-ray microanalysis. Figure 7.40 shows the SEM micrographs of original CP1 zeolite in A, the outer and inner surfaces of CP1 after copper exchange in B and C, respectively. In order to layout the differences in the structure of CP1 zeolite after copper exchange process in packed column, representative zeolite particles were taken and cut into two to see how the copper ions moved through the inner surface of the CP1 zeolite. The results of column exhaustion were given just for one experiment to be representative. In Figure 7.40-A, clear clinoptilolite crystals can easily be seen. However, after copper exchange, the outer surface of CP1 was covered with different structures (Figure 7.40-B). Finally, in Figure 7.40-C, although similar structures can be seen in the inner surface of CP1, crystals can still be perceived within the structure, which may indicate that slowly diffused copper ions into the zeolite could not be spread out easily.

EDX results of only exchangeable cations namely, Na^+, K^+, Mg^{2+}, Ca^{2+} and Cu^{2+} for the same CP1 zeolite particles given in Figure 7.40 was presented in Figure 7.41. Each bar represents the average results of 10 EDX analyses taken from different parts of CP1 structure in 1000 magnification. Standard deviations were calculated by using SPSS computer program (SPSS 10.0) and corresponding percent errors were calculated by dividing the standard deviations by mean and multipliying by 100. The calculated percent errors were presented on the bar graph as error bars (Figure 7.41).

When Figure 7.41 is investigated, it is seen that after copper exchange process, weight percentages of Na^+, K^+, Mg^{2+} and Ca^{2+} ions were decreased while weight percent of Cu^{2+} ions was increased. Also, the least exchange was observed between magnesium and copper ions as was proved by the ICP-OES results of batch studies for CP1 zeolite. Furthermore, for all exchangeable cations investigated except copper, the accumulation of the ions at the inner surface was greater, while accumulation of copper was greater at the outer surface. These results were consistent within each other. The amount of Na^+, K^+, Mg^{2+} and Ca^{2+} ions being less at the outer surface prove the presence of higher amount of exchanged copper ions at the outer surface.

7.4. Modeling of Breakthrough Curves

Since the feed solutions were kept at constant temperature water bath and the effect of slight temperature differences on the breakthrough curves was assumed to be negligible, the fixed bed system can be considered to be isothermal. When the

equilibrium relationship is not linear, it is generally not possible to determine the analytical solution for the breakthrough curve, however, by using the assumption of irreversible rectangular isotherm it is possible to obtain the analytical solution.

Also, plug flow was assumed because the Reynold's numbers tabulated in Figure 7.7 are quite low.

In the calculation of the Re, column diameter was used (Mc Cabe et al., 1988).

$$\mathrm{Re} = \frac{d_c u_s \rho}{\mu} \tag{7.1}$$

where u_s, μ and ρ are superficial fluid velocity, viscosity and density of fluid, respectively.

The correlation of Wilson and Geankoplis expressed in terms of Sherwood number for liquids is equivalent to

$$0.0015 < \mathrm{Re} < 55,\ Sh = \frac{1.09}{\varepsilon}\mathrm{Re}^{0.33}\ Sc^{0.33} \text{ (Ruthven, 1984).} \tag{7.2}$$

Peclet numbers and axial dispersion coefficients were calculated from

$\varepsilon Pe = 0.2 + 0.011 Re^{0.48}$ (Chung et al., 1968). (7.3)

$Pe = u_i * d_p / E_D$ (7.4)

Where u_i, ε and E_D are interstitial fluid velocity, bed voidage and axial dispersion coefficient, respectively.

The lower axial dispersion coefficients in Table 7.7 indicate that axial dispersion is negligible.

In order to determine mass transfer behavior of the system, Biot numbers were calculated. The Biot numbers, which measure the ratio of internal to external gradients, were defined by

$$Bi = \frac{k_f d_p}{3 D_m} \tag{7.5}$$

Where k_f and D_m are external fluid film mass transfer coefficient and molecular diffusivity, respectively. Biot numbers greater than 3 in Table 7.7 indicate that intraparticle mass transfer resistance controls the mass transfer rate (Ülkü et al., 1997).

Since the system is isothermal and one diffusional resistance is assumed, the solution for the uptake curve is:

$$\frac{m_t}{m_\infty} = 1 - \frac{6}{\pi^2}\sum_{n=1}^{\infty}\frac{1}{n^2}\exp\left(\frac{-n^2\pi^2 D_e t}{r_c^2}\right) \tag{7.6}$$

$\frac{m_t}{m_\infty}$ is the fractional approach to equilibrium. Since the higher terms of the summation become very small in the long time region, for fractional uptakes greater than 70% only the first term can be retained:

$$1-\frac{m_t}{m_\infty}=\frac{6}{\pi^2}\exp(\frac{-\pi^2 D_e t}{r_c^2}) \qquad (7.7)$$

In the long time region, a plot of ln $(1-m_t/m_\infty)$ versus t should be linear with slope $-\pi^2 D_e/r_c^2$.

For fractional uptakes smaller than 30%, short time approximation can be written:

$$\frac{m_t}{m_\infty}=\frac{6}{\sqrt{\pi}}(\frac{D_e t}{r_c^2})^{1/2} \qquad (7.8)$$

from which a plot of m_t/m_∞ vs $\sqrt{t}$ should be linear in the initial region with the slope $(\frac{6}{\sqrt{\pi}})(\frac{D_e}{r_o^2})^{1/2}$.

According to Equation 7.7, the effective diffusivities for all concentrations were calculated.

Table 7.23. Experimental Uptake Data for Cu^{2+} in CP1 crystals at 29°C.

	C_o= 50 mg/L	**C_o= 75 mg/L**	**C_o= 100 mg/L**	**C_o= 150 mg/L**	**C_o= 200 mg/L**
t [sec]	**M_t/M**	**M_t/M**	**M_t/M**	**M_t/M**	**M_t/M**
0	0	0	0	0	0
3600	0.85	0.79	0.68	0.68	0.66
21600	1.00	0.97	0.88	0.88	0.90
86400	1.00	0.97	0.91	0.95	0.97
108000	1	1	1	0.98	-
172800	-	-	-	1	1

Table 7.24. Effective Diffusivities with Varying Concentrations

Co [mg/L]	**$D*10^{11}$ [m^2/s]**
50	4.12
75	8.24
100	6.18
150	6.18
200	6.18

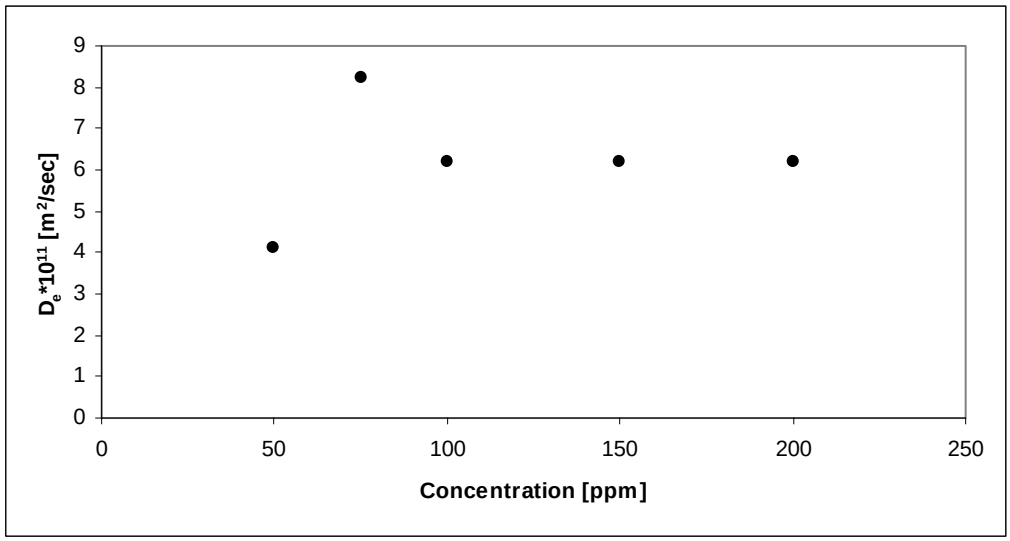

Figure 7.42. Variation of Diffusivity with Solution Concentration for Cu^{2+} in CP1 at 29°C

According to experimental results, it can be said that diffusivities slightly changed with increasing solution concentration but this may be due to the non-linearity of the equilibrium isotherm rather than to any variation in mobility (Figure 7.42). Thus, it can be said that diffusivities calculated from Equation 7.7 are practically independent of concentration.

Table 7.25. Dimensionless Numbers for Different Flow Rates in Packed Column

Flow Rate [ml/min]	**u_s [cm/s]**	**Re**	**Pe**	**E_D [m^2/s]*10^6**	**k_f [cm/s]*10^5**	**Bi**
2.86	0.027	3.64	0.711	1.74	1.47	4.249
3.60	0.034	4.58	0.719	2.17	1.58	4.584
4.75	0.045	6.04	0.729	2.83	1.73	5.024

After the assumptions discussed in this section yield the analytical solution of breakthrough curves for the limiting cases of solid diffusion control and solved by Cooper (Rutven, 1984).

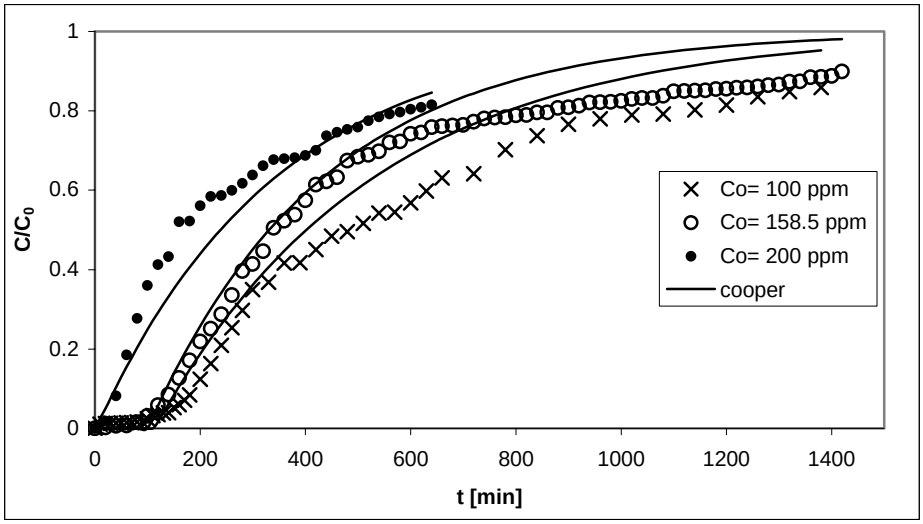

Figure 7.43. Breakthrough Curves for Cu^{2+} Exchange on CP1 and corresponding model fits with Respect to Concentration Ratio and Time at 29°C with varying Cu^{2+} Concentrations (Flow Rate= 4.75 ml/min, Packing Height= 18.75 cm).

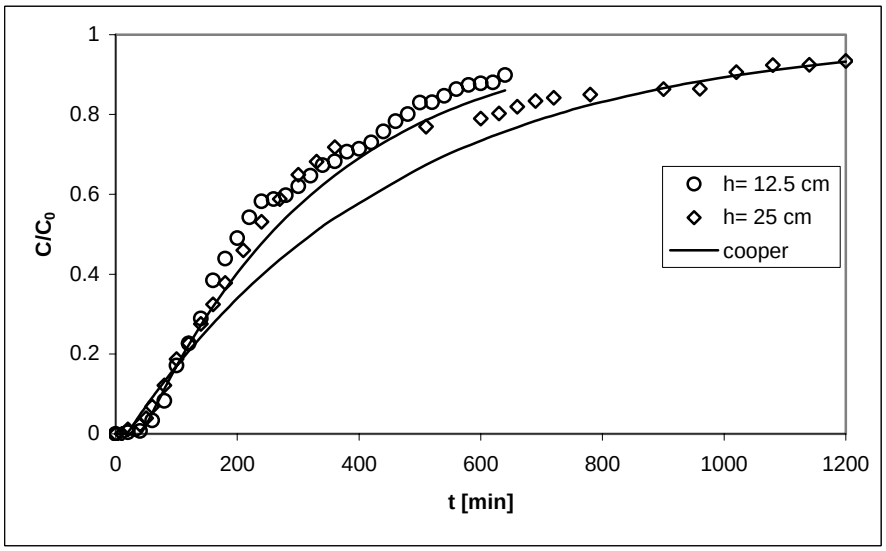

Figure 7.44. Breakthrough Curves for Cu^{2+} Exchange on CP1 and corresponding model fits with Respect to Concentration Ratio and Time at 29°C with Varying Packing Heights (Flow Rate= 4.75 ml/min, Initial Cu^{2+} Concentration= 200 mg/L).

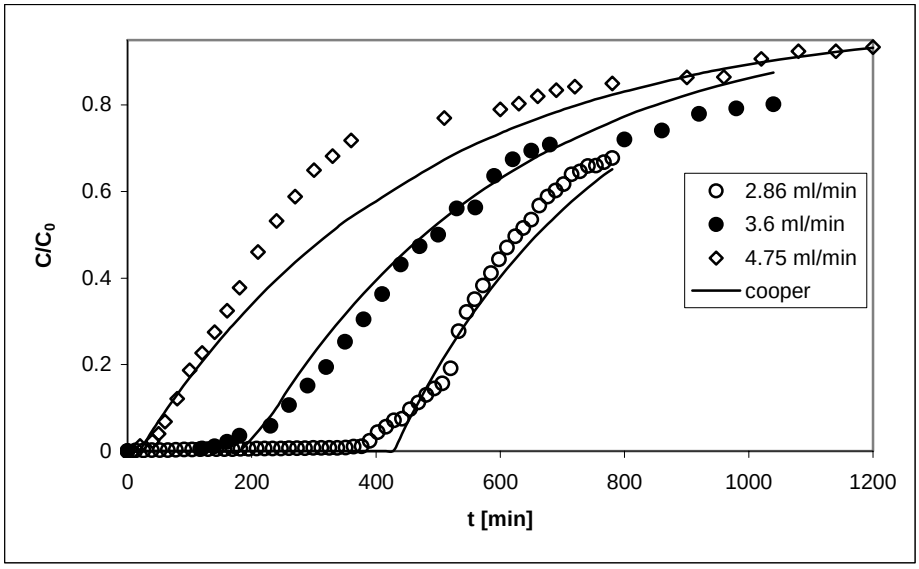

Figure 7.45. Breakthrough Curves for Cu^{2+} Exchange on CP1 and corresponding model fits with Respect to Concentration Ratio and Time at 29°C with Varying Flow Rates (Packing Height= 25 cm, Initial Cu^{2+} Concentration= 200 mg/L).

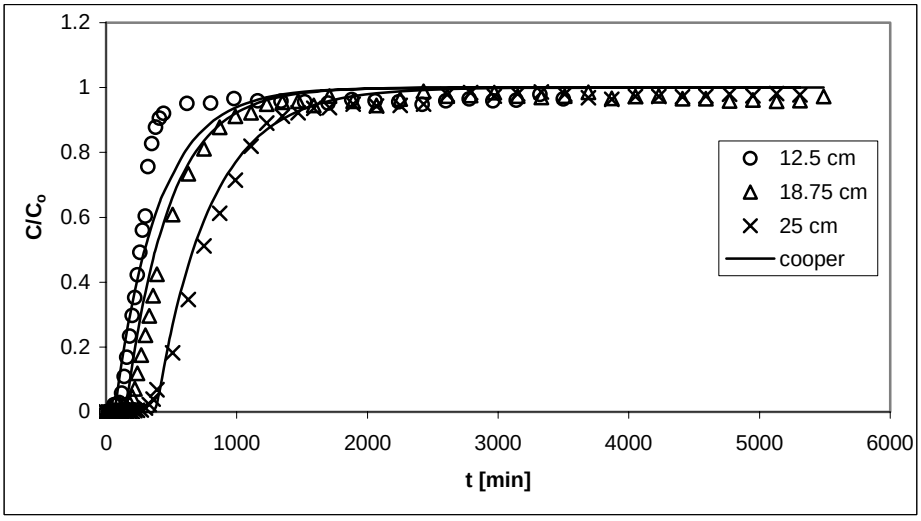

Figure 7.46. Breakthrough Curves for Cu^{2+} Exchange on CP2 and corresponding model fits with Respect to Concentration Ratio and Time at 29°C with Varying Packing Heights (Flow Rate= 1.87ml/min, Initial Cu^{2+} Concentration= 200 mg/L).

Table 7.26. Cooper Model Parameters Corresponding to Experimental Conditions

Experimental Parameters for Cu^{2+} Exchange			Cooper Model		
Packing Height [cm]	Flow Rate [ml/min]	C_o [mg/L]	$k*10^5$ [s^{-1}]	K	R
Effect of inlet Cu^{2+} concentration					
18.75	4.75	100	4.0	110	0.9976
18.75	4.75	158	5.0	90	0.9969
18.75	4.75	200	4.9	71	0.9776
Effect of packing height					
12.5	4.75	200	5.5	108	0.9953
25	4.75	200	5.0	71	0.9838
Effect of flow rate					
25	2.86	200	3.8	71	0.9962
25	3.6	200	4.1	71	0.9937
25	4.75	200	5.0	71	0.9838

In Figures 7.43-46, according to the Cooper model, breakthrough curves were constructed and model parameters corresponding to experimental conditions were given in Table 7.26. Effective mass transfer coefficient, k, and equilibrium constant, K were estimated to best describe the experimental data and correlation coefficient, R were given. Figures 7.43-46 show the superposition of experimental results and theoretical calculated points. It is also seen from Table 7.26, increasing flow rate was resulted in an increase in the effective mass transfer coefficients. Equilibrium constants were ranging between 71 and 110. As initial metal concentration increased from 100 mg/L to 200 mg/L, equilibrium constant decreased from 110 to 71, while for the initial metal concentration of 200 mg/L, K was not changed by changing flow rate. For higher packing height, flow rate and initial copper concentrations, the correlation between the experimental and the predicted values using the Cooper model deviated slightly.

As a result of this simulation, breakthrough was well predicted, whereas the whole breakthrough curve could not be defined.

CONCLUSIONS

Turkish natural clinoptilolites were examined to evaluate their ion exchange performance for the removal of copper, nickel and cobalt ions by performing both batch and packed column experiments at 29^{o}C. Zeolites were characterized by (RIR) Reference Intensity Ratio method using α-alumina (corundum) as an internal standard and reference clinoptilolites supplied from California and Idaho. Their clinoptilolite contents were determined quantitatively as 80 and 64 % for zeolites named as CP1 and CP2, respectively. The copper exchange capacities of CP1 and CP2 were determined from equilibrium studies as 10 mg (0.32 meq) Cu^{2+} / g CP1 and 8.33 mg (0.26 meq) Cu^{2+} / g CP2. Ion exchange capacity of CP2 zeolite was determined as 6.64 mg (0.23 meq) Ni^{2+} / g and 4.55 mg (0.15 meq) Co^{2+} / g. Langmuir model was best described the equilibrium behaviour of the system.

Design of experiments was applied to investigate significance of the interactions between the parameters of column studies such as packing height, inlet metal concentration and flow rate. When the interaction between concentration and packing height was investigated, it was found that the concentration effect was very small when the packing height was at the low level and relatively large when the packing height was at the high level, with the best results obtained with low concentration and high packing height. Concentration and flow rate interaction indicated that concentration had little effect at high flow rate but a large effect at low flow rate. The effect of packing height and flow rate interaction was more significant when packing height was at the high level and flow rate was at the low level. Therefore, the maximum breakthrough time, 850 minutes, would appear to be obtained when concentration and flow rate were at the low level and packing height was at the high level, which were 100 mg/L, 2.86 ml/min and 25 cm, respectively. Therefore, breakthrough times were well predicted by using 2^3 factorial design model. Correlation coefficient was calculated as 0.9999 for experimental and predicted data series.

Afterwards, breakthrough capacity and ion exchange capacity of natural zeolites were calculated. Decreasing the feed concentration increased the breakthrough time, which were 150, 120 and 30 min for initial copper concentrations of 100, 158 and 200 mg/L, respectively and thus shifted the breakthrough curve to the right. As the concentration of Cu^{2+} ions increased in the feed, the breakthrough curves became steeper. At lower flow rate, a steeper breakthrough curve was obtained and the

breakthrough point, set at C/C_o = 5%, was moved towards left. Increasing packing height increases the time for the system to reach eqilibrium, C/C_o=1. After 600 minutes, the column with 12.5 cm of packing height reached the saturation point, while 1200 and 1700 minutes were required to reach to this point for the columns having 18.75 and 25 cm packing heights, respectively. Also it is seen that increasing packing height from 12.5 cm to 18.75 cm increased the breakthrough time by 66% and operating capacity 5 %, while increasing packing height from 18.75 cm to 25 cm was increased the breakthrough time by 80% and operating capacity 20 %. The ion exchange capacity of CP2 zeolite was calculated as 8.04 mg Cu^{2+}/g CP2, which was consistent with the capacity calculated from batch experiments, 8.33 mg Cu^{2+}/g CP2.

When the column studies of CP1 and CP2 zeolites with Cu^{2+} ion were compared, it was determined that the breakthrough time for both zeolites were 380 min. Besides, the system has reached equilibrium at around 2500 and 4000 min for CP1 and CP2 at which the saturation point, C/C_o, for these zeolites were approximately 1. Although the breakthrough curves were generally close to each other, there was a slight difference between the time interval of 1000-4000 min, CP2 was on the right hand side of CP1 zeolite.

The breakthrough times obtained for Cu^{2+}, Ni^{2+} and Co^{2+} exchange on CP2 zeolite were 250, 119 and 118 min, respectively which were consistent with the results obtained from batch studies. As was also understood from the batch studies, the ion exchange capacity of CP2 zeolite towards Cu^{2+} was much higher than Ni^{2+} and Co^{2+} ions. In addition, breakthrough times for Co^{2+} and Ni^{2+} are nearly the same and the system has reached the saturation point ($C/C_o \approx 1$) at about 500 min for these ions. However, it took much greater time for the system to reach equilibrium for Cu^{2+} ion which was around 2000 min.

In addition to these, natural zeolite particles which have been ion exchanged throughout this process were regenerated using 0.2M and 1.7M of NaCl solutions. According to regeneration studies, it was determined that 94 and 95% of copper were recovered within the first 100 minutes for both experiments.

After the experiments were performed, model equations were applied to the system in order to be able to investigate the dynamic behavior of the system. As a result of this simulation, breakthrough was well predicted.

REFERENCES

1. Abusafa, A., Yücel, H., " Removal of ^{137}Cs from aqueous solutions using different cationic forms of a natural zeolite: clinoptilolite ", Separation and Purification Technology 28 (2002), 103-116.
2. Ahmed S., Chughtai S., Mark A.K., "The removal of cadmium and lead from aqueous solution by ion exchange with Na-Y zeolite," *Separation and Purification Technology*, 13 (1998) 57-64.
3. Ajmal M., Rao R., Siddiqui B., "Studies on removal and recovery of Cr(VI) from electroplating wastes," *Water Research*, 30 (1995) 1478-1482.
4. Armbruster T., Simoncic P., Döbelin N., Malsy A., Yang P., "Cu^{2+}-acetate and Cu^{2+}-ammine exchanged heulandite," *Microporous and Mesoporous Materials*, 57 (2003) 121-131.
5. Assenov A., Vassilev C., Kostova M., "Simultaneous sorption of metal ions on natural zeolite clinoptilolite", *Occurence, properties and utilization of natural zeolites, Budapest: Akademiai Kiado* (1998) 471-480.
6. Baptist J., Loos W.P., Verheijen P.J.T., Moulijn J.A., "Improved estimation of zeolite diffusion coefficients from zero-length column experiments," *Chemical Engineering Science*, 55 (2000) 51-65.
7. Belyaev M.V., "Model of reaction diffusion process during ion exchange in multicomponent glass," *Physical Chemistry*, 377 (2001) 783-785.
8. Beszedits S., Chromium removal from industrial wastewaters, B&L Information Services, Canada.
9. Blanchard G., Maunaye M., Martin G., "Removal of heavy metals from waters by means of natural zeolites", *Water Res.*, 18 (1984) 1501-1507.
10. Carta G., Cincotti A., "Film model approximation for non-linear adsorption and diffusion in spherical particles," *Chemical Engineering Science*, 53 (1998) 3483-3488.
11. Carta G., Cincotti A., Cao G., "Film model approximation for particle-diffusion-controlled binary ion exchange," *Separation Science and Technology*, 34 (1999) 1-15.
12. Chipera, S., J., Bish, D., L., "Multi-reflection RIR and Intensity Normalizations for Quantitative Analyses: Applications to Feldspars and Zeolites", *Powder Diffraction*, 10 (1995) 47-55.

13. Chmielewski A.G., Urbanski T.S., Migdal W., "Separation technologies for metals recovery from industrial wastes," *Hydrometallurgy*, 45 (1997) 333-344.

14. Cincotti A., Lai N., Orru R., Cao G., "Sardinian natural clinoptilolites for heavy metals and ammonium removal: experimental and modeling," *Chemical Engineering Journal*, 84 (2001) 275-282.

15. Curkovic L., Stefanovic S.C., Filipan T., "Metal ion exchange by natural and modified zeolites," *Water Research*, 31 (1997) 1379-1382.

16. Çulfaz M., Yağız M., "Ion exchange properties of natural clinoptilolite: lead-sodium and cadmium-sodium equilibria," *Separation and Purification Technology*, article in press.

17. Dimitrova, S., V., "Use of granular slag columns for lead removal", *Water Research*, 36 (2002) 4001-4008.

18. Doula M., Ioannou A., Dimirkou A., "Copper adsorption and Si, Al, Ca, Mg, and Na Release from clinoptilolite," *Journal of Colloid and Interface Science*, 245 (2002) 237-250.

19. Doula M.K., Ioannou A., "The effect of electrolyte anion on Cu adsorption-desorption by clinoptilolite," *Microporous and Mesoporous Materials*, 58 (2003) 115-130.

20. Durrani S.K., Dyer A., Blackburn R., "Self-diffusion of barium and caesium cations in neutron-and gamma-irradiated high-silica zeolites and boron zeotypes," *Zeolites*, 13 (1993) 2-13.

21. Dyer A., Aggarwal S., "Removal of fission products from mixed solvents using zeolites II. Caesium and strontium removal," *Journal of Radioanalytical and Nuclear Chemistry*, 221 (1997) 235-238.

22. Dyer A., Las T., Zubair M., "The use of natural zeolites for radioactive waste treatment: studies on leaching from zeolite/cement composites," *Journal of Radioanalytical and Nuclear Chemistry*, 243 (2000) 839-841.

23. Dyer A., White K.J., "Cation diffusion in the natural zeolite clinoptilolite," *Thermochimica Acta*, 340-341 (1999) 341-348.

24. Ersoy B., Çelik M.S., "Electrokinetic properties of clinoptilolite with mono- and multivalent electrolytes", *Microporous and Mesoporous Materials*, 55 (2002) 305-312.

25. Flores V., Cabassud C., "Cu^{2+} removal by ion-exchange in a membrane reactor comparison with a packed-bed reactor,"*Journal of Membrane Science*, 162 (1999) 257-267.

26. Gomonaj V.I., Golub N.P., Szekeresh K.Yu., Gomonaj P.V., Charmas B., Leboda R., "Adsorption of lead(II) ions on Transcarpathian clinoptilolite," 19 (2001) 465-473.

27. Guansheng Z., Xingzheng L., Guangju L., Quanchang Z., "Removal of copper from electroplating effluents (potch water) using clinoptilolite, *Occurence, properties and utilization of natural zeolites, Budapest: Akademiai Kiado* (1988) 529-539.

28. Güçlü G., Gürdağ G., Özgümüş S., "Competitive removal of heavy metal ions by cellulose graft copolymers," *Journal of Applied Polymer Science*, 90 (2003) 2034-2039.

29. Helfferich, F., Ion Exchange, McGraw-Hill, 1962.

30. Inglezakis V.J., Loizidou M.D., Grigoropoulou H.P., "Equilibrium and kinetic ion exchange studies of Pb^{2+}, Cr^{3+}, Fe^{3+} and Cu^{2+} on natural clinoptilolite," *Water Research*, 00 (2001) 1-10.

31. Inglezakis V.J., Loizidou M.D., Grigoropoulou H.P., "Ion exchange of Pb^{2+}, Cu^{2+}, Fe^{3+}, and Cr^{3+} on natural clinoptilolite: selectivity determination and influence of acidity on metal uptake," *Journal of Colloid and Interface Science*, 261 (2003) 49-54.

32. Inglezakis V.J., Loizidou M.D., Grigoropoulou H.P., "Liquid holdup and flow dispersion in zeolite packed beds," *Chemical Engineering Science*, 56 (2001) 5049-5057.

33. Inglezakis V.J., Zorpas A.A., Loizidou M.D., Grigoropoulou H.P., "Simultaneous removal of metals Cu^{2+}, Fe^{3+} and Cr^{3+} with anions SO_4^{2-} and HPO_4^{2-} using clinoptilolite," *Microporous and Mesoporous Materials*, 61 (2003) 167-171.

34. Iznaga I.R., Gomez A., Fuentes G., Aguilar A., Ballan J., "Natural clinoptilolite as an exchanger of Ni^{2+}, NH_4^+ ions under hydrothermal conditions and high ammonia concentration," *Microporous and Mesoporous Materials*, 53 (2002) 71-80.

35. Kaban, Y., Ülkü, S., Ağaçe, M., Çetin, A., Topçu, S., Türkcan, S., Alkan, N., "Porsuk Çayının kirlilik durumu ve tabii zeolit yataklarının su tasfiyesinde kullanılması", *VII. Bilim Kongresi Çevre Araştırmaları Grubu Tebliğleri*, 1980.

36. Langella A., Pansini M., Cappeletti P., de Gennaro B., de Gennaro M., Colella C., "NH_4^+, Cu^{2+}, Zn^{2+}, Cd^{2+} and Pb^{2+} exchange for Na^+ in a sedimentary clinoptilolite, North Sardinia, Italy," *Microporous and Mesoporous Materials*, 37 (2000) 337-343.

37. Lehmann M., Zouboulis Matis K.A., "Modelling the sorption of metals from aqueous solutions on goethite fixed-beds," *Environmental pollution*, 113 (2001) 121-128.

38. Liberti, L., Helfferich, F., G., Mass Transfer and Kinetics of Ion Exchange, Martinus Nijhoff Publishers, 1983.

39. Lin S.H., Kiang C.D., "Chromic acid recovery from waste acid solution by an ion exchange process: equilibrium and column ion exchange modeling," *Chemical Engineering Journal*, 92 (2003) 193-199.

40. Malherbe, R.R., " Applications of Natural Zeolites in Pollution Abatement and Industry ", Handbook of Surfaces and Interfaces of Materials, edited by H.S. Nalwa, Volume 5: Biomolecules, Biointerfaces and Applications, 2001, 495-520.

41. Mark A.K., "The removal of copper and nickel from aqueous solution using Y zeolite ion exchangers," *Colloids and Surfaces A: Phsicochemical and Engineering Aspects*, 138 (1998) 11-20.

42. McCabe, W., L., Smith, J., C., Harriot, P., Unit operations of chemical engineering, McGraw-Hill, 1985.

43. Mier M.V., Callejas R.L., Gehr R., Cisneros B.J., Alvarez P.J.J., "Heavy metal removal with Mexican clinoptilolite: multi-component ionic exchange," *Water Research*, 35 (2001) 373-378.

44. Mondale K.D., Carland R.M., Aplan F.F., "The comparative ion exchange capacities of natural sedimentary and synthetic zeolites", Miner Eng., 4/5 (8) (1995) 535-548.

45. Möller T., Harjula R., Lehto J., "Ion exchange of ^{85}Sr, ^{134}Cs and ^{57}Co in sodium titanoosilicate and the effect of crystallinity on selectivity," *Separation and Purification Technology*, 28 (2002) 13-23.

46. Nikashina V.A., Tyurina V.A., Mironova L.I., "Sorption of copper (II) ions on the sodium and the calcium form of zeolites", J Chromatogr, 201 (1984) 107-112.

47. Nikashina V.A., Galkina N.K., Komarova V., Anfilov B.G., Argin M.A., "Evaluation of clinoptilolite rich tuffs as ion-exchangers," Natural Zeolites 93: Occurrence, Properties, Use, Ming, D.W. and Mumpton, F.A., 1995, pp 289-297.

48. Nikolova N., Stamenov S., Ninova V.K., Using of modified zeolites for purification of heavy metals ions from wastewater, Annual of the university of mining and geology, St.Ivan Rilski, vol.44-45, part II, Mining and Mineral Processing, Sofia, 2002, pp.151-154.

49. Panayotova M.I., "Kinetics and thermodynamics of copper ions removal from wastewater by use of zeolite," *Waste Management*, 21 (2001) 671-676.

50. Peric J., Trgo M., Medvidovic N.V., "Removal of zinc, copper and lead by natural zeolite- a comparison of adsorption isotherms," *Water Research,* 38 (2004) 1893-1899.

51. Perraki Th., Orfanoudaki A., "Minerological study of zeolites from Pentalofos area, Thrace, Greece, 25 (2004) 9-16.

52. Petrus R., Warchol J., "Ion exchange equilibria between clinoptilolite and aqueous solutions of Na^{+}/Cu^{2+}, Na^{+}/Cd^{2+} and Na^{+}/Pb^{2+}," 61 (2003) 137-146.

53. Rivera, A., Rodriguez-Fuentes, G., Altshuler, E., "Time evolution of a natural clinoptilolite in aqueous medium: conductivity and pH experiments", *Microporous and Mesoporous Materials*, 40 (2000) 173-179.

54. Rubcumintara T., Han K.N., "The effect of concentration and temperature on diffusivity on metal compounds," *Metallurgical Transactions B*, 21B (1990) 429-438

55. Ruthven D.M., Principles of Adsorption Processes ,John Wiley and Sons, 1984.

56. Sağ Y., Aktay Y., "Application of equilibrium and mass transfer models to dynamic removal of Cr(VI) ions by chitin in packed column reactor," *Process Biochemistry*, 36 (2001) 1187-1197.

57. Sapari N., Idris A., Hisham N., Hamid Ab., "Total removal of heavy metal from mixed plating rinse wastewater," *Desalination*, 106 (1996) 419-422.

58. Semmens J.M., Martin P.W., " The influence of pre-treatment on the capacity and selectivity of clinoptilolite for metal ions," *Water Research*, 22 (1988) 537-542.

59. Sherman J., "Ion exchange separations with molecular sieve zeolites," *AIChE Symposium Series*, 179 (1978) 33-39.

60. Top A., "Cation exchange (Ag^{+}, Zn^{2+}, Cu^{2+}) behavior of natural zeolites", *M.S. Thesis*, İzmir Institute of Technology, 2001.

61. Top A., Ülkü S., "Silver, zinc, and copper exchange in a Na-clinoptilolite and resulting effect on antibacterial activity," *Applied Clay Science*, 00 (2004), 1-7.

62. Tsitsishvili G.V., Andronikashvili, T.G., Kirov, G.N., Filizova, L.D., Natural Zeolites, Ellis Horwood, New York, 1992.

63. Türkmen M., "Removal of heavy metals from waste waters by use of natural zeolites", *M.S. Thesis*, İzmir Institute of Technology, 2001.

64. Ülkü S., 1984, "Application of natural zeolites in water treatment", *Umwelt'84*, (1984) 26-29.

65. Ülkü S., Balköse D., Çağa T., Özkan F., Ulutan S., "A study of adsorption of water vapour on wool under static and dynamic conditions," *Adsorption*, 4 (1998) 63-73.

66. Wang Y., Lin S., Juang R., "Removal of heavy metalions from aqueous solutions using various low-cost adsorbents," *Journal of Hazardous Materials*, B102 (2003) 291-302.

67. Xu Y., Nakajima T., Ohki A., "Adsorption and removal of arsenic(V) from drinking water by aluminum-loaded Shirasu-zeolite," *Journal of Hazardous Materials,* B92 (2002) 275-282.

68. Yaşyerli, S., Ar, I., Doğu, G., Doğu, T., " Removal of hydrogen sulfide by clinoptilolite in a fixed bed adsorber", *Chemical Engineering and Processing*, 00 (2002) 1-8.

69. Zamzow M.J., Schultze L.E., "Treatment of acid mine drainage using natural zeolites", Natural Zeolites 93: Occurrence, Properties, Use, Ming, D.W. and Mumpton, F.A., 1995, pp 405-413.

APPENDICES

A.1. Interpretation of Characterization Studies

In order to determine the optimum grinding time to reduce the particles under 25 μm, the same amount of samples (30 g) were ground with different time intervals such as 1, 2 and 4 minutes and then the samples were analysed using Sedigraph. To determine if the zeolite particles were dispersed or not within the solution, a drop of the solution was analysed under optic microscope and scanning electron microscopy. As a result of this optic microscope and scanning electron microscope pictures were obtained as shown in Figures A.1 and A.2, respectively.

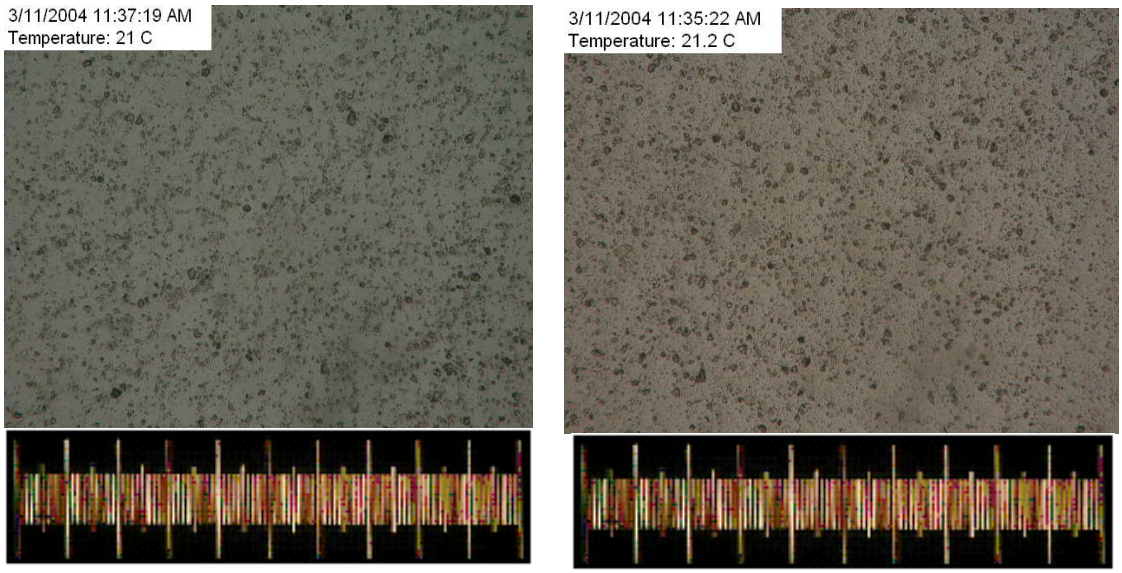

(100 μm) (100 μm)

Figure A.1. Optic Microscope Pictures of Dispersed Zeolite Particles

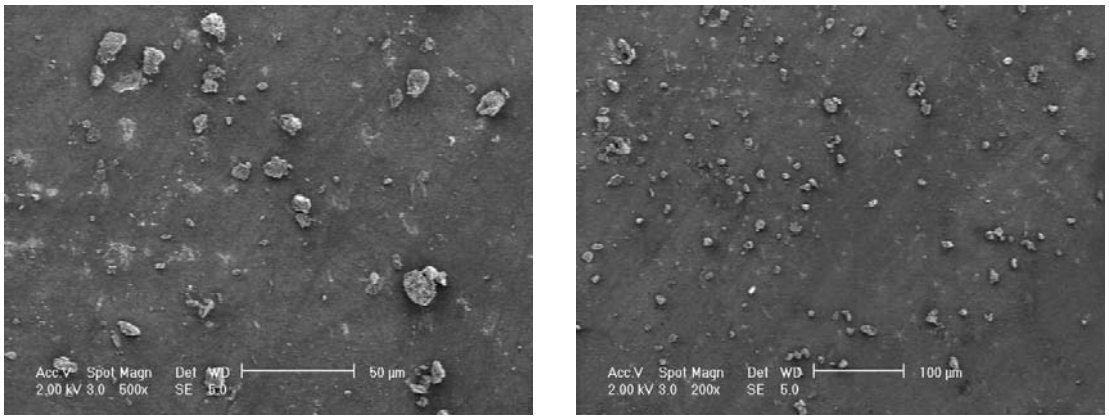

Figure A.2. SEM Pictures of Dispersed Zeolite Particles

As was proved by the optic microscope and SEM pictures, the particles were well dispersed within the solution therefore they were ready to be investigated with the sedigraph.

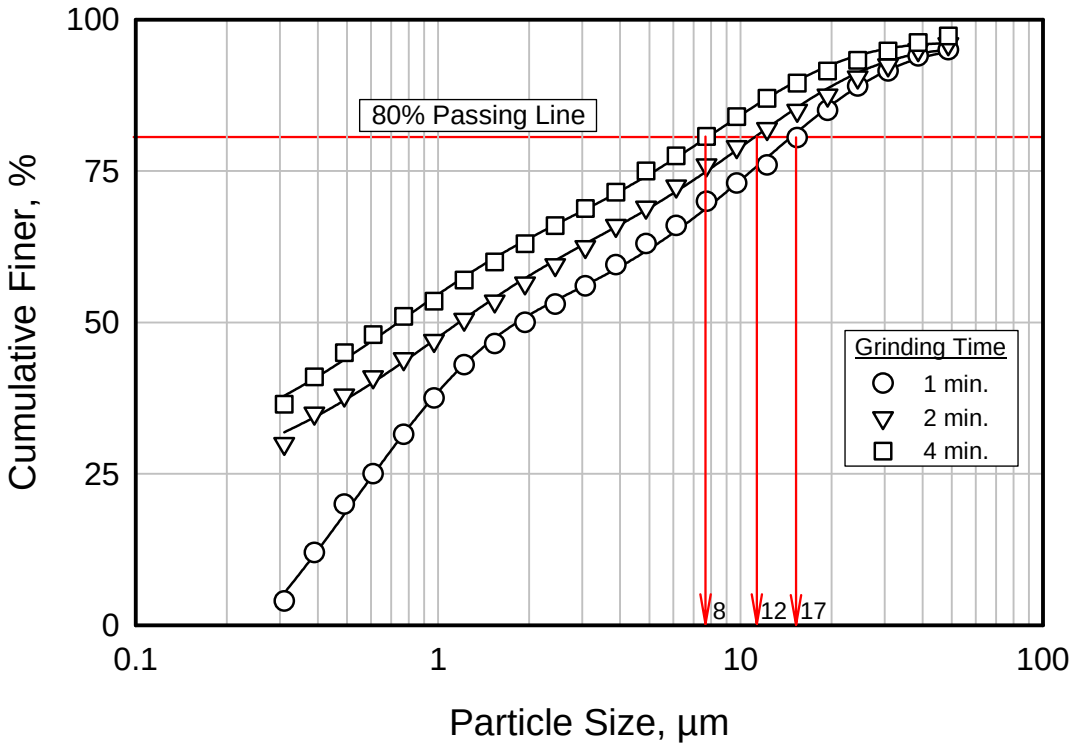

Figure A.3. Particle Size Distribution of Zeolite Particles for the Selection of Grinding Times

As can be seen from Figure A.3, 80% of the particles are under 8, 12, and 17 µm for 1, 2, and 4 minute grinding times respectively. In order to obtain particle size under 10 µm, 2 minute grinding time was determined to be optimum.

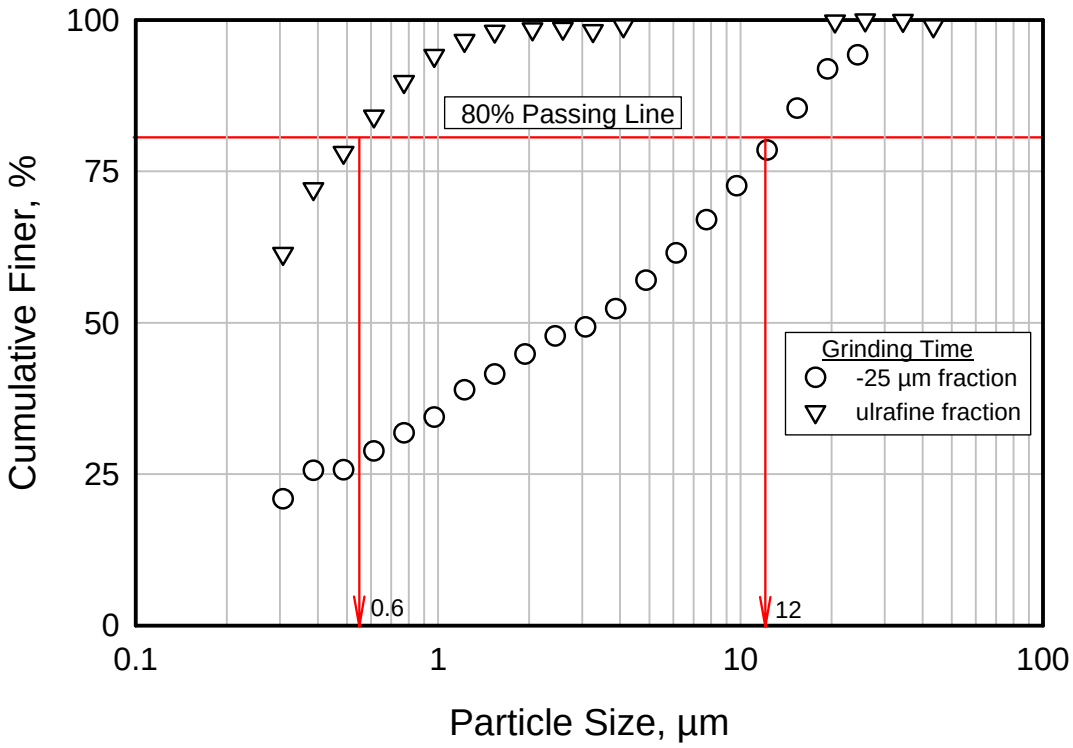

Figure A.4. Particle Size Distribution of Zeolite Particles less than 25 µm

Figure A.4 shows that 80% of the fraction under 25 µm has particle size below 12 µm, while 80% of ultrafine fraction has particle size below 0.6 µm.

A.1.1. Reference Intensity Ratio for Quantitative Analyses Using X-ray Diffraction

The natural material used in this work namely, CP2 was characterized by X-ray diffractometry (XRD) on a Philips X'pert Pro employing the Cu Kα radiation of power settings of 30 kV and 30 mA.

In order to determine the particle size effect for quantitative analyses, six particle size range of CP2 zeolite were investigated in Figures A.5 and A.6. As can be seen from Figure A.5, no significant differences were observed in the x-ray patterns of the particles sizes namely, >1.7, 425µ - 1.7mm, 106 - 425µ, 25-106µ. As can be understood from this result mineralogical content of CP2 zeolite didn't change with different particle sizes and hence sample preparation plays an important role in the characterization studies as was discussed in chapter 6. Accurate x-ray diffraction intensities from a powder sample require that the grain (i.e. crystallite) size be small, at

least 10 μm and preferably smaller (Bish, 1994). Therefore, the zeolites were ground more effectively with the aid of a grinding machine under 10 μm and that the peak intensities of ground zeolites were slightly higher than the unground ones.

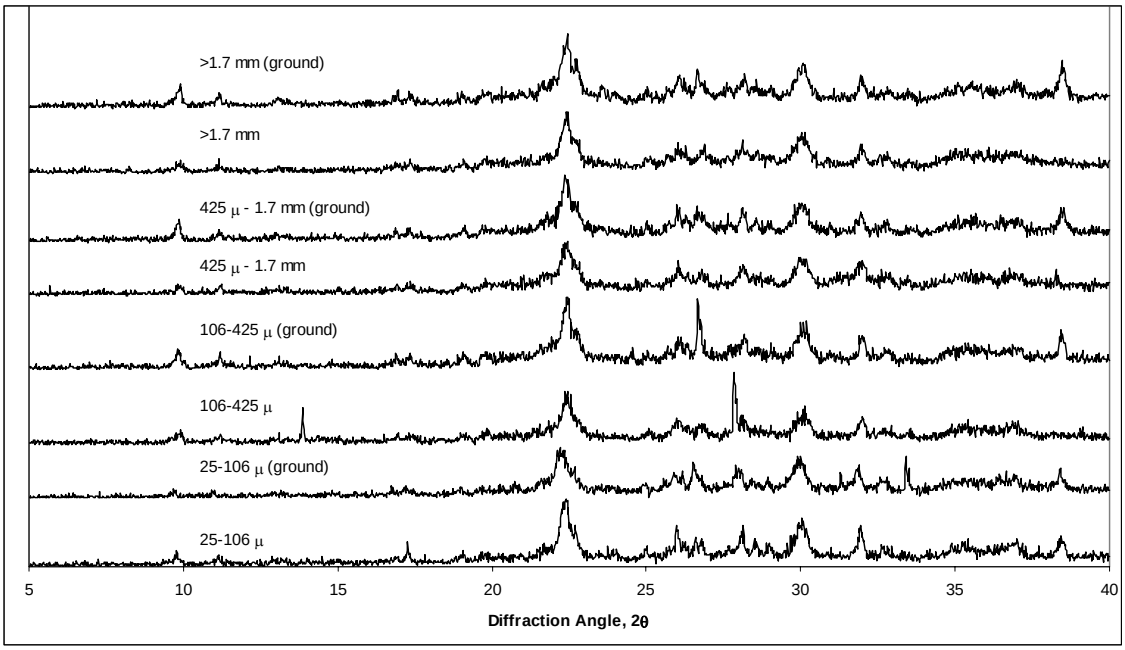

Figure A.5. XRD Spectrums of the CP2 higher than 25 μm Compared with Ground Samples

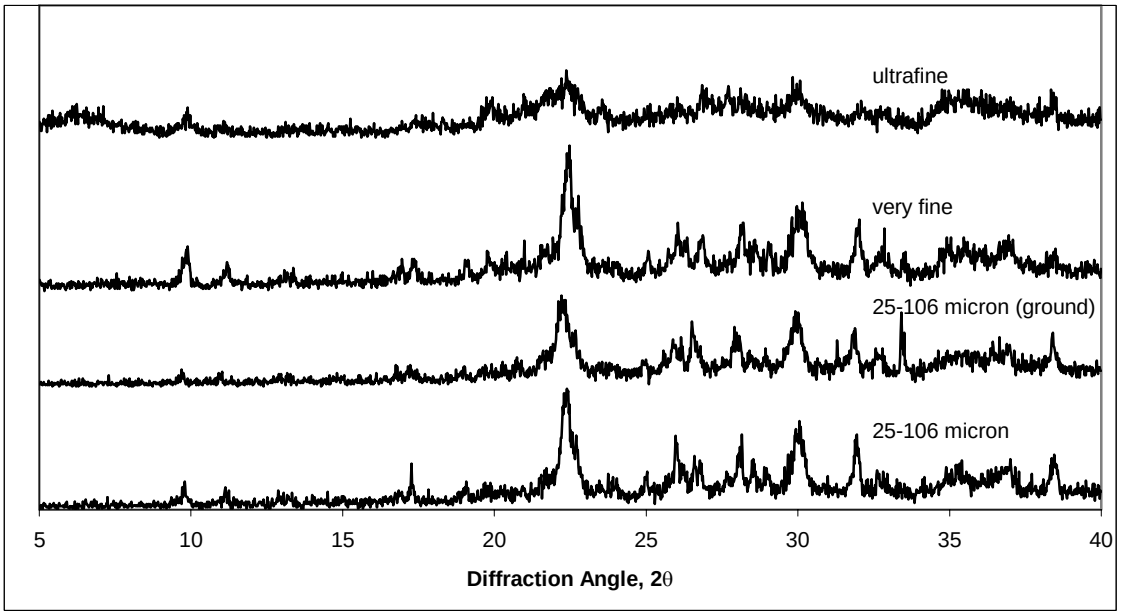

Figure A.6. XRD Spectrums of the CP2 less than 25 μm

In Figure A.6, it can be said that, although there aren't much intensity differences between the particle sizes, zeolite particles coded with "very fine" have the highest peak intensities because they were already under 10 μm without a need of further grinding process for XRD analyses. This particle size range which is under 10 μm represents the crystal size of clinoptilolite sample used in the study. For the quantitative determination of clinoptilolite content in the zeolite, particle size range under 10 μm was used due to the reasons indicated. It's also clearly seen that the crystal structure of ultrafine particles have collapsed since their peak intensities are quite low.

Figure A.7 represents the XRD patterns of standard clinoptilolites namely IDA and CAL used in the study. They have much higher intensities when compared to CP2 zeolite as can be seen from the figure. Figure A.7 shows the XRD patterns of α-alumina powder (corundum), which was used as the internal standard. In the quantitative determination, 2θ ranges between 5 and 40^{o} 2θ were used to measure only the reflections of interest which involves the highest peak as 35.21^{o} 2θ of corundum.

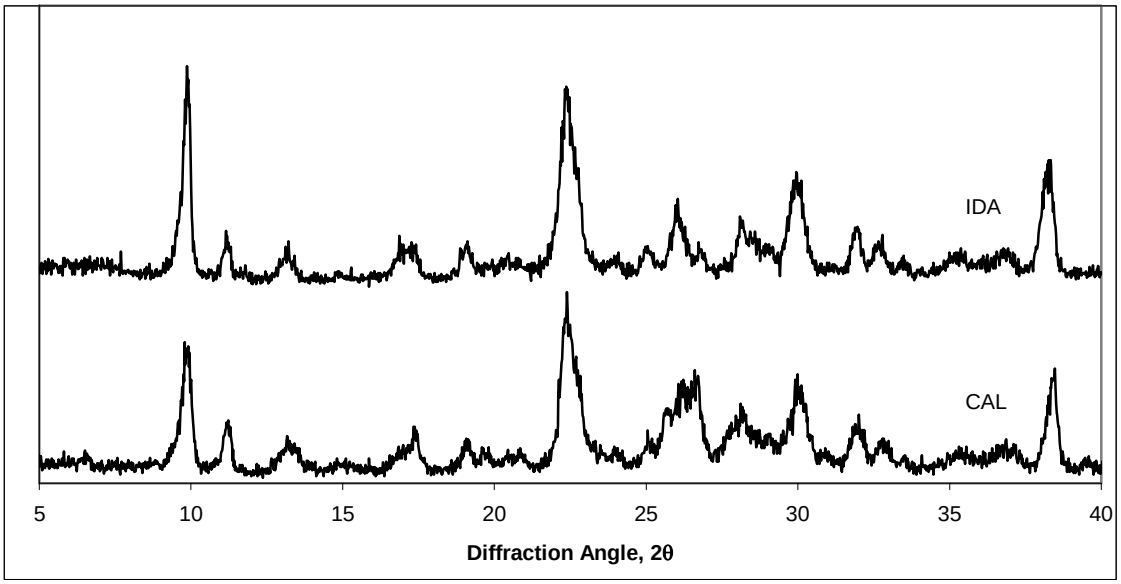

Figure A.7. XRD Spectrums of the Standard Clinoptilolite Particles (Idaho, California) less than 10 μm

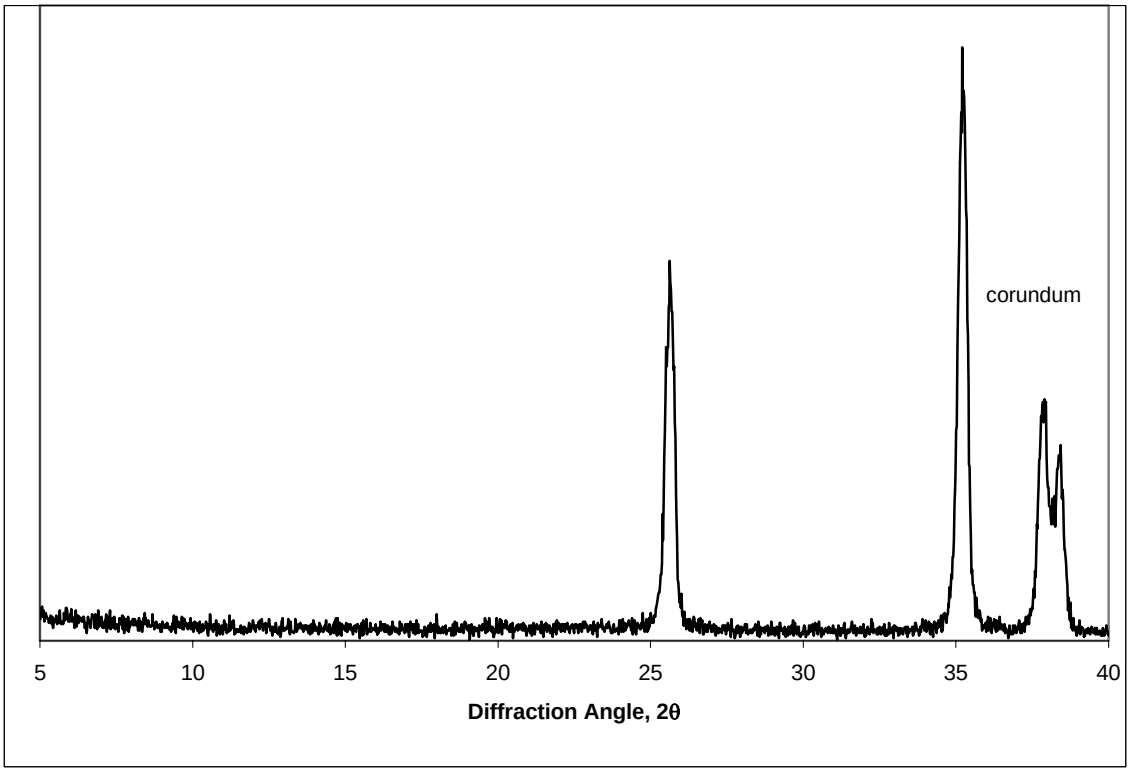

Figure A.8. XRD Spectrum of the Corundum (CT 3000 SG) less than 0.7 μm as an Internal Standard

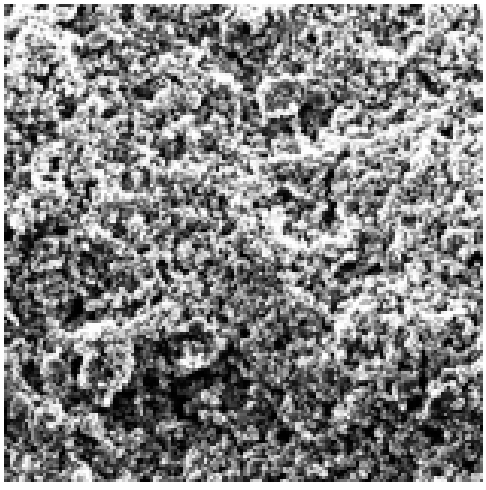

Figure A.9. SEM Micrograph of Corundum (CT 3000 SG)

As can be seen from the SEM micrograph (Figure A.9), the particle size of corundum used was less than 1 μm.

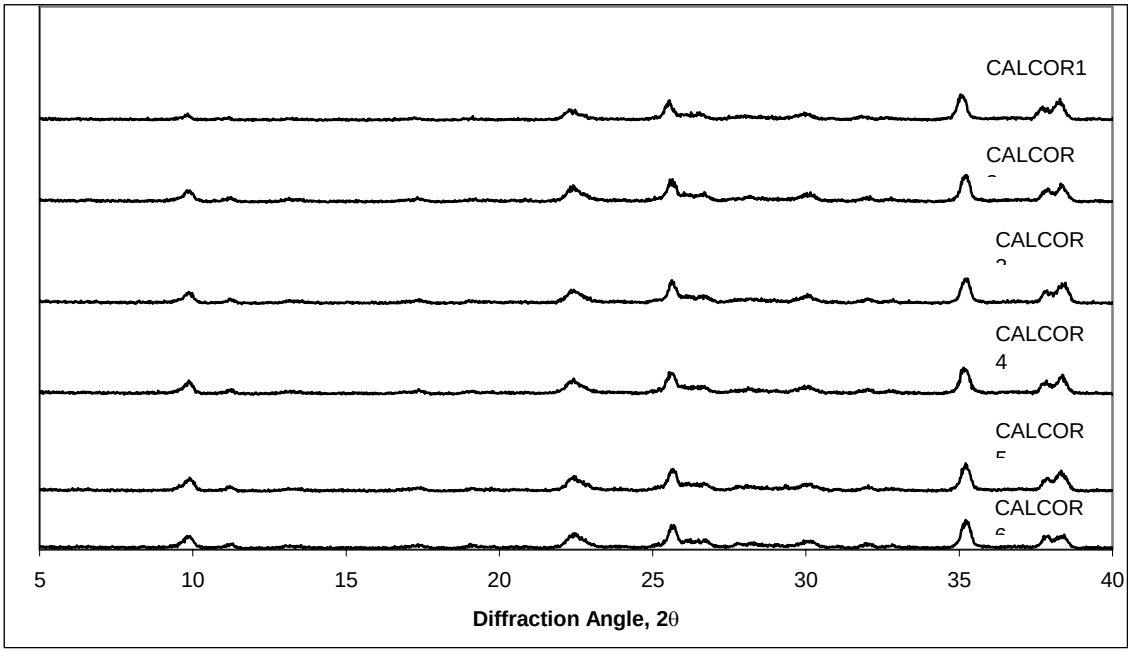

Figure A.10. Six XRD Spectrums of the Clinoptilolite Standard Particles (California) less than 10 μm

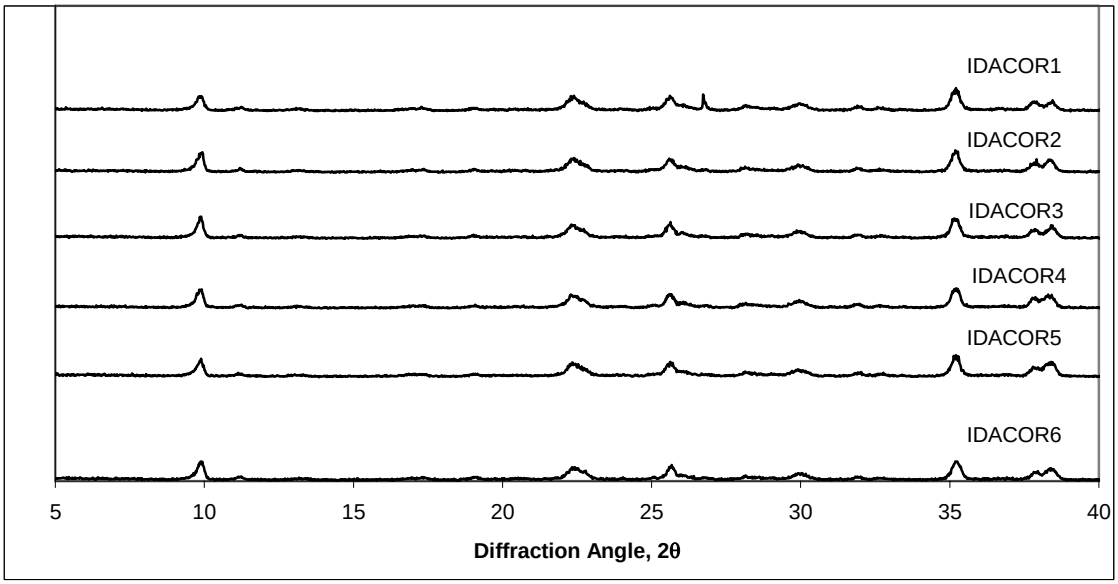

Figure A.11. Six XRD Spectrums of the Clinoptilolite Standard Particles (Idaho) less than 10 μm

In order to determine the accuracy of the measurements, XRD spectrums of six replicate runs for CAL and IDA were constructed in Figures A.10 and A.11. As can be seen from these figures, there were no significant differences between the x-ray patterns of the standard samples with small exceptions.

Quantitative determination of phase abundances using XRD is a technique in wide use today. Of the various methods employed, RIR method, is one of the most common because it can provide reliable results for all sample types. The RIR method requires that reference intensity ratios have been measured for one or more reflection for each phase to be analysed before analyses of unknowns. The reference intensity ratio is defined as the intensity of the peak of interest for a given phase divided by the intensity of a peak from a standard in a 50:50 mixture (Chipera et al., 1994).

Generally, it's more desirable to use the sum of reflections from a localized region in the diffraction pattern than to use individual reflections from a phase. Thus, for clinoptilolite, two separate intensity regions were chosen: the 020 reflection at 9.8^{o} 2θ and the sum of the intensity in the range 22.1-23.0^{o} 2θ (Chipera et al., 1994). To determine the RIR values for clinoptilolite, six replicate XRD scans were conducted on each RIR standard. Before each replicate analyses, the standard was removed from the sample mount, remixed with the standard remaining in the sample bottle, and the sample mount was remade. For phases with chemical or preferred orientation variability such as clinoptilolite, two RIR standards were prepared with six replicate runs conducted on each as outlined above.

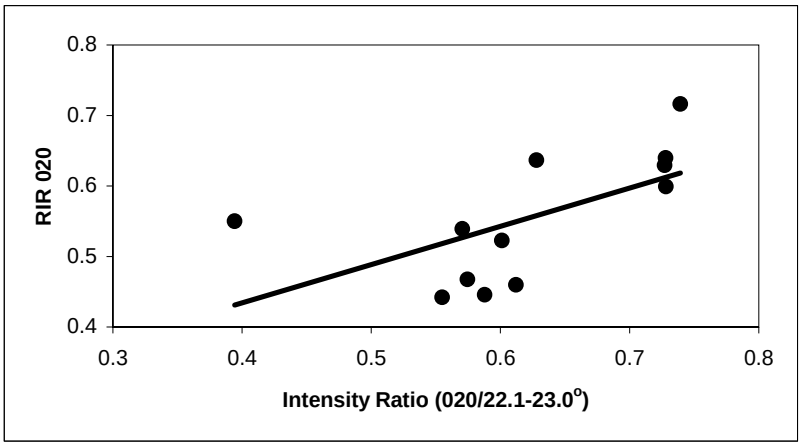

Figure A.12. RIR Normalization Curve for Quantitative Determination

For the 020 clinoptilolite reflection, Figure A.12 was constructed by plotting the measured RIR value for the 020 reflection versus the intensity ratio between the 020 reflection and the (22.1-23^{o}2θ) sum peak for each of two clinoptilolite standards. In a study performed by Chipera et al., 1994, they stated that precise RIR values for a reflection or sum peak can be obtained by plotting the RIR for a given peak versus the ratio of the intensities measured for this peak to a second peak or reflection as in the

case of Figure A.12. This technique minimizes the effects of both preferred orientation and chemical variabilities by producing the curve of RIR values. From this curve, improved RIR values can be obtained during analysis of unknowns and can thus provide more precise and accurate determination of clinoptilolite abundance.

By the help of the intensity ratios and corresponding RIR values (Figure A.12), the below expressed equation was obtained which is unique for the zeolite being used.

$$RIR_{020} = 0.2169 + 0.5431 * (INT_{020} / INT_{22.1\text{-}23}{}^{o}) \quad (A.1)$$

It is important to note that although RIR values and determinative equations were given in this study or in other scientists' studies, RIR values are dependent also on the instrument geometry and physical dimensions of the sample holder. Therefore, RIR values should be measured for each instrument/sample configuration (Chipera et al., 1994).

As a result of the quantitative analyses performed, the natural zeolite tuff used in this study was determined to contain 64 ± 5.36 % of clinoptilolite mineral. Also, other zeolite samples, which have not been used in ion exchange experiments, analysed quantitatively for comparing them with the quantitative analyses results kindly supplied by Fahri Esenli and given in Table A1.

Table A.1. Quantitative Analyses Results of some Zeolite Samples

	w% (Fahri Esenli)	w% ± 5.36 (This Study)
bigadiç	80-85	69.96
gördes	60-70	70.73
kıranköy	80-85	79.36
avdaldere	60-70	71.49

The other constituents of the CP2 zeolite were determined qualitatively by using the search match program (Graphic and Identify). According to this, clay and quartz were the other major constituents of the natural zeolite as shown in Figure A.13.

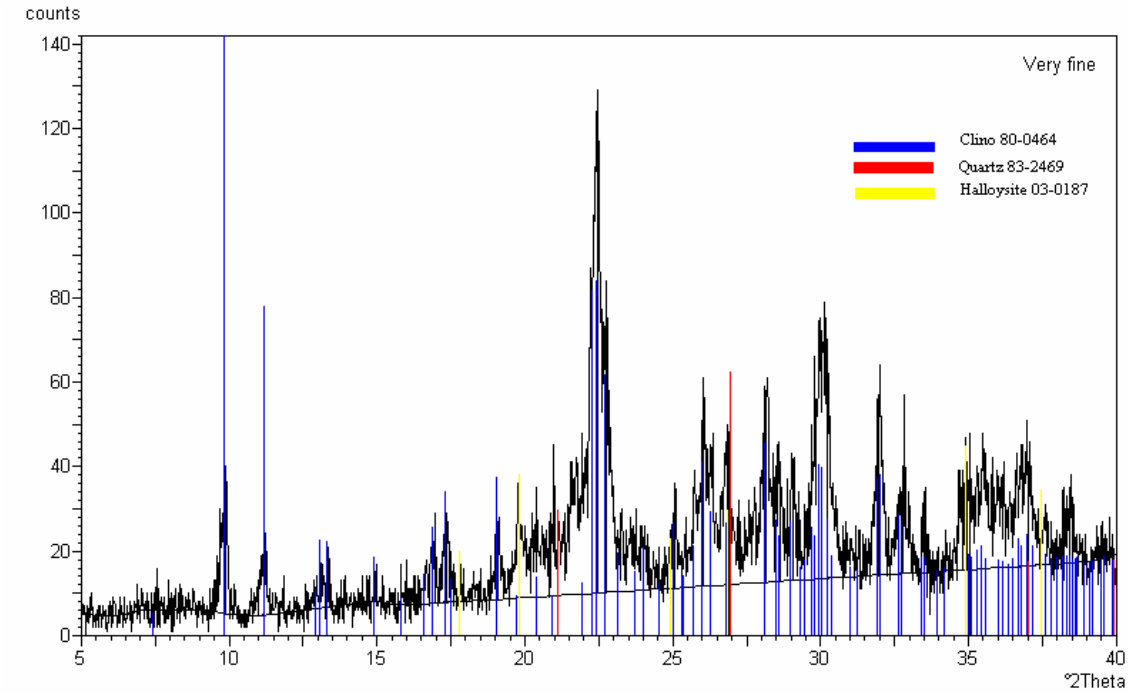

Figure A.13. Search Match Results of CP2 Sample

A.1.2. Scanning Electron Microscopy Analyses

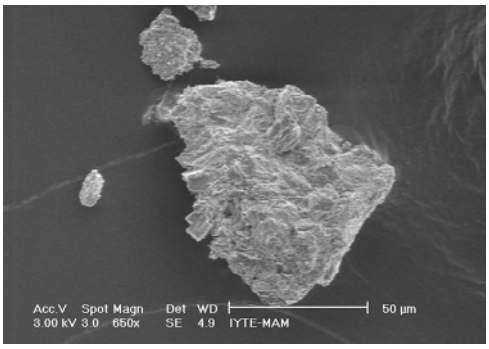

25µm–106µm (original)

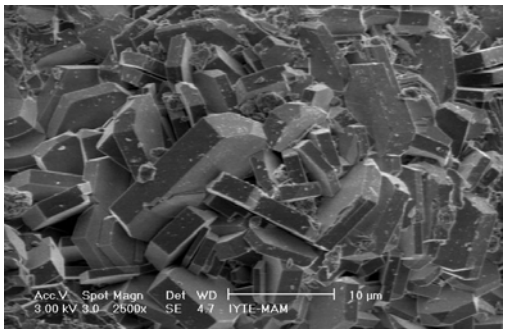

25 µm – 106µ m (original)

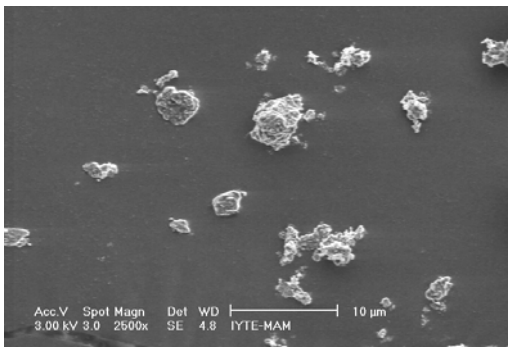

25µm–106µm (2 min ground, <25 µm)

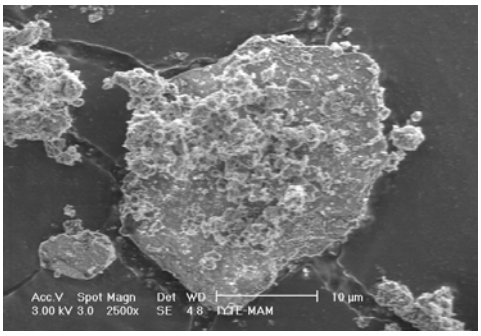

25 µm – 106µ m (2 min ground, <25 µm)

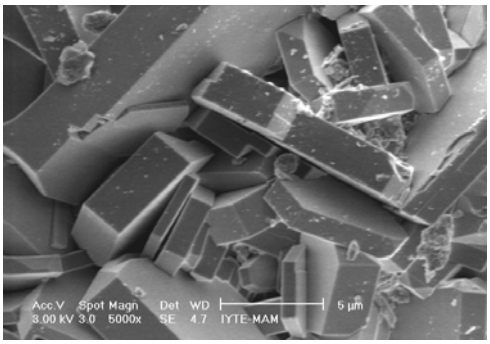

25 µm – 106µ m (original)

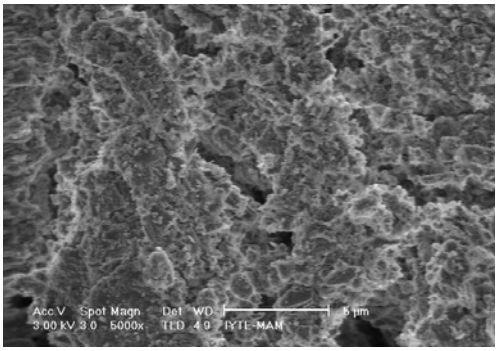

25µm–106µm (2 min ground, <25µm)

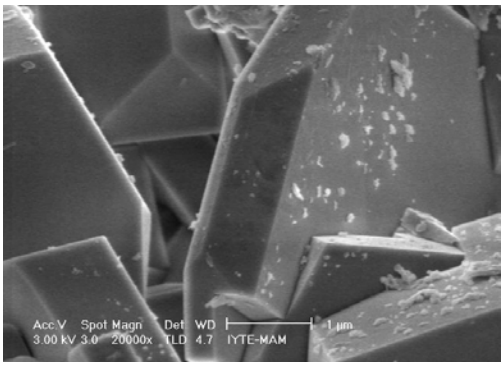

25 µm – 106µ m (original)

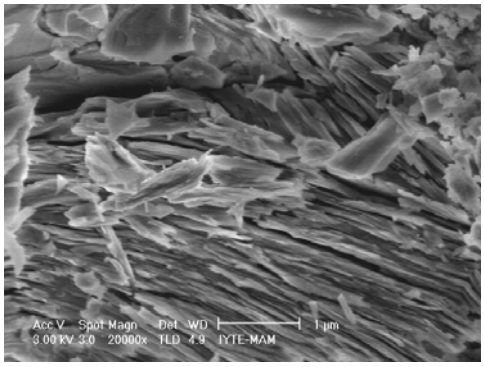

25µm–106µm (2 min ground, <25 µm)

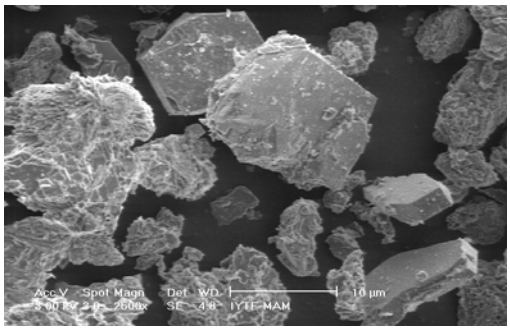

Very Fine

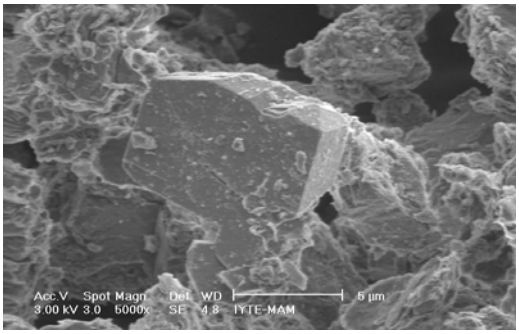

Very Fine

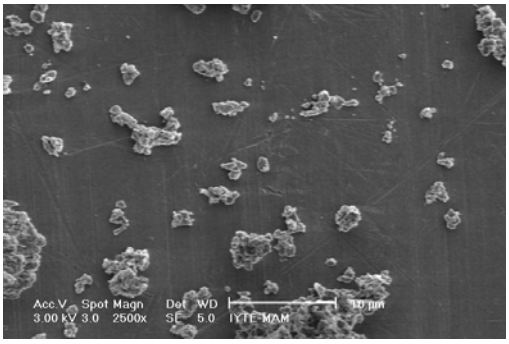

Ultra Fine

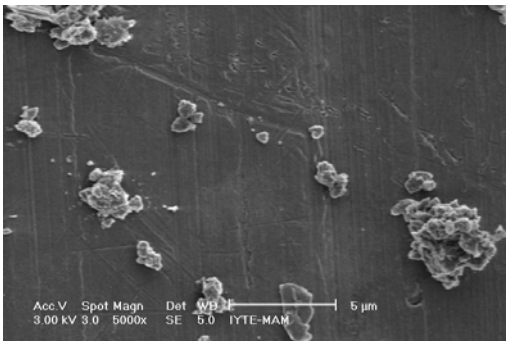

Ultra Fine

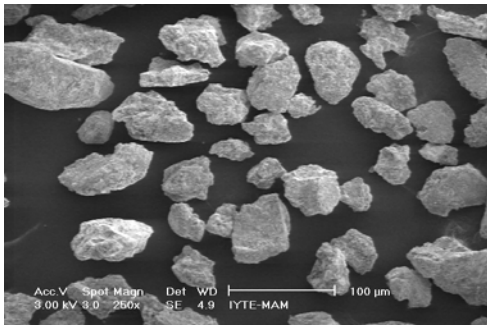

106µm–425µm (original)

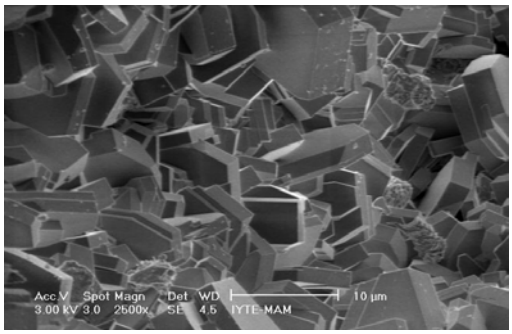

106µ m – 425µ m (original)

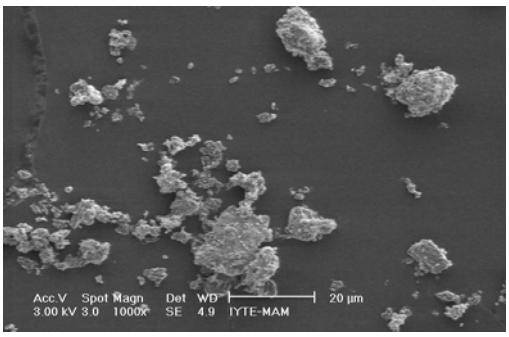

106µm–425µm (2 min ground, <25 µm)

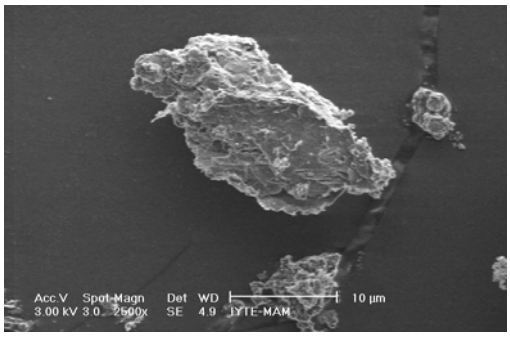

106µm–425µm (2 min ground, <25 µm)

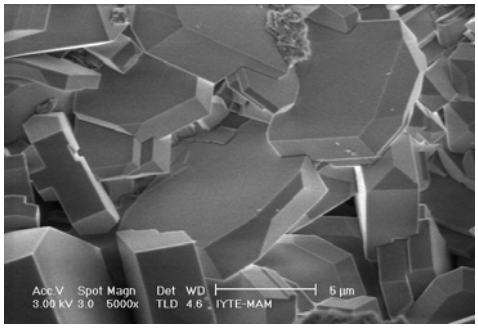

106µm–425µm (original)

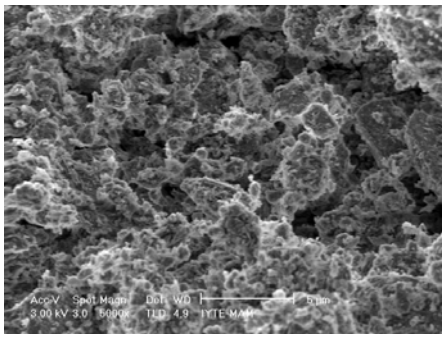

106µm–425µm (2 min ground, <25 µm)

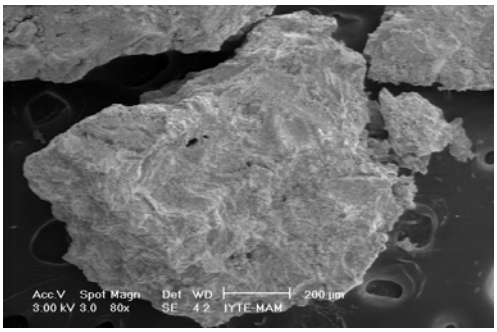

425µm–1.7mm (original)

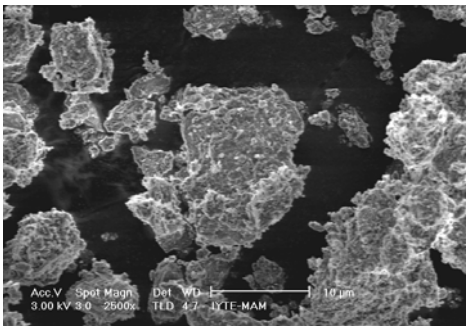

425µm–1.7mm (2 min ground, <25µm)

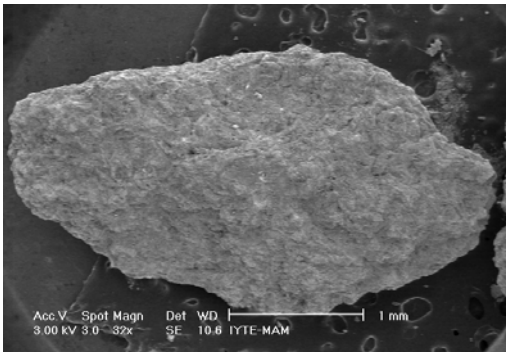

>1.7mm (original)

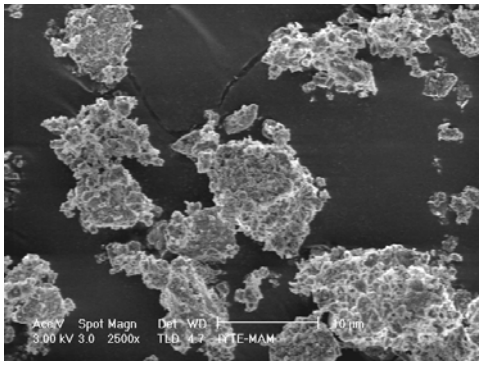

>1.7mm (2 min ground, <25µm)

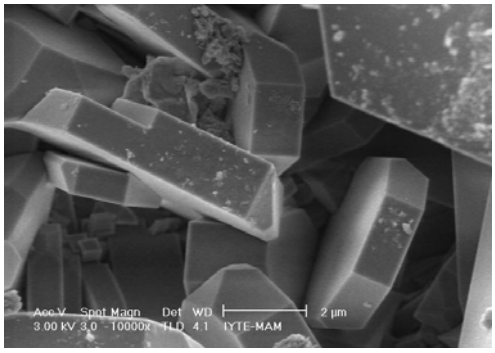

>1.7mm (original)

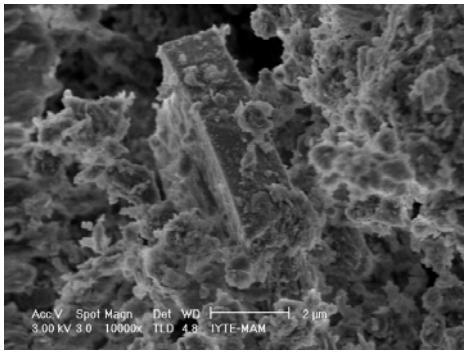

>1.7mm (2 min ground, <25 µm)

Figure A.14. SEM Micrographs of Zeolites

The crystal structures of all the fractions and their ground forms were investigated using SEM pictures in different magnifications (Figure A.14). When taking the SEM pictures indicating crystal structures, first of all, individual particles as a whole were investigated. Afterwards, their micrographs were taken with different magnifications in order to determine the crystal structure more clearly. Generally, original zeolite particles preserve their crystal structures while, their ground forms have some deformations such that some of their crystals which are greater than 10 μm have been broken. From the figures, it's seen that the size of the crystals are between 5-10 μm. Also the presence of some amorphous structure was observed after grinding operation as in the case of 25-106 μm due to overgrinding. As was also proved by the x-ray analyses, as particle size decreased, better crystal structure was observed.

A.2. Design of Experiments

Factorial designs are widely used in experiments involving several factors where it is necessary to study the joint effect of the factors on a response. There are several special cases of the general factorial design that are important because they are widely used in research work and also because they form the basis of other designs of considerable practical value.

The most important of these special cases is that of k factors, each at only two levels. High and low values of these levels were given in Table A.2. A complete replicate of such a design requires 2^k observations and is called a 2^k factorial design. The 2^k design is particularly useful in the early stages of experimental work, when there are likely to be many factors to be investigated. It provides the smallest number of runs with which k factors can be studied in a complete factorial design.

Breakthrough time, which was selected as the time when the effluent concentration was reaching a 5% of the influent concentration, was chosen as a response for this study. Since there are only two levels for each factor, it was assumed that the response was approximately linear over the range of the factor levels chosen. As it's stated in literature (Montgomery, 2001), in many factor screening experiments, when it's been just started to study the process or system this is often a reasonable assumption.

In this study, there were three factors such as A, B and C namely concentration, packing height and flow rate, respectively. Therefore, the design was called a 2^3 factorial design and the eight treatment combinations were given in Table A.2.

Table A.2. Packed Column Studies for Design of Experiments

Run C: Flow Rate	Factor 1 A: Conc. [mg/L]	Factor 2 B: Packing Height [cm]	Factor 3 C: Flow Rate [ml/min]	Response (B.T.)* exp [min]	Response (B.T.)* model [min]
1	100.00	18.75	4.75	146	141.88
2	100.00	25.00	4.75	330	334.13
3	200.00	25.00	4.75	54	49.88
4	200.00	18.75	4.75	30	34.13
5	200.00	25.00	2.86	390	394.13
6	200.00	18.75	2.86	143	138.88
7	100.00	18.75	2.86	410	414.13
8	100.00	25.00	2.86	850	845.88

* B.T. is the Breakthrough Time

In order to be able to construct Table A.2, eight packed column runs were performed. Figures A.15-A.21 represent breakthrough curves at varying concentrations, packing heights and flow rates. Consequently, breakthrough times corresponding to these experiments were then calculated experimentally by the help of the figures constructed. Design of experiment studies were all performed using "Design of Expert 6.0.10" computer program. Results of model predictions for breakthrough time were given in Table A.2. According to this, it can be said that breakthrough times were well predicted by using 2^3 factorial design model. Correlation coefficient was calculated as 0.9999 for two data series.

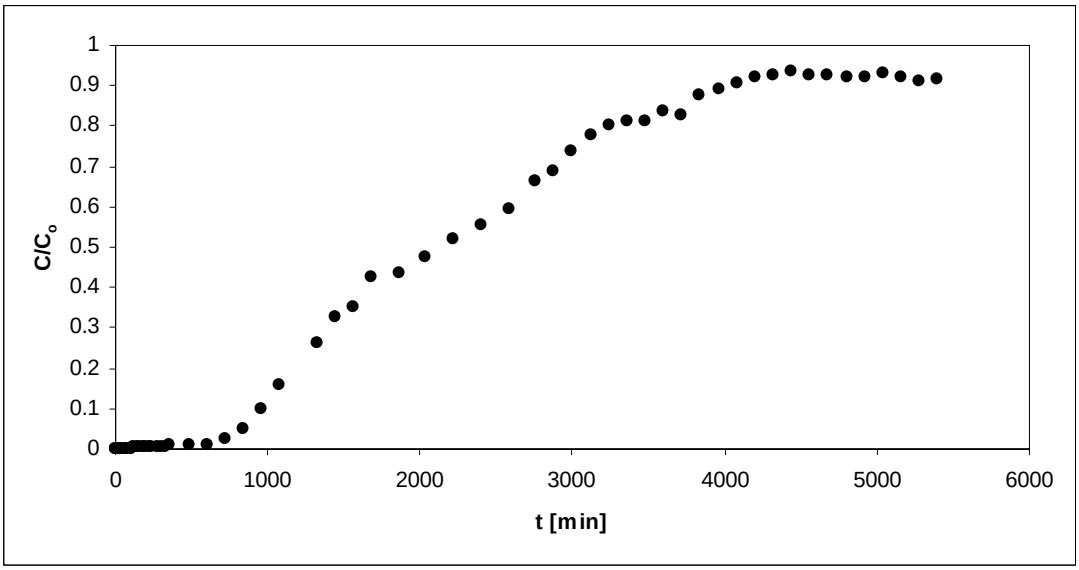

Figure A.15. Breakthrough Curve for Cu^{2+} Exchange on CP1 with Respect to Concentration Ratio and Time at 29°C with a flow rate of 2.86 ml/min (Packing Height= 25 cm, Initial Cu^{2+} Concentration= 100 mg/L).

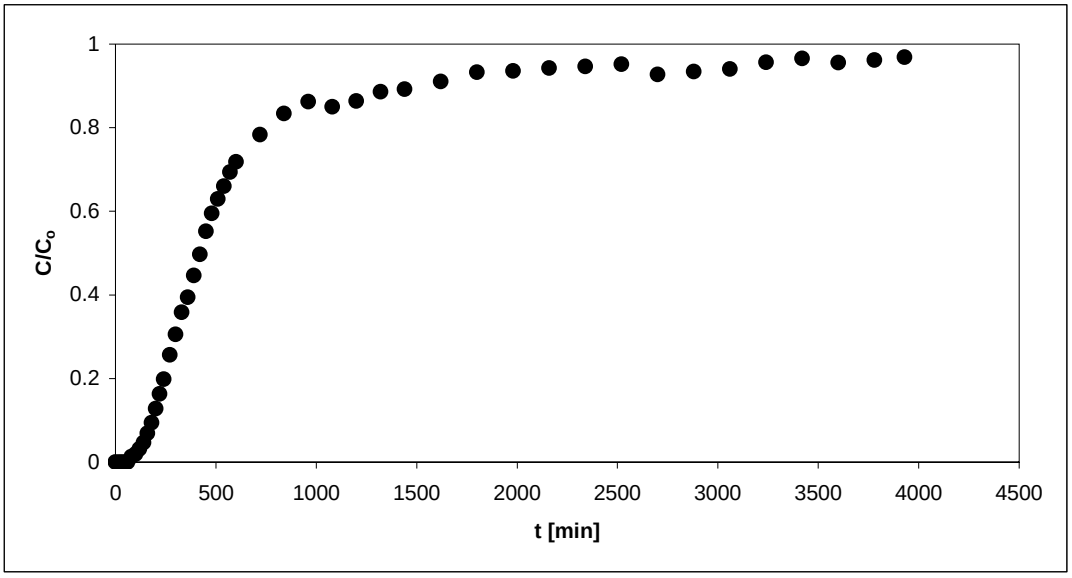

Figure A.16. Breakthrough Curve for Cu^{2+} Exchange on CP1 with Respect to Concentration Ratio and Time at 29°C with a flow rate of 2.86 ml/min (Packing Height= 18.75 cm, Initial Cu^{2+} Concentration= 200 mg/L).

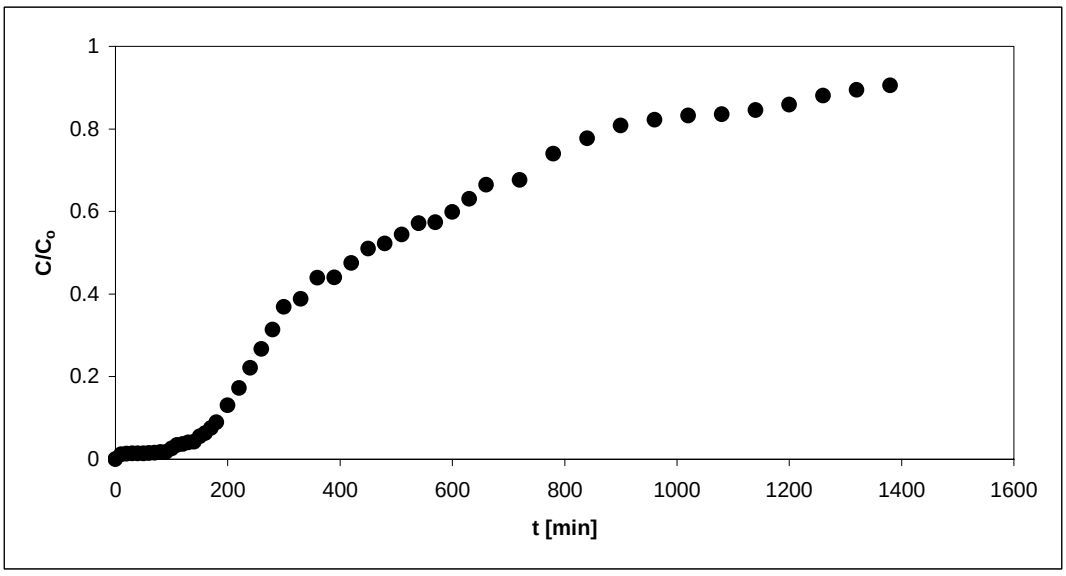

Figure A.17. Breakthrough Curve for Cu^{2+} Exchange on CP1 with Respect to Concentration Ratio and Time at 29°C with a flow rate of 4.75 ml/min (Packing Height= 18.75 cm, Initial Cu^{2+} Concentration= 100 mg/L).

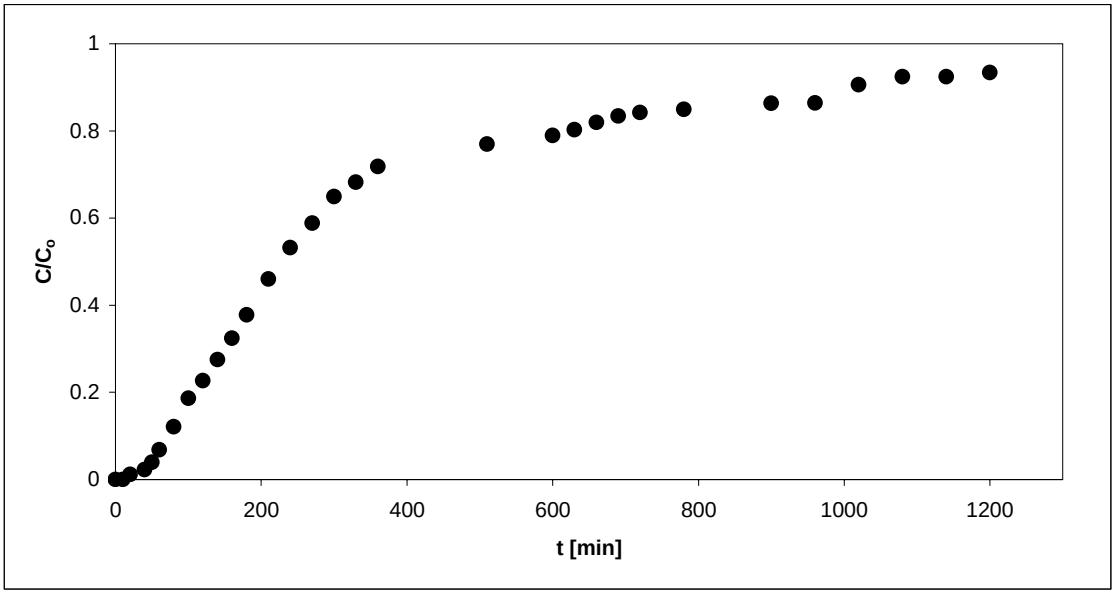

Figure A.18. Breakthrough Curve for Cu^{2+} Exchange on CP1 with Respect to Concentration Ratio and Time at 29°C with a flow rate of 4.75 ml/min (Packing Height= 25 cm, Initial Cu^{2+} Concentration= 200 mg/L).

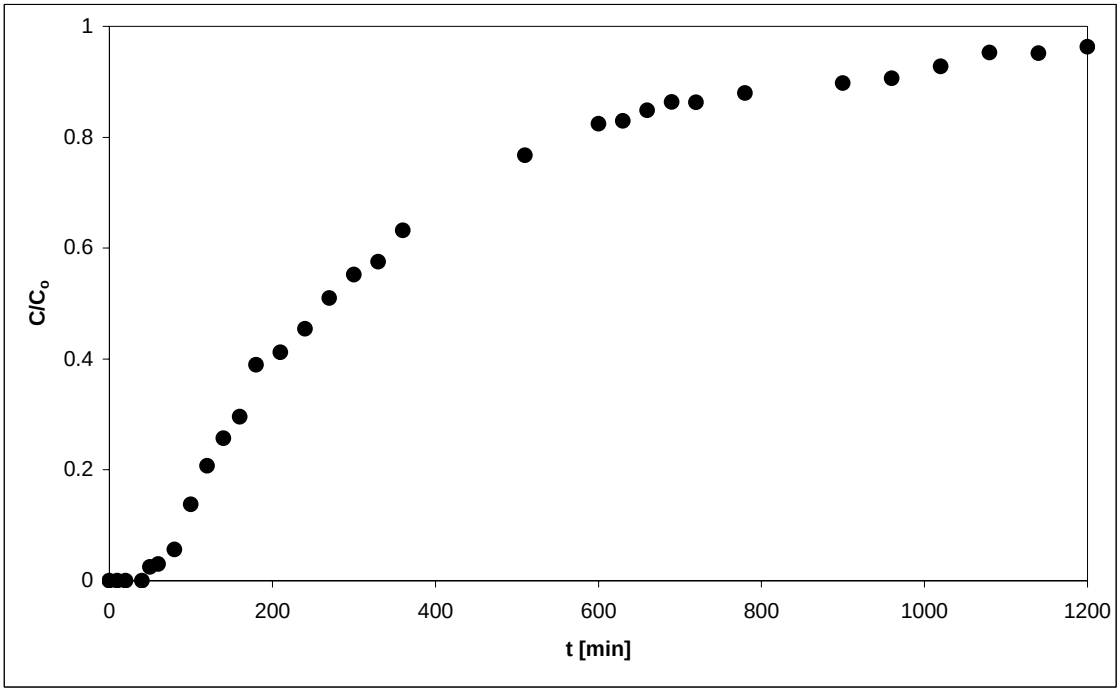

Figure A.19. Breakthrough Curve for Cu^{2+} Exchange on CP1 with Respect to Concentration Ratio and Time at 29°C with a flow rate of 2.86 ml/min (Packing Height= 18.75 cm, Initial Cu^{2+} Concentration= 100 mg/L).

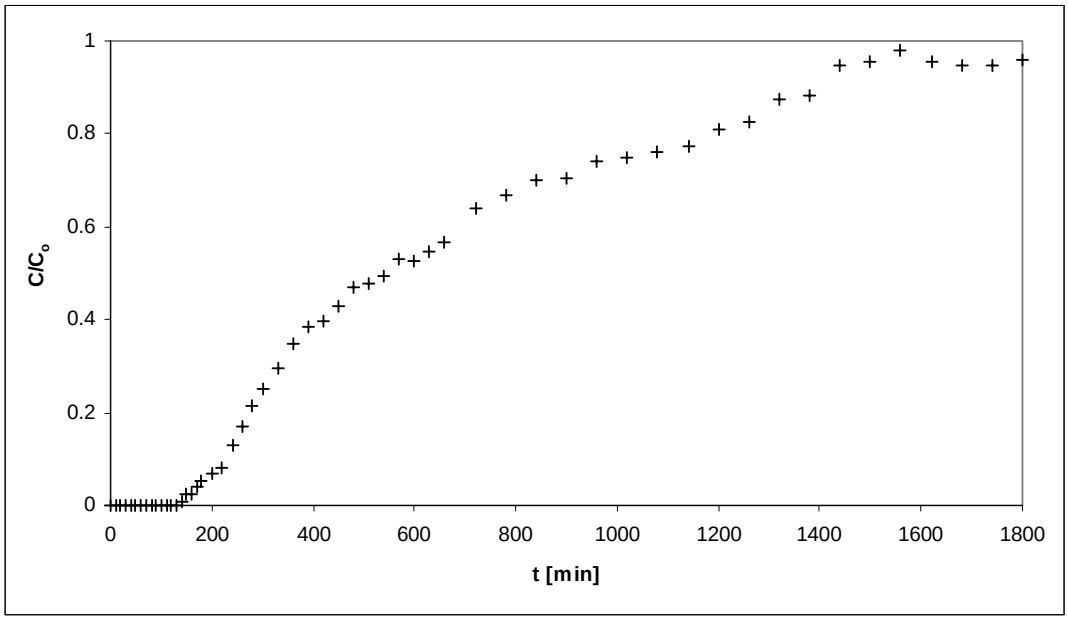

Figure A.20. Breakthrough Curve for Cu^{2+} Exchange on CP1 with Respect to Concentration Ratio and Time at 29°C with a flow rate of 4.75 ml/min (Packing Height= 25 cm, Initial Cu^{2+} Concentration= 100 mg/L).

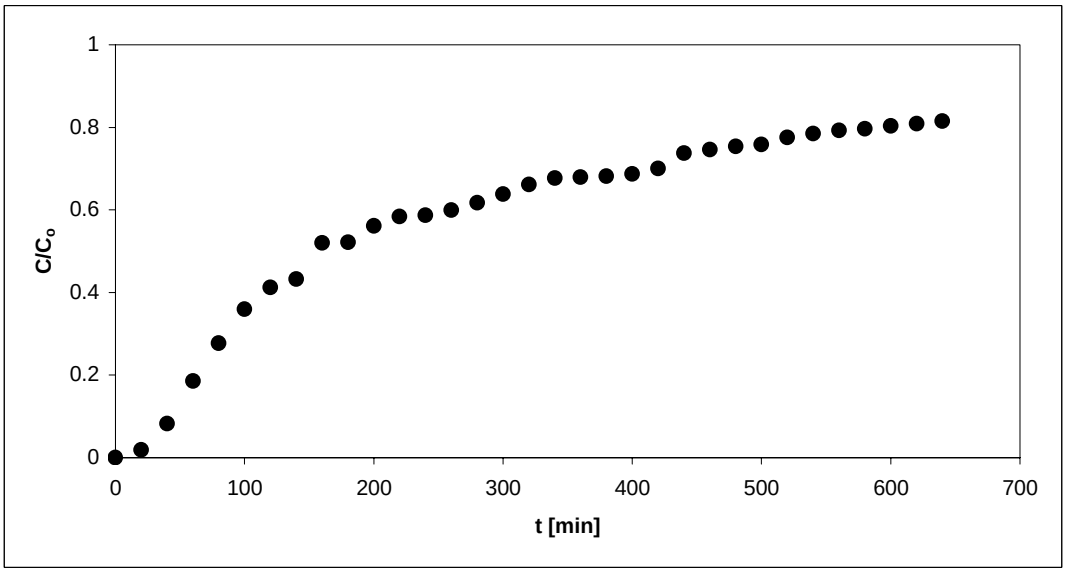

Figure A.21. Breakthrough Curve for Cu^{2+} Exchange on CP1 with Respect to Concentration Ratio and Time at 29°C with a flow rate of 4.75 ml/min (Packing Height= 18.75 cm, Initial Cu^{2+} Concentration= 200 mg/L).

Interpretation of the results:

As can be seen from Table A.3., the Model F-value of 618.27 implies the model is significant. There is only a 3.08% chance that a "Model F-Value" this large could occur due to noise.

Table A.3. Statistical Data for Design of Experiments

Source	Sum of squares	DF	Mean Square	F Value	Prob>F	
Model	5.050E+005	6	84161.46	618.27	0.0308	Significant
A	*1.565E+005*	*1*	*1.565E+005*	*1149.83*	*0.0188*	
B	*1.001E+005*	*1*	*1.001E+005*	*735.56*	*0.0235*	
C	*1.900E+005*	*1*	*1.900E+005*	*1396.04*	*0.0170*	
AB	*15576.12*	*1*	*15576.12*	*114.43*	*0.0593*	
AC	*14028.13*	*1*	*14028.13*	*103.05*	*0.0625*	
BC	*28680.12*	*1*	*28680.12*	*210.69*	*0.0438*	

- Values of "Prob > F" less than 0.0500 indicate model terms are significant. In this case A, B, C, BC are significant model terms as can be seen from Table A3.
- Values greater than 0.1000 indicate the model terms are not significant.

The straight line on the half-normal plot always passes through the origin. From Figure A.22 it's seen that the large effects are far from the line, which are the main effects of A, B and C and the BC interaction.

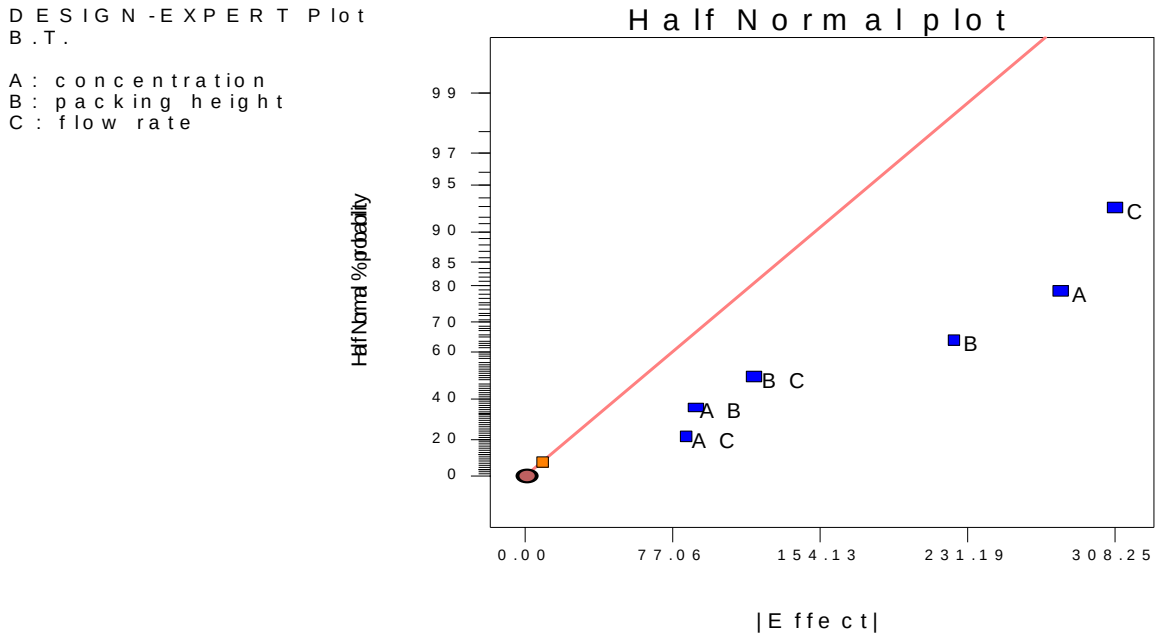

Figure A.22. Half Normal Plot for Determining the Effects of Concentration, Packing Height and Flow Rate

The AB, AC and BC interactions were plotted in Figures A.23-A.25. These interactions were the key to solving the problem. When investigating the interaction between two factors, the third one was taken at the mid-level. For example in Figure A.23, from the AB interaction that the concentration effect was very small when the packing height was at the low level and relatively large when the packing height was at the high level, with the best results obtained with low concentration and high packing height. The AC interaction indicated that concentration had little effect at high flow rate but a large effect at low flow rate. Finally, as can be seen from Figure A.25, the effect of BC interaction was more significant when B was at the high level and C was at the low level. Therefore, the maximum breakthrough time would appear to be obtained when A and C were at the low level and B was at the high level.

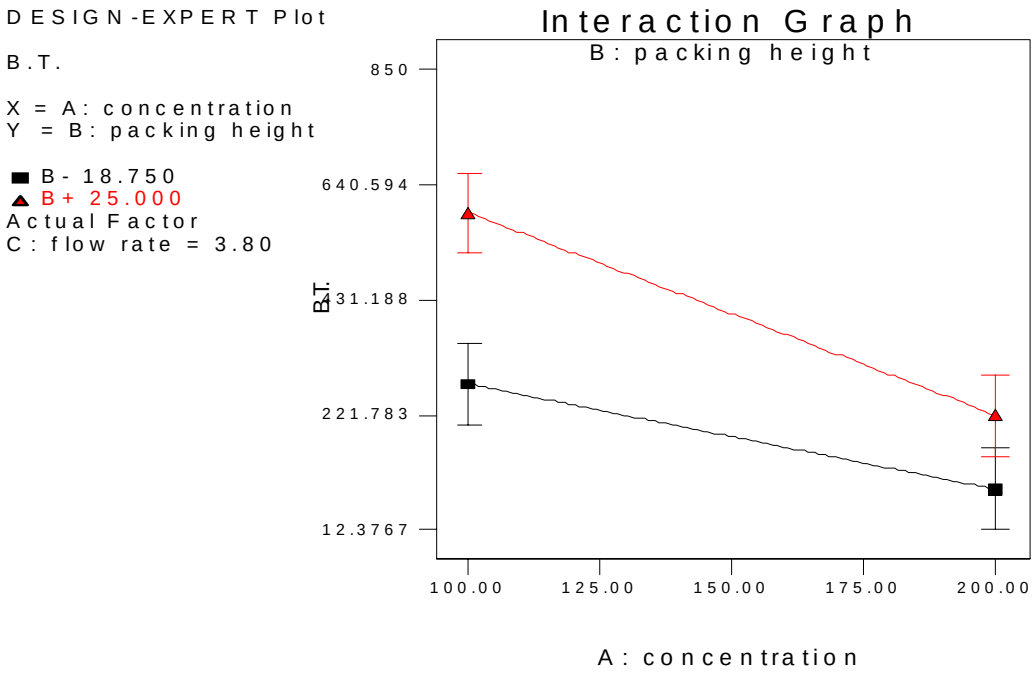

Figure A.23. Interaction of the Heavy Metal Concentration and Packing Height

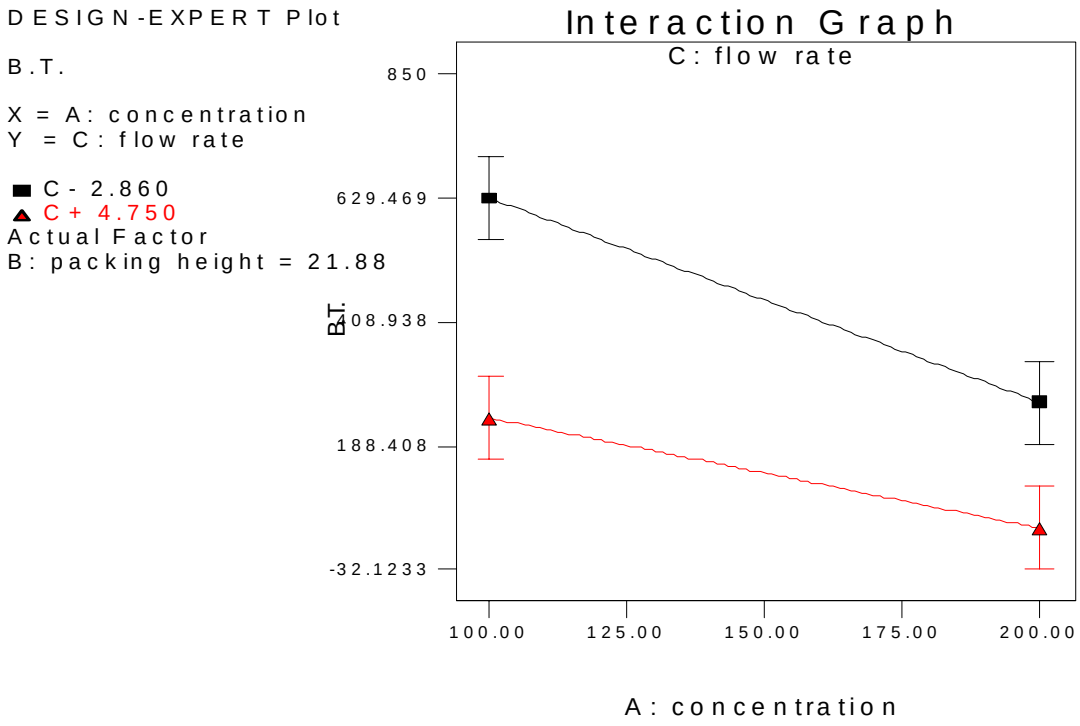

Figure A.24. Interaction of the Heavy Metal Concentration and Flow Rate

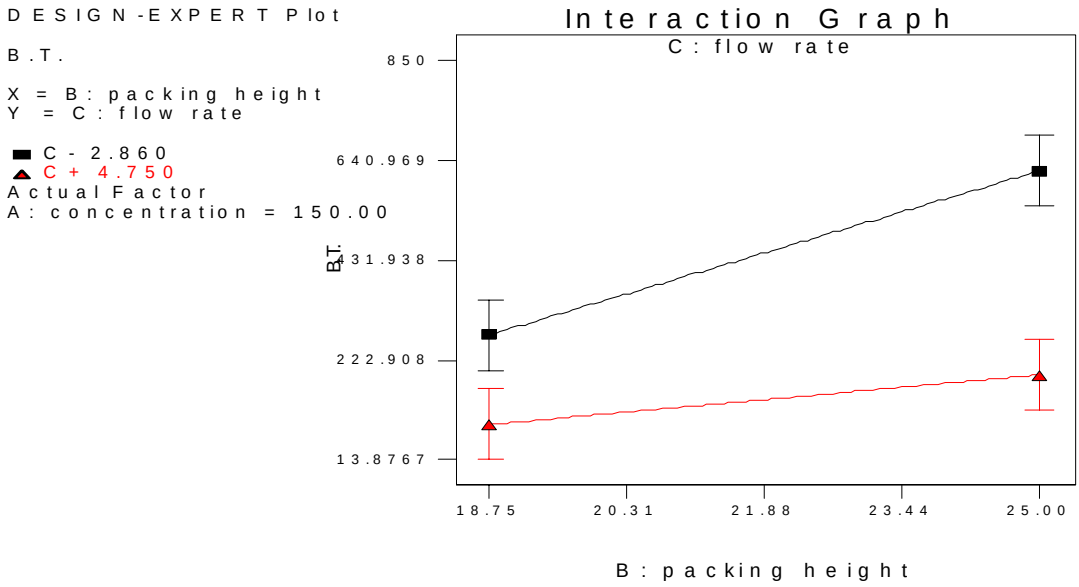

Figure A.25. Interaction of the Packing Height and Flow Rate

Also, breakthrough time was predicted by using Design-Expert computer program when three factors were at the mid-level and the final equation in terms of actual factors were given;

B.T. = -1557.19 + 0.0078 * concentration + 155.31 * packing height + 147.49 * flow rate - 0.28 * concentration * packing height + 0.88 * concentration * flow rate - 20.27 * packing height * flow rate (A.1)

Table A.4. Prediction of Breakthrough Time from Design of Experiments (From Design-Expert)

Factor	Name	Level	Low Level	High Level
A	concentration	150.00	100.00	200.00
B	packing height	21.88	18.75	25.00
C	flow rate	3.80	2.86	4.75

Prediction	SE Mean	95% CI low	95% CI high	SE Pred	95% PI low	95% PI high
*B.T. 294.12	4.12	241.71	346.54	12.37	136.8	451.36

Table A.5. 95% Confidence Interval for the Different Effects

Factor	Coefficient Estimate	Standard Error	95% CI Low	95% CI High
Intercept	294.13	4.12	241.71	346.54
A-concentration	-139.88	4.12	-192.29	-87.46
B-packing height	111.88	4.12	59.46	164.29
C-flow rate	-154.13	4.12	-206.54	-101.71
AB	-44.12	4.12	-96.54	8.29
AC	41.88	4.12	-10.54	94.29
BC	-59.87	4.12	-112.29	-7.46

Table A.6. Diagnostics Case Statistics

Standard Order	Actual Value	Predicted Value	Residual	Order
1	410.00	414.13	-4.13	7
2	143.00	138.87	4.13	6
3	850.00	845.88	4.12	8
4	390.00	394.13	-4.13	5
5	146.00	141.88	4.12	1
6	30.00	34.12	-4.12	4
7	330.00	334.13	-4.13	2
8	54.00	49.88	4.12	3

Table A.7. Percent Contribution of Different Effects

Require	Term Intercept	Effect	Sum Sqr	% Contribution
Model	A	-279.75	156520	30.9876
Model	B	223.75	100128	19.8232
Model	C	-308.25	190036	37.6231
Model	AB	-88.25	15576.1	3.08374
Model	AC	83.75	14028.1	2.77727
Model	BC	-119.75	28680.1	5.67805
Error	ABC	8.25	136.125	0.0269498